

INFORMATION TO USERS

This manuscript has been reproduced from the microfilm master. UMI films the text directly from the original or copy submitted. Thus, some thesis and dissertation copies are in typewriter face, while others may be from any type of computer printer.

The quality of this reproduction is dependent upon the quality of the copy submitted. Broken or indistinct print, colored or poor quality illustrations and photographs, print bleedthrough, substandard margins, and improper alignment can adversely affect reproduction.

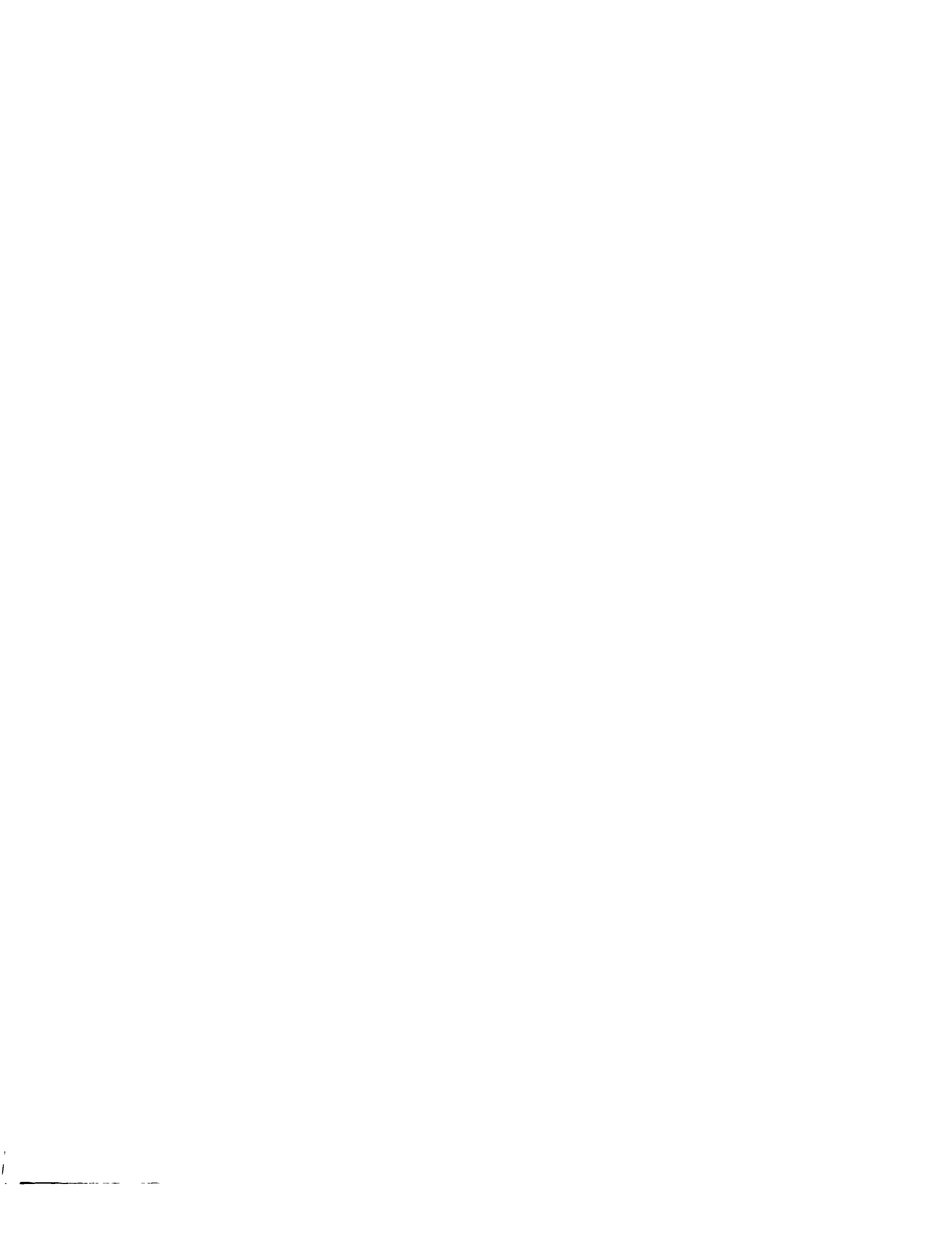
In the unlikely event that the author did not send UMI a complete manuscript and there are missing pages, these will be noted. Also, if unauthorized copyright material had to be removed, a note will indicate the deletion.

Oversize materials (e.g., maps, drawings, charts) are reproduced by sectioning the original, beginning at the upper left-hand corner and continuing from left to right in equal sections with small overlaps. Each original is also photographed in one exposure and is included in reduced form at the back of the book.

Photographs included in the original manuscript have been reproduced xerographically in this copy. Higher quality 6" x 9" black and white photographic prints are available for any photographs or illustrations appearing in this copy for an additional charge. Contact UMI directly to order.

UMI

**A Bell & Howell Information Company
300 North Zeeb Road, Ann Arbor MI 48106-1346 USA
313/761-4700 800/521-0600**



UNIVERSITY OF OKLAHOMA
GRADUATE COLLEGE

HEAT FLOW IN OKLAHOMA

A DISSERTATION
SUBMITTED TO THE GRADUATE FACULTY
in partial fulfillment of the requirements for the
degree of
Doctor of Philosophy

By
CONSTANTIN CRANGANU
Norman, Oklahoma
1997

UMI Number: 9810311

UMI Microform 9810311
Copyright 1997, by UMI Company. All rights reserved.

**This microform edition is protected against unauthorized
copying under Title 17, United States Code.**

UMI
300 North Zeeb Road
Ann Arbor, MI 48103

© Copyright by Constantin Cranganu 1997
All Rights Reserved

HEAT FLOW IN OKLAHOMA

A DISSERTATION APPROVED FOR THE
SCHOOL OF GEOLOGY AND GEOPHYSICS

BY

cc c.

RRP

Judson L. Chess

James E. ...

James E. ...

To the memory of my mother

ACKNOWLEDGMENTS

Many people have contributed, in small ways and large, to the creation of this thesis. Foremost among them has been Dr. David Deming, who provided a continuous, useful guidance and thorough, creative criticism of successive versions of this study. My Committee members, Dr. Jud Ahern, Dr. Paul Philp, Dr. Anuj Gupta, and Dr. Douglas Waples, oriented me during the time of course work and various stages of research. Dr. David D. Blackwell (Southern Methodist University in Dallas) generously offered three unpublished heat flow values and other useful information. Thanks are also due to the U. S. Information Agency Fulbright Program, School of Geology and Geophysics (Director Dr. M. C. Gilbert) and Oklahoma Geological Survey (Director Dr. Charles Mankin) which offered financial support during the time of my research. Dr. Kenneth S. Johnston, Dr. Kenneth V. Luza, Dr. Robert O. Fay, and Dr. Jock Campbell (from Oklahoma Geological Survey), Dr. Stephen R. Kraemer (from United States Environmental Protection Agency in Ada), and Scott Christenson (from United States Geological Survey in Oklahoma City) provided useful information in various stages of manuscript preparation. My colleague, Youngmin Lee, shared with me his knowledge and competence in UNIX, FORTRAN, and Tecplot. Core and Sample Library in Norman (Manager Walter Esry), Log Library in Norman (Manager Michael Mercer), and Oklahoma City Geological Society Library were the sources for drilling cuttings and gamma-ray logs. Undergraduate students Patrick Doherty and Travis Wilson helped me with thermal conductivity measurements. And last, but not least, I would like to thank my family, without whose support this study would not have been possible.

TABLE OF CONTENTS

	Page
1. INTRODUCTION.....	1
1.1. Thermal regime of sedimentary basins.....	2
1.2. Thermal anomalies related to Paleozoic fluid migrations.....	3
2. GEOLOGIC FRAMEWORK.....	5
2.1. General considerations.....	5
2.2. Basement rocks of Oklahoma.....	10
2.3. Sedimentary rocks of Oklahoma.....	13
2.3.1. Early Paleozoic (523 - 440 m.y. ago).....	13
2.3.2. Middle Paleozoic (440 - 333 m.y. ago).....	15
2.3.3. Late Paleozoic (333 - 245 m.y. ago).....	16
2.3.4. Post Paleozoic.....	17
3. THERMAL METHODOLOGY.....	18
3.1. Temperature data.....	18
3.2. Thermal gradients.....	20
3.2.1. Thermal gradient corrections.....	24
3.3. Thermal conductivity.....	24
3.3.1. Anisotropy correction.....	29
3.3.2. Temperature correction.....	30
3.3.3. Porosity correction.....	31
3.4. Heat production.....	36
3.5. Heat flow.....	37
4. RESULTS.....	38
4.1. Thermal gradients.....	38
4.2. Thermal conductivity.....	38
4.3. Heat production.....	46

	Page
4.4. Heat flow.....	52
5. ERROR ANALYSIS.....	57
5.1. Temperature data.....	57
5.2. Thermal gradients.....	58
5.3. Thermal conductivity.....	58
5.3.1. Sampling error.....	58
5.3.2. Measurement error.....	59
5.3.3. Correction errors.....	60
5.4. Heat production error.....	61
5.5. Heat flow error.....	62
6. INTERPRETATION OF RESULTS AND DISCUSSION.....	63
6.1. Introduction.....	63
6.2. Transient effects of sedimentary processes and metamorphic/igneous activity.....	65
6.3. Climatic effects.....	67
6.4. Effects of variable distribution of heat generation sources.....	67
6.5. Effects due to contrasts in thermal conductivity.....	72
6.6. Effects due to groundwater movement.....	73
7. SUMMARY AND CONCLUSIONS.....	84
Appendix A.....	88
Appendix B.....	129
Appendix C.....	130
Appendix D	149
REFERENCES.....	150

LIST OF TABLES

	Page
Table 1 - Well Data Including Geothermal Gradients, In-situ Conductivities, and Surface Heat Flow.....	22
Table 2 - Thermal Conductivity Measurements.....	25
Table 3 - Porosity Estimates.....	32
Table 4 - Thermal Conductivities in central Oklahoma.....	35
Table 5 - Heat Production Estimates.....	47

LIST OF ILLUSTRATIONS

	Page
Fig. 1: Geologic provinces of Oklahoma (simplified after Northcutt and Campbell, 1996).....	7
Fig. 2: Map of the southwestern United States, showing the approximate boundary of the Oklahoma Basin and other major features that existed in Early and Middle Paleozoic time (after Johnson et al., 1988).....	8
Fig. 3: Distribution of basement rocks in Oklahoma (simplified after Denison et al., 1984).....	12
Fig. 4: Generalized correlation of rock units in Oklahoma (after Johnson and Cardott, 1992).....	14
Fig. 5: Temperature (a), thermal gradient (b), thermal conductivity (c), and heat flow (d) distribution with depth at site #16.....	20
Fig. 6: Stratigraphic map of Booch sand at site #16.....	21
Fig. 7: Thermal conductivity distribution with depth and geologic ages at sites #1, #2, #3, and #4 (for location, see Table 2 and Figures A2, A4, A6, and A8).....	40
Fig. 8: Thermal conductivity distribution with depth and geologic ages at sites #5, #6, #7, and #8 (for location, see Table 2 and Figures A10, A12, A14, and A16).....	41

	Page
Fig. 9: Thermal conductivity distribution with depth and geologic ages at sites #9, #10, #11, and #12 (for location, see Table 2 and Figures A18, A20, A22, and A24).....	42
Fig. 10: Thermal conductivity distribution with depth and geologic ages at sites #13, #14, #15, and #16 (for location, see Table 2 and Figures A26, A28, A30, and A32).....	43
Fig. 11: Thermal conductivity distribution with depth and geologic ages at sites #17, #18, #19, and #20 (for location, see Table 2 and Figures A34, A36, A38, and A40).....	44
Fig. 12: Heat Generation Map of Oklahoma.....	49
Fig. 13: Heat Flow Map of Oklahoma.....	53
Fig. 14: Geologic cross-section A - A' (after Stratigraphic Committee, 1971) with heat generation and heat flow distribution.....	54
Fig. 15: Geologic cross-section B - B' (after Johnson et al., 1972) with heat generation and heat flow distribution.....	55
Fig. 16: Heat generation (A) - heat flow (q) relationship for Oklahoma.....	71
Fig. 17: Equivalent freshwater head, in ft (1 ft = 0.30 m), in Cambrian and Ordovician rocks of the Central United States (modified from Jorgensen,	

	Page
1989).....	75
Fig. 18: Concentration of total dissolved solids, in mg/l, in groundwater from Cambrian and Ordovician rocks of the Central United States (modified from Jorgensen, 1989).....	76

ABSTRACT

Twenty new heat flow values are incorporated, along with 40 previously published data, into a heat flow map of Oklahoma. The new heat flow data were estimated using previous temperature measurements in boreholes made by American Petroleum Institute researchers and 1,498 thermal conductivity measurements on drill cuttings.

The mean of 20 average thermal gradients is 30.50°C/km. In general, thermal gradients increase from SW (14.11°C/km) to NE (42.24°C/km). The range of 1,498 in situ thermal conductivity measurements (after corrections for anisotropy, in situ temperature, and porosity) is 0.90 - 6.1 W/m-K; the average is 1.68 W/m-K. Estimated near-surface heat flow ($\pm 20\%$) at 20 new sites in Oklahoma varies between 22 ± 4 mW/m² and 86 ± 17 mW/m²; the average is 50 mW/m². Heat flow is relatively low (< 30 mW/m²) in SW Oklahoma and is relatively high in NE Oklahoma (> 70 mW/m²). There are areas with low-to-intermediate heat flow (30 - 50 mW/m²) in central and SE Oklahoma, and areas with intermediate-to-high heat flow (50 - 70 mW/m²) in the Oklahoma Panhandle, Cherokee Platform, and SE corner of the state.

Twenty-seven new heat-generation estimates, along with 22 previously published data, are used to create a heat generation map of Oklahoma. The range of heat production estimates is 1.1 - 3.5 $\mu\text{W}/\text{m}^3$, with an average of 2.5 $\mu\text{W}/\text{m}^3$. Heat production rates vary with basement rock type. The area with the lowest heat production (< 1.5 $\mu\text{W}/\text{m}^3$) lies in the SE parts of the Arkoma Basin and the Arbuckle Uplift. Areas with the highest heat generation (> 3 $\mu\text{W}/\text{m}^3$) occupy the northwestern part of the state, as well as small portions in NE.

The heat flow regime in Oklahoma is primarily conductive in nature, except for a zone in northeast. Transient effects due to sedimentary processes

and metamorphic/igneous activity, as well as past climatic changes, do not significantly influence the thermal state of the Oklahoma crust. Heat flow near the margins of the Arkoma and Anadarko Basins may be depressed or elevated by 5 - 13 mW/m² by refraction of heat from sedimentary rocks of relatively low thermal conductivity (1 - 2 W/m-K) into crystalline basement rocks of relatively high thermal conductivity (~ 3 - 4 W/m-K).

The linear heat production - heat flow relationship found empirically in plutonic provinces by other investigators does not apply to Oklahoma. A modest correlation between heat generation and heat flow implies that heat production in basement rocks exerts some control on regional heat flow variations in Oklahoma. The relatively high heat flow (~ 70 - 80 mW/m²) in part of northeastern Oklahoma suggests that the thermal regime there may be perturbed by regional groundwater flow originating in the fractured outcrops of the Arbuckle-Simpson aquifer in the Arbuckle Mountains.

1. INTRODUCTION

The aim of this study is to establish the present-day thermal regime of Oklahoma by incorporating 20 new heat flow values and 27 new heat-production determinations into previously published data, thus creating the first heat flow and heat production maps of Oklahoma.

Even though the distribution of heat flow values on many continental areas is well estimated (Pollack et al., 1993), Oklahoma is a region with few heat flow and heat production data. For example, the geothermal map of North America (Blackwell and Steele, 1991) contains a single heat flow value (the one determined by Roy et al., 1968, in the northeast corner of the state). In recent years, several new heat flow data were added to the map of Oklahoma. These include seven values reported by Carter et al. (1996) for the Anadarko Basin. These values were determined using high-precision temperature logs and thermal conductivity measurements on nearly 300 core plugs. Borel (1995) estimated heat flow at a site in north-central Oklahoma. from high-precision temperature logs and thermal conductivity measurements on 18 core samples. Lee et al. (1996) estimated heat flow at eleven sites in the Arkoma Basin and Oklahoma Platform to the north using corrected bottom-hole temperatures (BHTs) and thermal conductivity measurements on drill cuttings. Lee and Deming (1997) reported seventeen values for the Anadarko Basin, using the same procedure as Lee et al. (1996). The present thesis also contains three values estimated by D. D. Blackwell and his co-workers at Southern Methodist University in Dallas (pers. comm., Blackwell, 1996).

Other previous thermal investigations in Oklahoma include thermal gradient maps published by Gilarranz (1964); Cheung (1978, 1979); Harrison et al. (1983); and Harrison and Luza (1986) for the state of Oklahoma; American Association of Petroleum Geologists and U.S. Geological Survey (1976),

Guffanti and Nathenson (1981) and Nathenson and Guffanti (1988), for the United States, including Oklahoma. However, discussing the relative importance of such thermal gradient maps, Birch (1954) stressed that the principal variable affecting temperature gradient in the outer layers of the crust is thermal conductivity (and, locally, groundwater movement). Consequently, a geothermal gradient map alone is expected to tell us as much about the variations in thermal conductivity (and, locally, groundwater circulation) as about variations in the more fundamental quantity, heat flow.

1.1. Thermal regime of sedimentary basins

Oklahoma is well known for oil and gas production. From the Anadarko Basin alone, 82.4 trillion cubic feet of gas and 5.37 billion barrels of oil were produced through 1985 (Davis and Northcutt, 1989). Hundreds of thousands of wells have been drilled in the Anadarko, Ardmore, Arkoma, Hollis, and Marietta Basins, and in other places throughout the state.

Temperature is a critical parameter in the transformation of organic matter into gas and/or oil and in the maturation of crude oils in reservoirs (Waples, 1980; 1995a; 1995b; Quigley et al., 1987; Tissot et al., 1987; Ungerer et al., 1990; Barker, 1996). The temperature-dependent degradation of crude oils will produce lighter oils, then condensate, and finally, dry gas. Temperature also plays an important role in controlling inorganic reactions, such as the dewatering of clays and the mineral transformations that can create or destroy porosity. Reconstruction of the thermal history of a sedimentary basin allows: (1) the prediction of oil/gas windows in evaluating potential hydrocarbon source rocks; (2) an understanding of the geologic and tectonic history of a sedimentary basin; and (3) an understanding and evaluation of the timing of hydrocarbon generation and expulsion from a defined source rock (Barker,

1996). Levels of thermal maturity for Paleozoic strata, including the Woodford shale, the most important source rock for Oklahoma oil and gas, have been estimated for the Anadarko Basin, the Arkoma Basin or for the entire state of Oklahoma by Cardott (1989), Schmoker (1989), Houseknecht et al. (1992), Hester et al. (1992) and Pawlewicz (1992). These studies constrain hydrocarbon-generation models by indicating, according to maturation stage, the type of production (oil, dry gas) and the volume of production. Any future study concerning hydrocarbon-generation modeling in Oklahoma will find thermal information available from the present thesis.

In addition to the above considerations, heat-flow studies in some sedimentary basins, such as the Anadarko Basin, may provide a better understanding of overpressures. Several processes can cause abnormal pressures (Sahay and Fertl, 1989; Fertl et al., 1994; Osborne and Swarbrick, 1997): (1) compaction disequilibrium; (2) petroleum generation; (3) petroleum cracking; (4) thermal expansion of water; (5) other mechanisms (lateral tectonic compression, clay diagenesis and dewatering, and reverse osmosis). Some of the preceding processes (e.g., hydrocarbon generation, aquathermal pressuring) are thermally driven and the present-day heat flow values can offer a constraint for modeling these processes.

1.2. Thermal anomalies related to Paleozoic fluid migrations

Briny hydrothermal fluids were once ubiquitous in the Middle and Late Paleozoic (~250 - 360 m.y. ago) country rocks of the midcontinent (Oliver, 1986; 1992; Sverjensky, 1986; Bethke and Marshak, 1990; Garven et al., 1993). Although these brines have an unknown origin, their existence is documented by: (1) the presence of ore bodies that were deposited from metal-bearing brines, such as Mississippi Valley - Type ores (MVT) (Anderson and

Macqueen, 1982; Kisvarsanyi et al., 1983); (2) metal-rich Pennsylvanian shales (Zangerl and Richardson, 1963; Vine and Tourtelot, 1970; Coveney and Martin, 1983); (3) epigenetic dolomite cements in ore bodies and deep aquifers (Zenger and Dunham, 1980; Mattes and Mountjoy, 1980); (4) paleomagnetization (Van der Voo and French, 1975; McCabe et al., 1983; Bagley et al., 1992), and (5) fluid inclusions indicating unusually high homogenization temperatures (up to 200°C) at shallow depths (< 1.5 - 2 km) (Roedder, 1979; Leach, 1979; Coveney et al., 1987; Shelton et al., 1992). There may also exist a link between continental-scale fluid migrations and occurrences of oil fields (Oliver, 1992; Coveney, 1992) that might explain, for example, the presence of a major oil and gas area in the Ouachita trend - including West Texas, Oklahoma, and Kansas.

The origin of the heat source of these warm brines is still controversial, and reconstructing the complete thermal history of the midcontinent region is a complex task. The present-day heat flow values can act as a boundary condition for those studies that investigate (1) the effects of convective heat transfer on the thermal history of sediments by evaluating the ratio of conductive to convective heat transfer (thermal Peclet number: Person et al., 1995); (2) the thermal effect of depositing of cold sediments on top of the lithosphere ("blanketing effect"), especially in those areas where the sedimentation rate exceeded a certain lower limit (250 m/m.y.) and the sedimentation period lasted for some time (Wangen, 1995); and (3) past fluid migrations by constraining regional scale permeabilities of the present day groundwater flow (Deming et al., 1992, 1996).

2. GEOLOGIC FRAMEWORK

2.1. General considerations

In this chapter I review aspects of Oklahoma geology relevant to the thermal structure and history of Oklahoma. Basement rocks contain radioactive isotopes of U, Th, and K which, by radioactive decay, provide about 40% of the global near-surface heat flow (Pollack and Chapman, 1977). The sedimentary cover over the basement, by its lithology and thermal conductivity, partly controls the distribution of thermal gradients. The thermal conductivity of sedimentary rocks ranges over more than an order of magnitude, from coal (0.33 - 0.45 W/m-K, Pollack and Cercone, 1994; Herrin and Deming, 1996) to evaporites (~6.0 W/m-K, Clark, 1966; Horai, 1971). Accordingly, for a fixed heat flow, geothermal gradient is inversely related to thermal conductivity. Highly conductive rocks give low gradients, while poor conductors give high gradients.

The permeability of sedimentary rocks is a key parameter in groundwater movement which, in turn, controls the convective distribution of heat flow in sedimentary basins. The permeability of sedimentary rocks extends over several orders of magnitude. The permeability of sandstone ranges from 10^{-13} to 10^{-17} m² (10^2 to 10^{-2} mD); limestone, 10^{-13} to 10^{-16} m² (10^2 to 10^{-1} mD); shale, 10^{-16} to 10^{-20} m² (10^{-1} to 10^{-5} mD) (Brace, 1980; Neuzil, 1994). Thus, sandstone beds may be good conduits for groundwater, while shales can act as low-permeability barriers in overpressuring or groundwater movement.

The following presentation draws on Johnson et al. (1988), Johnson and Cardott (1992), and Denison et al. (1984).

The geology of Oklahoma is complex but very well explained, owing to a plethora of information provided by many thousands of wells drilled for oil

and gas, and by extensive seismic exploration.

Oklahoma is a part of the southern Midcontinent characterized by great thickness of sediments preserved in a series of major depositional and structural basins separated by orogenic uplifts created mainly during Pennsylvanian time (Johnson et al., 1988; Northcutt and Campbell, 1996; Fig. 1).

The major sedimentary basins contain as much as 6,000 to 12,000 m of sediments, most of which are Paleozoic and marine. These sediments rest upon a basement complex of igneous rocks and some low-rank metasedimentary rocks (Denison et al., 1984; Johnson et al., 1988; Johnson and Cardott, 1992). Thick sedimentary deposits accumulated along the southern margin of the North American Craton during Paleozoic episodes of subsidence of the Anadarko, Ardmore, and Marietta Basins (Fig. 1), and of the foredeep areas north and west of the Ouachita Trough (Johnson et al, 1988; Arbenz, 1989). The west-northwest trending trough comprising the Anadarko, Ardmore, and Marietta Basins and associated uplifts is known as the Southern Oklahoma Geosyncline (Ham et al., 1964; Ham and Wilson, 1967) or the Southern Oklahoma Aulacogen (Gilbert, 1983; Brewer et al., 1983; see Fig. 2).

By Early Paleozoic time (570 m.y. ago), Oklahoma included three major tectonic/depositional provinces: the Oklahoma basin, the Southern Oklahoma aulacogen, and the Ouachita trough (Johnson and Cardott, 1992; see Fig. 2). The Oklahoma basin consisted of a broad, shelf-like area covered with thick carbonates interbedded with marine shales and sandstones (Johnson et al, 1988). The Southern Oklahoma aulacogen, which was the depocenter for the Oklahoma basin (Johnson and Cardott, 1992), extended from the Ouachita trough (the Paleozoic continental margin of North

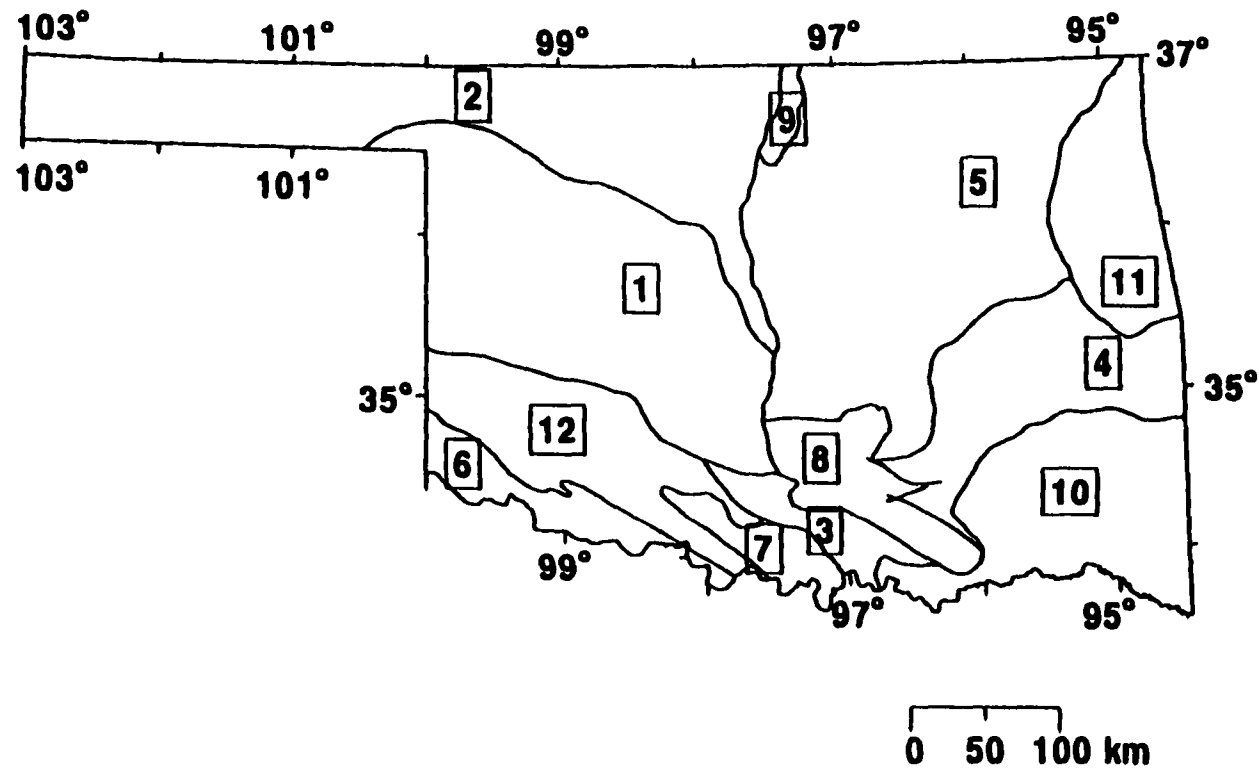


Fig. 1. Geologic provinces of Oklahoma (simplified after Northcutt and Campbell, 1996)
 1 - Anadarko Basin; 2 - Anadarko Shelf; 3 - Ardmore Basin; 4 - Arkoma Basin; 5 - Cherokee Platform; 6 - Hollis Basin; 7 - Marietta Basin; 8 - Arbuckle Uplift; 9 - Nemaha Uplift; 10 - Ouachita Mountains Uplift; 11 - Ozark Uplift; 12 - Wichita Uplift.

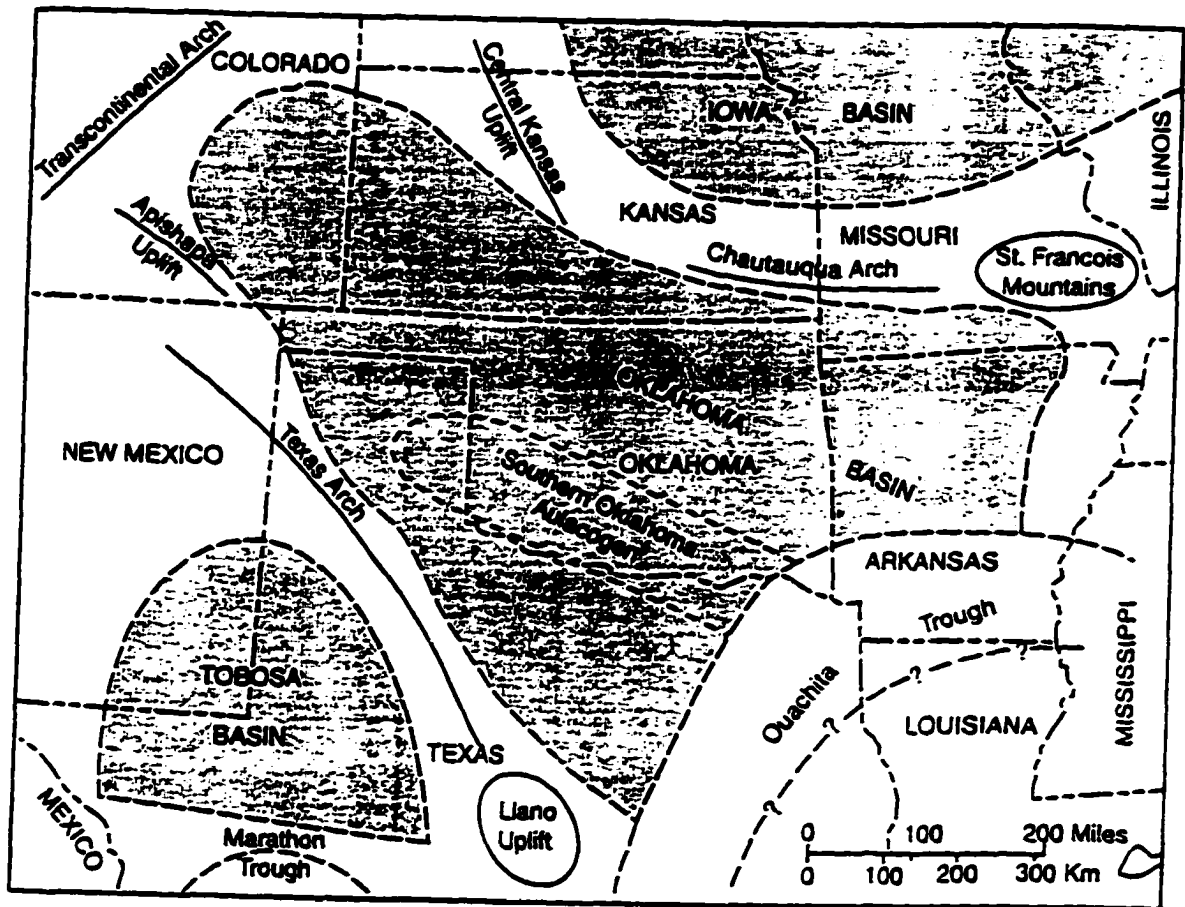


Fig. 2. Map of the southwestern United States, showing the approximate boundary of the Oklahoma Basin and other major features that existed in Early and Middle Paleozoic time (after Johnson et al., 1988).

America) 700 km west-northwest into the Midcontinent, through southwestern Oklahoma and northern Texas (Feinstein, 1981). Three stages of evolution of the aulacogen have been defined by Ham et al. (1964); Ham (1969); Pruatt (1975), and Thompson (1976, 1978): (a) a thermally related rifting stage from Late Precambrian through Middle Cambrian (900 - 523 m.y. ago), associated with intensive igneous activity and graben formation; (b) a stage of passive subsidence and sediment accumulation, dominated by shallow carbonate rocks from Late Cambrian through Devonian (523 - 360 m.y. ago); and (c) termination of the aulacogen stage by intensive deformation and deep burial from the Late Devonian to the Early Permian (360 - 258 m.y. ago).

The Southern Oklahoma aulacogen comprised the Anadarko, Ardmore, and Marietta protobasins, together with the Arbuckle anticline and the Wichita Mountain uplift (Gilbert, 1983; Johnson and Cardott, 1992). The third province, the Ouachita trough, was a deep-water sedimentation site along a rift at the southern margin of the North American Craton (Arbenz, 1989; Johnson and Cardott, 1992).

These three provinces persisted through the middle Paleozoic until Pennsylvanian time (~410 - ~290 m.y. ago), when two of them (the Oklahoma basin and the aulacogen) were divided into a series of well-defined marine basins by uplifted crustal blocks (Johnson and Cardott, 1992). The Ouachita trough was destroyed by Pennsylvanian uplift and northward thrusting (Arbenz, 1989). Orogenic activity throughout Oklahoma was limited, during its tectonic history, to folding, faulting, and uplift, and was not generally accompanied by igneous or high-grade metamorphic activity (Johnson et al., 1988; Johnson and Cardott, 1992).

Oklahoma is separated today into five major uplifts and six major basins, or low areas, on which a significant accumulation of sedimentary

rocks occurs (Fig. 1). According to Northcutt and Campbell (1996), they can be described as follow: 1 - Anadarko Basin; 2 - Anadarko Shelf (the boundary between 1 and 2 is placed near the 700 ft isochore of the Atokan and Desmonian Series at which there is a marked rate of change of thickening southward into the basin); 3 - Ardmore Basin; 4 - Arkoma Basin, including Franks Graben and Wapanucka Graben (the northern limit approximates the striking rate of change of thickness of Atokan strata southward from the Cherokee Platform into the Arkoma Basin); 5 - Cherokee Platform, including Seminole structure; 6 - Hollis Basin; 7 - Marietta Basin; 8 - Arbuckle Uplift, including the Ada high (This structure is apparently the northern faulted extension of a high that is part of the Pauls Valley - Hunton and Lawrence Horst blocks (Ham et al., 1964). This province also includes the Arbuckle Mountains, Tishomingo - Belton Horst, and Clarita Horst); 9 - Nemaha Uplift, formerly known as Nemaha Ridge, is defined by a horst-block complex in north-central Oklahoma and continuing northward in Kansas; 10 - Ouachita Uplift, including Broken Arrow Uplift, Ouachita central region, Ouachita frontal thrust belt, and Potato Hills; 11 - Ozark Uplift; 12 - Wichita Uplift, including Criner Uplift, Waurika - Muenster Uplift, and Wichita frontal fault zone.

Between and within these geologic provinces there are eighteen major faults (Northcutt and Campbell, 1996). For the sake of simplicity, they are not depicted in Figure 1.

2.2. Basement rocks of Oklahoma

The composition of basement rocks is important in any regional continental heat flow study because it controls to a large extent the surface heat flow values. This is due to their content of radioactive isotopes of U, Th,

and K. On a global average, the heat produced by radioactive decay of near-surface radiogenic sources contributes approximately 40% of the total heat flux measured at the surface on continents (Pollack and Chapman, 1977). The difference in composition among different types of basement rocks (granites, rhyolites, gabbros, or metamorphic rocks) is responsible for different rates of heat generation, and hence for variations of heat flow values. Granites (mesozonal or epizonal) usually produce more heat than other types of rocks due to their enhanced concentration of radioactive isotopes: the average heat production of granites/rhyolites is $\sim 2.5 \mu\text{W}/\text{m}^3$ (Rybach, 1976). Sedimentary rocks that cover the basement and fill the basins are less radioactive than basement rocks ($\sim 1 \mu\text{W}/\text{m}^3$ vs. $\sim 2.5 \mu\text{W}/\text{m}^3$, Keen and Lewis, 1982; Rybach, 1986, 1988; Fountain et al., 1987).

There are two important outcrops of basement rocks in the Wichita and Arbuckle Mountains in the southern part of Oklahoma (Fig. 1 and 3). In addition, several small outcrops of granite are exposed in northeast Oklahoma near the town of Spavinaw (Johnson et al., 1988). In most areas the basement, represented by silicic volcanic rocks and associated epizonal and mesozonal granitic plutons, is buried beneath Paleozoic rocks less than 3,000 m thick. The exceptions are in the Arkoma, Anadarko, and Ardmore basins where the sediment cover reaches 12,000 m (Johnson et al., 1988). A large number of wells drilled in search for oil, gas, and other minerals have penetrated the basement in all but the deepest basins.

Oklahoma is underlain by an extensive terrane of silicic volcanic rocks and associated epizonal and mesozonal granitic plutons (Denison et al., 1984) (Fig. 3). These rocks were formed between 1,500 and 1,300 m.y. ago. The Wichita Province (Fig. 3) is much younger (510 - 530 m.y. ago) and is composed of basalt, rhyolite, epizonal granite plutons, and a large body of

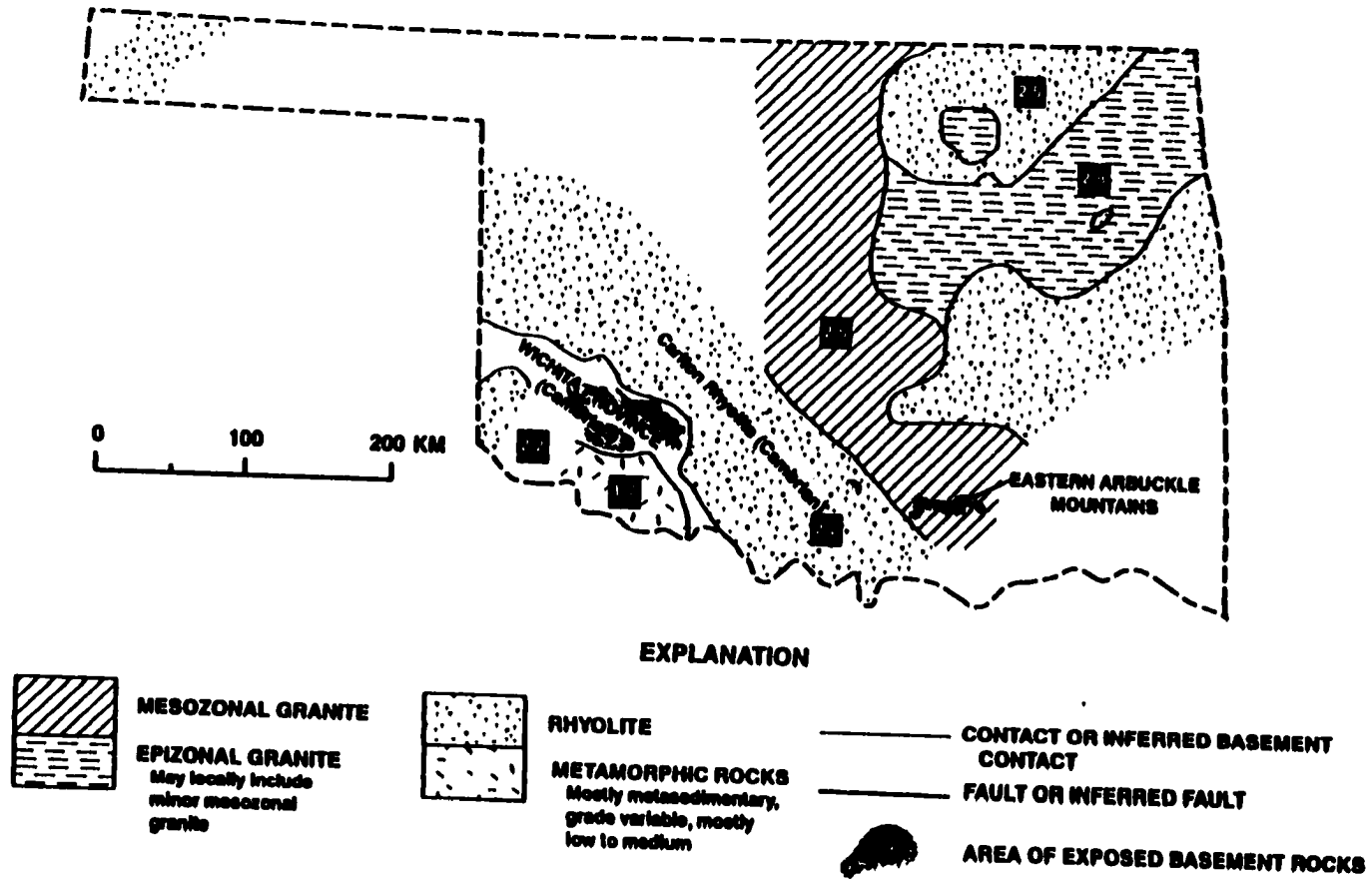


Fig. 3. Distribution of basement rocks in Oklahoma (simplified after Denison et al., 1984). The numbers indicate average heat-production measurements and estimates.

gabbroic rocks (Ham et al., 1964). The Carlton Rhyolite, also of Cambrian age (Fig. 3), is found on northern side of Wichita Province. A small area of metamorphic basement is shown on southeastern side of Wichita Province.

2.3. Sedimentary rocks of Oklahoma

The distribution of shales, sandstones, and carbonates, with their different permeabilities and thermal conductivities within a sedimentary basin, controls the distribution of groundwater movement, overpressure regime, and to some degree, the thermal gradient values.

The sedimentary rocks of Oklahoma and their associated tectonic history can be grouped into four major time periods (Johnson and Cardott, 1992): early Paleozoic (Late Cambrian and Ordovician), middle Paleozoic (Silurian, Devonian, and Mississippian), late Paleozoic (Pennsylvanian and Permian), and post Paleozoic (Triassic through Holocene) (Fig. 4).

2.3.1 Early Paleozoic (523 - 440 m.y. ago)

The layers deposited in this period are 300 - 3,000 m thick and consist mainly of carbonates (limestone and dolomite) interbedded with several quartzose sandstone and green shale units (Johnson and Cardott, 1992).

The basal Reagan sandstone, along with the Honey Creek limestone, forms the Timbered Hills Group (Fig. 4). This group is overlain by the Arbuckle Group, which consists of six limestone units interbedded with dolomites. The thickness of this group ranges from 2,500 m in the aulacogen, on the flank of the Arbuckle anticline (Fay, 1989) to about 300 - 1,200 m in most shelf areas of the Oklahoma basin (Johnson et al., 1988).

During the Middle Ordovician the Simpson Group strata were deposited (Fig. 4). They consist of quartzose sandstones, interbedded with

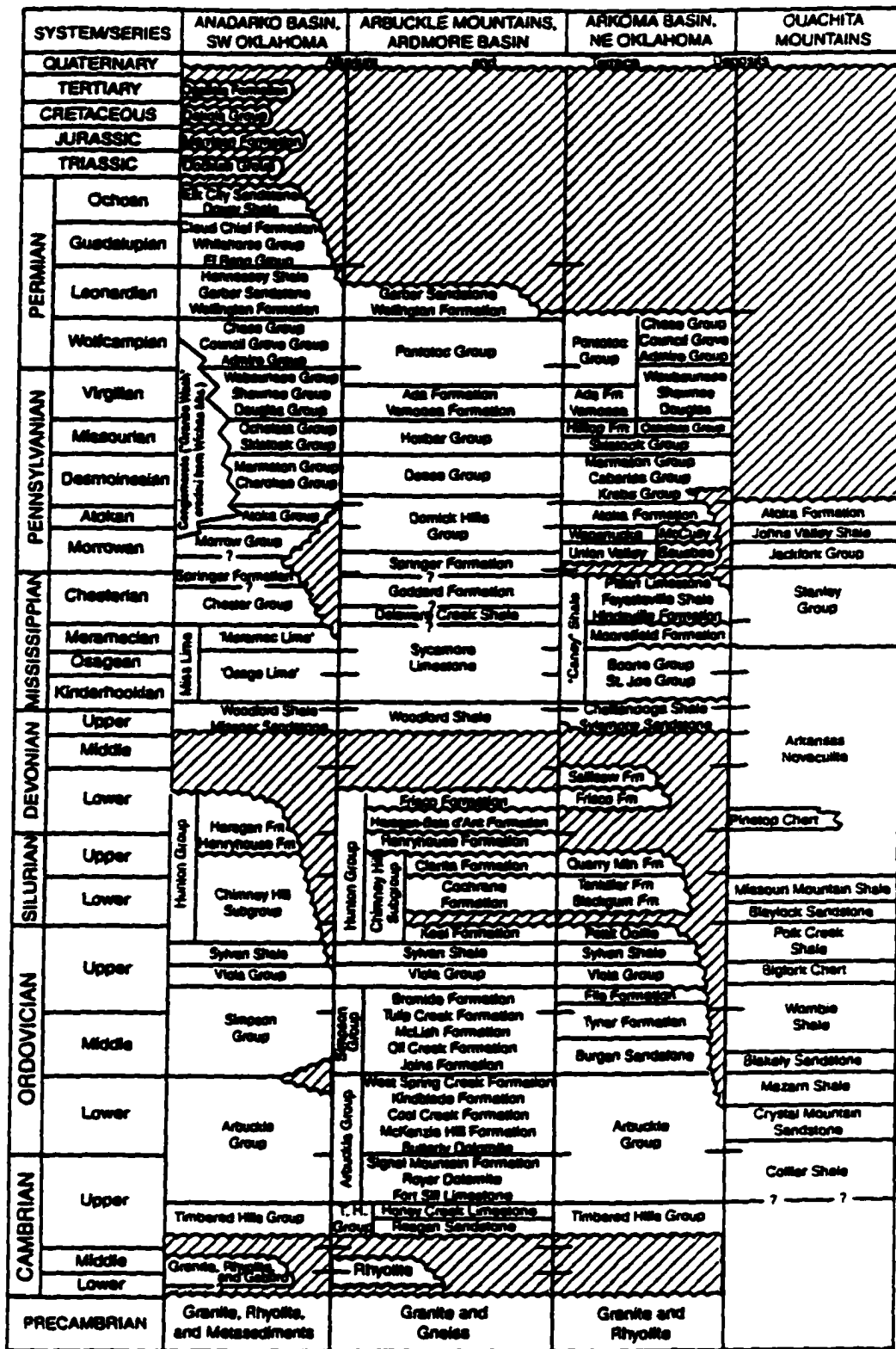


Fig. 4. Generalized correlation of rock units in Oklahoma (after Johnson and Cardott, 1992). Height of boxes is not related to thickness of rock units.

thick limestones and thin to moderately thick greenish-gray shales. Small deposits of red shale are interbedded with green shales in east - central Oklahoma, and minor amounts of dark - gray and black shales outcrop in southeastern Oklahoma (Statler, 1965; Johnson et al., 1988; Johnson and Cardott, 1992).

The next geologic unit, deposited in the Late Ordovician, is the Viola Group. This group contains terrigenous detritus (lower part) and skeletal limestones (upper part) (Johnson et al., 1988).

The Sylvan shale, with a large spread from western Arkansas into central Oklahoma, is a green and greenish - gray shale, with thicknesses ranging from 90 - 1,200 m in the aulacogen to 1 - 60 m in most shelf areas (Johnson et al., 1988; Johnson and Cardott, 1992).

In the Ouachita Mountains, Lower Paleozoic sediments include the Collier, Crystal Mountains, Mazarn, Blakely, Womble, Bigfork, and Polk Creek formations (Johnson and Cardott, 1992; see Fig. 4). These formations consist of black shales interbedded with sandstones, limestones, siliceous shales and cherts, and are equivalent of the Arbuckle facies. They are exposed over a total thickness of ~750 m (Johnson and Cardott, 1992). The Viersen and Cochran no. 25 - 1 Weyerhauser well, drilled in the core of the Broken Bow uplift, penetrated ~3,000 m of highly folded and faulted black phyllite, quartzite, and dolomitic marble without reaching basement (Goldstein, 1975).

2.3.2. Middle Paleozoic (440 - 333 m.y. ago)

During Silurian and Early Devonian times the Oklahoma basin was the site for deposition of the Hunton Group, which consists of mainly limestones in the lower part (Chimney Hill Subgroup), argillaceous and silty carbonates in the middle (Henryhouse and Haragan - Bois d'Arc Formations),

and limestones at the top (Frisco Formation) (Johnson et al., 1988; Fay, 1989; Johnson and Cardott, 1992).

Overlying the Hunton Group is the Woodford Shale (recognized as being the most prolific source rock for oil and gas in Oklahoma: Cardott, 1989), which is equivalent to the Chattanooga Shale to the northeast (Fig. 4). The Woodford shale is present throughout most parts of the Oklahoma basin, ranging from 60 - 270 m thickness in the aulacogen to 15 - 30 m thickness in most of the shelf areas (Amsden, 1975; Johnson et al., 1988; Johnson and Cardott, 1992).

Mississippian strata, which overlie the Woodford Shale, are represented by limestones and shales in most parts of the Oklahoma basin. These deposits generally range from 60 m to 600 m in the northern shelf areas and 600 - 1,500 m in the aulacogen (Fay, 1989; Johnson and Cardott, 1992).

During the same period of time (Silurian through Early Devonian), the Ouachita trough received nearly 300 m of shales and sandstones in the Blaylock and Missouri Mountain Formations, followed by at least 180 m of Arkansas Novaculite (Fig. 4, Johnson and Cardott, 1992). The Ouachita trough then subsided quickly and received 2,100 - 4,200 m of Stanley Shale (Arbenz, 1989; Johnson and Cardott, 1992).

2.2.3. Late Paleozoic (333 - 245 m.y. ago)

During the Late Mississippian and Pennsylvanian Oklahoma was affected by major changes. Initially, an episode of Late Mississippian - Early Pennsylvanian epeirogenic uplift throughout most of the state produced a widespread pre-Pennsylvanian unconformity, except in the deep Anadarko and Ardmore basins, where the sedimentation was apparently continuous (Johnson et al., 1988; Elmore et al., 1990). Subsequently, a series of pulses in

the aulacogen and the Ouachita trough during Early through Middle Pennsylvanian time produced, or contributed to, the following geologic events: folding and thrusting of the Ouachita Foldbelt; raising of the Wichita, Criner, Arbuckle, Nemaha, and Ozark uplifts; and increased subsidence of the Anadarko, Ardmore, Marietta, Arkoma, and Hollis basins (Ham and Wilson, 1967; Johnson et al., 1988).

Pennsylvanian strata in Oklahoma consist of shales, sandstones, conglomerates, and limestones, with thicknesses ranging from 3,000 to 4,500 m (McKee et al., 1975). Thin coal beds are found in Desmoinesian strata, mainly in the Arkoma Basin and on the Cherokee Platform (Johnson and Cardott, 1992).

In the Ouachita trough about 1,800 m of flysch sediments were deposited in the Mississippian through Morrowan and Atokan times (Arbenz, 1989). The trough was then destroyed during the Ouachita orogeny (Desmoinesian) with northward thrusting and complex folding of the basin rocks, forming the present-day Ouachita Mountains (Johnson and Cardott, 1992).

Permian rocks are exposed in the northwest corner of the Oklahoma basin (Johnson et al., 1988) and in isolated locations in the southeast part (Hollis basin). They consist of nearly 500 m of alluvial-deltaic and marine sandstones, mudstones, carbonates, and shales.

2.2.4. Post Paleozoic

Post-Paleozoic rocks were not presently found at the sites I studied. However, in other parts of Oklahoma, Johnson and Cardott (1992) described Jurassic, Cretaceous and Tertiary strata in the west; Cretaceous strata in the south east; and Quaternary deposits at many places throughout Oklahoma.

3. THERMAL METHODOLOGY

3.1. Temperature data

The temperature data used in this study were obtained by the American Petroleum Institute from 1926 to 1929 and the results were published in 1930 (McCutchin, 1930). The aim of API research was to study "deep Earth temperatures" and the possible relationship between temperature, geologic structure, and petroleum occurrence (Heald, 1930). Measurements were made with maximum-reading mercury thermometers (Van Orstrand, 1930). McCutchin (1930) reported the results of measurements made in 153 wells, including 119 boreholes in Oklahoma. These measurements and others were later compiled by Spicer (1964). Subsequently, Guffanti and Nathenson (1981) used Spicer's (1964) original data set when they created their geothermal map of the United States (Nathenson and Guffanti, 1987; 1988).

In this study, I use API temperature data from 20 boreholes filled with salt water or rotary mud in Oklahoma which met the following two criteria established by Guffanti and Nathenson (1981): (1) the temperature measurements were made to depths of 600 m or greater while at thermal equilibrium; (2) the temperature-depth profile appeared to be "conductive" (i.e., linear or piecewise linear) without obvious perturbations due to drilling disturbances or groundwater flow. The second criterion is imposed by the fact that gas evolution and expansion in the producing wells (as is frequently encountered in Oklahoma) will cause a temperature drop in the producing reservoir. Even if a test well was shut-in, any neighboring well which has been producing from the same reservoir for some time will lower the temperature of the reservoir rock near the test well due to such effects. The underground migration of fluids such as oil or water also has the potential to

cause temperature disturbances. The quality of the temperature data is discussed later in Sec. 5.1.

The 20 boreholes used in this study cover a central area of the state of Oklahoma, between about 34°N and 37°N latitude and about 96°W and 98°W longitude. They are shown in Figure 13 and in Figures A2, A4, A6, A8, A10, A12, A14, A16, A18, A20, A22, A24, A26, A28, A30, A32, A34, A36, A38, and A40 under the name "Temperature Well" (Appendix A). The exact locations are listed in Table 1. The temperature data were recorded with maximum thermometers at discrete depths (McCutchin, 1930) and are shown in Figures A1a, A3a, A5a, A7a, A9a, A11a, A13a, A15a, A17a, A19a, A21a, A23a, A25a, A27a, A29a, A31a, A33a, A35a, A37a, and A39a (Appendix A). An example of recorded temperatures is presented in Figure 5a.

In order to mitigate the possible influence of the topographic surface and recent climatic changes, temperature measurements in the first 150 m below the topographic surface were not used in this study to calculate thermal gradients or heat flow.

3.2. Thermal gradients

Based on temperature data measured in the 20 boreholes (Figures A1a, A3a, A5a, A7a, A9a, A11a, A13a, A15a, A17a, A19a, A21a, A23a, A25a, A27a, A29a, A31a, A33a, A35a, A37a, and A39a), interval thermal gradients were calculated between consecutive temperature measurements. They are depicted in Figures A1b, A3b, A5b, A7b, A9b, A11b, A13b, A15b, A17b, A19b, A21b, A23b, A25b, A27b, A29b, A31b, A33b, A35b, A37b, and A39b (Appendix A). An example of calculated thermal gradient is shown in Figure 5b. An average thermal gradient was also calculated for each well in which the temperature was measured. The method used to calculate average thermal

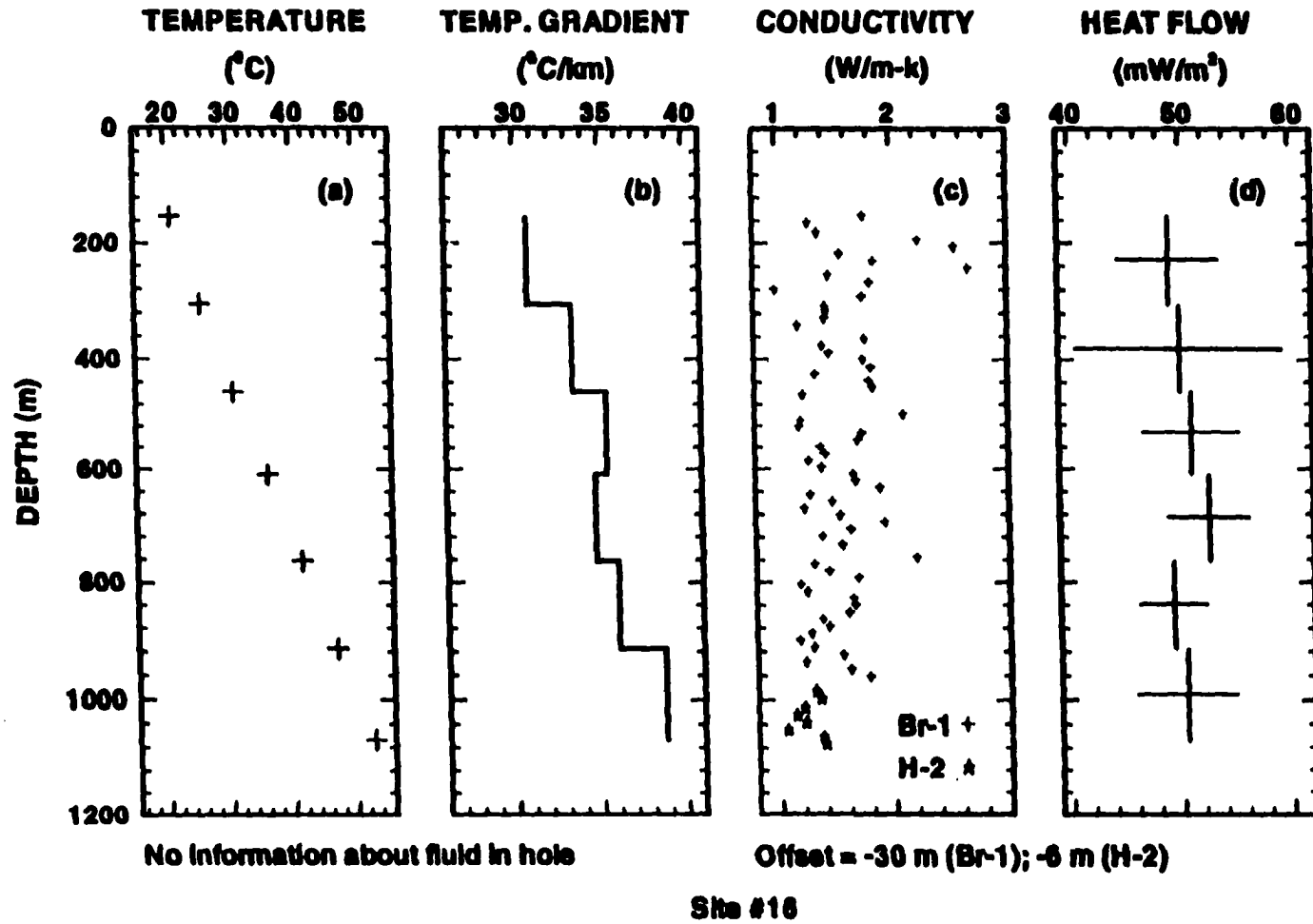


Fig. 5. Temperature (a), thermal gradient (b), thermal conductivity (c), and heat flow (d) distribution with depth at site #16 (for location, see Table 1 and Fig. A32)

BOOCH SAND MAP
(Contours are in meters below sea level)

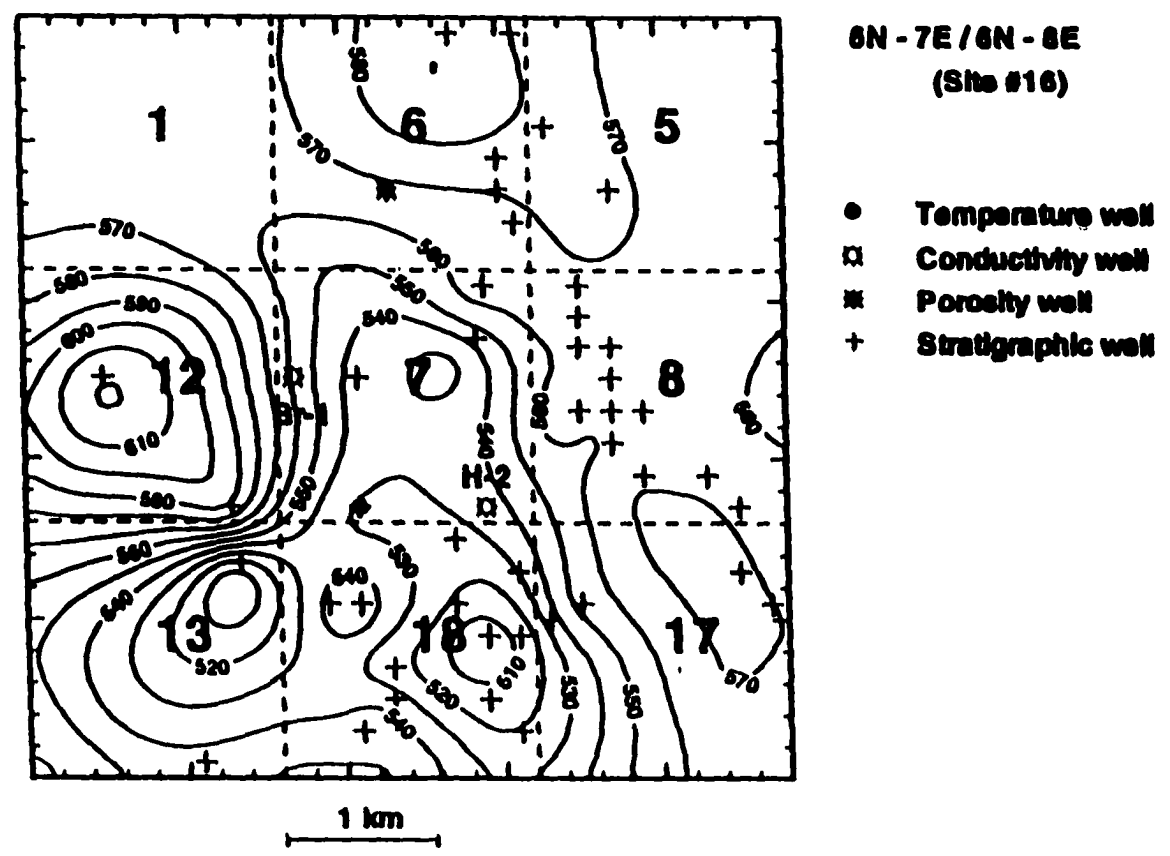


Fig. 6. Stratigraphic map of Booch sand at site #16. The bold numbers in the center of dashed squares represent section numbers of the township and range indicated on the top right side of the figure.

TABLE 1
Well Data Including Geothermal Gradients, In-situ Conductivities, and Surface Heat Flow

Site #	Name of site ¹	Lat. (°N)	Long. (°W)	Section-Township-Range	Elevation (m)	Depth range ² (m)	Thermal gradient (°C/km)	N ³	In-situ conductivity ⁴ (W/m-K)	Heat flow (mW/m ²) ⁵
1	B - 11	36.85	97.22	8-28N-1E	340	157 - 1020	36.63	78	1.11±0.03	41±8
2	110	36.75	97.35	12-26N-2W	310	460 - 875	38.36	52	1.38±0.02	53±11
3	T-1	36.59	97.28	2-24N-1W	293	168 - 860	34.75	74	1.49±0.05	52±10
4	T-16	36.52	97.34	20-24N-1W	305	152 - 831	34.80	76	1.30±0.03	45±9
5	114	36.22	97.41	9-20N-2W	366	152 - 913	31.12	83	1.53±0.05	48±9
6	CU-16	35.94	96.57	16-17N-7E	274	152 - 838	31.77	59	1.96±0.11	62±12
7	OC-2	35.52	97.50	15-12N-3W	357	152 - 1219	17.37	60	1.80±0.23	31±6
8	117	35.47	96.20	36-12N-10E	408	152 - 838	42.11	53	2.04±0.14	86±17
9	OC-1	35.43	97.46	13-11N-3W	382	306 - 1829	21.15	89	1.33±0.03	28±6
10	C-4	35.36	96.45	10-10N-8E	273	152 - 914	41.09	77	1.85±0.09	76±15
11	P-2	35.29	96.32	35-10N-9E	250	212 - 825	42.24	60	1.77±0.10	75±15
12	E-5	35.23	96.72	19-9N-6E	279	152 - 914	30.07	85	1.93±0.06	58±11
13	29	35.18	96.76	10-8N-5E	279	152 - 1067	28.97	91	1.63±0.05	47±9
14	BO-2	35.17	96.67	16-8N-6E	285	152 - 971	29.13	81	1.59±0.06	46±9
15	WE-5	35.17	96.45	15-8N-8E	259	152 - 914	39.01	103	1.64±0.05	64±12
16	128	35.00	96.50	7-6N-8E	258	152 - 1067	34.92	71	1.47±0.04	51±6
17	1	34.91	96.53	14-5N-7E	274	146 - 799	28.72	90	1.53±0.07	44±9
18	SA-1	34.47	97.56	18-1S-3W	290	152 - 686	14.11	86	2.22±0.04	31±6
19	W-6	34.42	98.26	4-2S-10W	315	212 - 599	16.50	77	1.35±0.01	22±4
20	HE-7	34.19	97.39	22-4S-2W	262	160 - 838	17.10	53	2.02±0.07	35±7

¹The well in which the temperature was measured, after Guffanti and Nathenson (1981) notation.

²Depth range for which both temperature and conductivity measurements were available.

³Number of thermal conductivity measurements.

⁴Harmonic mean of measurements after corrections for anisotropy, temperature, and porosity. The error is one standard error of the arithmetic mean.

⁵The error is one standard error of the arithmetic mean.

gradients was a least-squares linear regression of the temperature measurements below 150 m depth. Numerical values of average thermal gradients are given in Table 1.

3.2.1 Thermal gradient corrections

The topography of central Oklahoma where the 20 wells are located is nearly flat, with elevation above sea level ranging from 250 m (site #11) to 408 m (site #8). The topographic gradient for the 20 sites is less than 3%, based on interpolation of contour lines of topographic maps.

The correction for heat flow through a surface which slopes less than 3% is less than 1% at depths greater than 20 m (Lachenbruch, 1969). Therefore, no topographic correction was applied to calculated thermal gradients or estimated heat flows.

3.3. Thermal conductivity

Thermal conductivity measurements were made with a divided-bar apparatus (Birch, 1950; Beck, 1957; Roy et al., 1981; Sass et al., 1984) using the cell technique of Sass et al. (1971), which allows the determination of the thermal conductivity of a randomly oriented aggregate of rock matrix at room temperature (λ_{ag}). To estimate λ_{pr} , the *in situ* thermal conductivity of a porous rock perpendicular to bedding, corrections must be made for the effects of anisotropy, temperature, and porosity.

I made 1,498 thermal conductivity measurements (Table 2) on drill cuttings from 28 wells (locations indicated in Table 2 and shown in Figures A2, A4, A6, A8, A10, A12, A14, A16, A18, A20, A22, A24, A26, A28, A30, A32, A34, A36, A38, and A40 (Appendix A) under the name "Conductivity Well"). Some sites (#3, Fig. A5c; # 6, Fig. A11c; #9, Fig. A17c; #12, Fig. A23c; #15, Fig.

TABLE 2
Thermal Conductivity Measurements

Site #	Well name	Section-Township-Range	Depth interval(s) (m)	L ¹	Offset ² (m)	N ³	In-situ conductivity ⁴ (W/m-K)
1	Herman #3	8-28N-16	157 - 1020	1000	+ 9	78	1.11±0.03
2	McCulloch #1	12-26N-2W	460 - 1131	652	+ 47	52	1.38±0.02
3	McAninch #1 (M-1)	1-24N-1W	168 -1033; 1310 -1478	1848	- 28	48	1.18±0.03
	L. Shower #93 (L-93)	2-24N-1W	1046 - 1290	1040	+ 28	26	1.80±0.07
4	Gravel #1	20-24N-1W	105 - 831	565	- 6	76	1.30±0.03
5	Providence #1	4-20N-2W	148 - 913	2348	- 4	83	1.53±0.05
6	Stewart #1 (S-1)	16-17N-7E	151 - 398	187	+ 1	23	2.10±0.10
	Dacon #37 (D-37)	16-17N-7E	414 - 853	345	+ 2	36	1.82±0.12
7	Thompson #1	15-12N-3W	111 - 1224	10	0	60	1.80±0.23
8	Skeleton #2	30-12N-10E	131 - 850	1826	+ 5	53	2.04±0.14
9	Wheeler #4 (W-4)	13-11N-3W	306 - 1175	870	+ 32	54	1.37±0.04
	Wheeler #2 (W-2)	13-11N-3W	1190 - 1832	783	+ 25	35	1.26±0.05
10	Johnson #1	10-10N-8E	105 - 922	652	+ 26	77	1.85±0.10
11	Williams #3	34-10N-9E	212 - 825	1783	- 16	60	1.77±0.10
12	Fixico #5 (F-5)	20-9N-6E	147 - 240	1478	+ 8	11	2.50±0.03
	Chowing #7 (C-7)	19-9N-6E	252 - 921	565	+ 5	74	1.87±0.05
13	Tiger #3	3-8N-5E	145 - 1081	2087	- 3	91	1.63±0.05
14	Livingstone #13	15-8N-6E	148 - 971	739	+ 37	81	1.59±0.06
15	Beard #1 (B-1)	21-8N-8E	151 - 233; 745 - 918	1783	- 4	37	1.56±0.07
	Harper #1 (H-1)	15-8N-8E	238 - 734	434	- 1	66	1.68±0.07
16	Bryant #1 (Br-1)	7-6N-8E	151 - 961	935	- 30	63	1.68±0.07
	Holotka #2 (H-2)	7-6N-8E	985 - 1072	826	- 6	8	1.25±0.03
17	Cully #2	13-5N-7E	142 - 819	870	+ 14	90	1.53±0.07
18	Edge Hardin #11 (EH-11)	18-1S-3W	152 - 476	760	- 82	53	2.14±0.05
	Hardin Heirs #2 (HH-2)	18-1S-3W	488 - 695	870	+ 32	33	2.40±0.05

19	Beard #1	32-1S-10W	212 - 599	1783	0	77	1.35±0.01
20	Dillard #115	22-4S-2W	160 -844	304	- 59	53	2.02±0.07

¹Distance from the temperature well (m). The range is 10 - 2348 m; average distance is 1013 ± 23 m. Error is one standard error of the arithmetic mean.

²Stratigraphic offset above (+) or below (-) the temperature well. Range is between -82 m and + 32 m; average is + 4.4 ± 0.88 m. Error is one standard error of the arithmetic mean.

³Number of thermal conductivity measurements.

⁴Harmonic mean of measurements of all intervals after corrections for anisotropy, temperature, and porosity. The error is one standard error of the arithmetic mean. The average thermal conductivity for 1498 measurements is 1.68 ± 0.07 W/m-K (range 0.90 - 6.10 W/m-K).

A29c; #16, Fig. A31c; and #18, Fig. A35c) required more than one "conductivity" well in order to sample the whole depth of the "temperature" well.

Drill cuttings and core samples were not available from the wells in which the API temperature measurements were made. I therefore utilized measurements on rock samples from the closest available well. All of the rock samples used for thermal conductivity measurements in this study came from the Core Library of the Oklahoma Geological Survey in Norman. Searching carefully the catalog for core samples to be used in this study for thermal conductivity or heat production measurements, I found that very few core samples were available and the existing ones covered limited depth intervals. Therefore, drill cuttings were used instead of core samples for thermal conductivity measurements in this study.

The horizontal distance between "temperature" well and "conductivity" well varies from 10 m (site #7, Fig. A14) to 2,348 m (site #5, Fig. A10) (Table 2, see also Figures A2, A4, A6, A8, A10, A12, A14, A16, A18, A20, A22, A24, A26, A28, A30, A32, A34, A36, A38, and A40 (Appendix A). The average horizontal distance between the "temperature" well and "conductivity" well was 1,013 m.

The sampling strategy was intended to provide as uniform as possible coverage of all lithologies found in a well. I usually sampled every 20 ft (~6 m) of depth for wells with highly variable lithology, and every 30 - 40 ft (~9 - 12 m) for wells with uniform lithology over long depths. The sampling intervals were chosen after tests have shown that thermal-conductivity average values and their associated errors do not change significantly with decreasing sampling intervals.

Because the wells in which the temperature and thermal conductivity

measurements were made were not at the same stratigraphic level or elevation, it was necessary to correct for the stratigraphic offset. This was done by constructing a correlation map for each site (Figures A2, A4, A6, A8, A10, A12, A14, A16, A18, A20, A22, A24, A26, A28, A30, A32, A34, A36, A38, and A40 (Appendix A). An example is shown in Figure 6. Stratigraphic maps were constructed by using formation tops (as indicated by logs) found in the completion cards on file at the University of Oklahoma Geology Library and Core and Sample Library in Norman.

There is a vertical offset between the "temperature" well and the "conductivity" well (Figures A2, A4, A6, A8, A10, A12, A14, A16, A18, A20, A22, A24, A26, A28, A30, A32, A34, A36, A38, and A40 (Appendix A). Figures 5c, A1c, A3c, A5c, A7c, A9c, A11c, A13c, A15c, A17c, A19c, A21c, A23c, A25c, A27c, A29c, A31c, A33c, A35c, A37c, and A39c (Appendix A) show the determined conductivity values and, under each panel, the offset value is given (positive offset values mean that the "temperature" well is at a higher stratigraphic elevation than "conductivity" well, while negative offset values mean that the "temperature" well has a lower stratigraphic elevation than the "conductivity" well). The stratigraphic offset ranges between -82 m (site #18, Fig. A36) and +32 m (site #9, Fig. A18) (Table 2). The stratigraphic offsets were used in calculating heat flow intervals by matching thermal gradients to corresponding stratigraphic intervals with thermal conductivity measurements.

There is an inherent uncertainty in the stratigraphic maps due to diversity of names used to define the same stratigraphic formation. Depending on time the well was drilled and the company that performed it, the names I found, even for close locations, were sometimes variable. For example, the Layton sand is described by some drilling company geologists as

having two or more horizons. In some cases, the name of an upper or lower horizon is replaced by another name, which has a local use. Some horizons, of no interest for oil or gas, have been omitted from some scout cards. In all such situations, I tried to be very consistent to avoid misnaming. Overcoming this difficulty and obtaining the most accurate stratigraphic map possible was due to using the correlation charts of Paleozoic formations kindly provided by Dr. Robert Fay from Oklahoma Geological Survey (pers. comm., 1996).

3.3.1. Anisotropy correction

The relevant thermal conductivity for the estimation of heat flow is usually the thermal conductivity perpendicular to bedding, but many sedimentary rocks are highly anisotropic, especially shales. The *in situ* thermal conductivity of shales parallel to bedding (λ_{xy}) may be two or three times higher than that perpendicular to bedding (λ_z) (Deming , 1994a). Rock fragments that are more or less randomly oriented in the cell is likely to give a conductivity that is intermediate between λ_{xy} and λ_z . I made an anisotropy correction using the method of Deming (1994a), calibrated by measurements on Pennsylvanian age sedimentary rocks in north-central Oklahoma (determined by needle-probe measurements on cores in both perpendicular and longitudinal directions and reported by Deming and Borel, 1995). Matrix conductivity perpendicular to bedding (λ_z) was calculated as

$$\lambda_z = \exp \{[\log_e (\lambda_{ag}) - 0.6145] / 0.5568\} \quad (1)$$

for $1.87 < \lambda_{ag} < 4.0$ W/m-K. For $\lambda_{ag} > 4.0$ W/m-K no correction is needed, and for $\lambda_{ag} < 1.87$ W/m-K, λ_z was taken as 1.0 W/m-K.

3.3.2. Temperature correction

In a rock aggregate filled with water, both matrix and water conductivity are functions of temperature. Generally, matrix conductivity tends to decrease with increasing temperature for rocks whose matrix conductivity at room temperature (22°C) is higher than about 2.0 W/m-K. However, the opposite tends to be true for rocks whose matrix conductivity at room temperature (22°C) is lower than 2.0 W/m-K: their matrix conductivity tends to increase with increasing temperature (Birch and Clark, 1940). The temperature behavior of these rocks is not so well known as for crystalline rocks for which a more extensive data base exists. Unfortunately, nearly all measurements made with the cell technique and reported in the literature are on sedimentary rocks, many of which tend to have relatively low matrix conductivities (< 2.0 W/m-K) at room temperature (22°C). The temperature correction applied was that recommended by Sekiguchi (1984):

$$\lambda_T = \lambda_m + \{ [T_0 - T_m / (T_m - T_0)] \times [\lambda_z - \lambda_m] \times [(1/T) - (1/T_m)] \} \quad (2)$$

where T is the estimated *in situ* temperature in kelvin, λ_T is the estimated matrix conductivity perpendicular to bedding at *in situ* temperature T , λ_m and T_m are the thermal conductivity and absolute temperature (kelvin) at what Sekiguchi (1984, p. 75) refers to as "the assumed point", and λ_z is the matrix thermal conductivity perpendicular to bedding at room temperature T_0 . The values suggested by Sekiguchi (1984, p. 75) for λ_m and T_m are 1.8418 W/m-K and 1473 K, respectively. For sedimentary rocks over a range of temperatures corresponding to *in situ* temperatures in the Arkoma basin and the Oklahoma Platform (~20 - 140°C), it was found (Lee et al., 1996) that the

Sekiguchi (1984) method matched available experimental temperature/thermal conductivity data better than alternative corrections (Zoth and Haenel, 1988; Sass et al., 1992), especially for rocks with conductivities at 25°C lower than 2.0 W/m-K.

For the temperature range found in wells studied here 16.6°C (at 152 m, site #9, Fig. A17a) to 56.8°C (at 991 m, site #11, Fig. A21a) the temperature correction is about $\pm 2\%$.

3.3.3. Porosity correction

The cell measurements yield only an estimate of the matrix conductivity. The *in situ* conductivity of a rock depends not only upon the matrix conductivity, but also upon the thermal conductivity of the fluid saturating its pores. Therefore, in order to estimate the *in situ* conductivity one must have some estimate of *in situ* porosity. I used density logs to estimate *in situ* porosities for the closest possible site to the conductivity wells. The porosities obtained from density logs were calibrated by using matrix density measurements on drill cuttings used for thermal conductivity measurements.

The "porosity" wells (used to estimate *in situ* porosity necessary for porosity correction, see eq. 3) are listed in Table 3 and are shown in Figures A2, A4, A6, A8, A10, A12, A14, A16, A18, A20, A22, A24, A26, A28, A30, A32, A34, A36, A38, and A40 (Appendix A) under the name "Porosity Well". The depth intervals available for porosity determination vary between 16 m (site #20) and 2224 m (site #7). The length of depth intervals used for porosity logging ranges 290 m (site #1) - 1311 m (site #9); the average length of depth intervals is 651 m. The horizontal distance between the "conductivity" well(s) and "porosity" well range from 434 m (site #7, Fig. A14) to 3,826 m (site #3,

TABLE 3
Porosity Estimates

Site #	Well name	Section-Township-Range	Elevation (m)	Depth interval (m)	L ¹	Offset ² (m)	Average porosity
1	Sims #1	7-28N-1E	337	37 - 327	1435	+ 5	0.17
2	North #15	12-26N-2W	315	518 - 945	1087	- 70	0.09
3	Christa #1	10-24N-1W	320	214 - 820	3239 (L-93) 3826 (M-1)	- 35 + 21	0.13
4	Carter #1-B	20-24N-1W	330	118 - 471	478	+ 2	0.21
5	Cox #2	9-20N-2W	367	973 - 1585	1870	- 2	0.04
6	Shamrock Royalty-Tract 3 #W-22	21-17N-7E	287	427 - 850	739 (S-1) 1130 (D-37)	- 28 - 29	0.05
7	Henderson #1-14	14-12N-3W	343	1538 - 2224	434	- 1	0.02
8	Burnett #1-36	36-12N-10E	292	618 - 1157	2261	- 1	0.05
9	Jennings "A" #4	13-11N-3W	381	332 - 1643	740 (W-4) 739 (W-2)	- 38 - 31	0.20
10	Standon Little #6	10-10N-8E	276	454 - 1249	1000	- 47	0.07
11	Thomas Ryan #1-35	35-10N-9E	248	115 - 1111	1435	+ 1	0.08
12	Nichols #6	19-9N-6E	286	792 - 1331	1304 (F-5) 957 (C-7)	+ 5 + 8	0.08
13	Hurst #1	10-8N-5E	275	79 - 1310	2304	- 2	0.14
14	Goforth #24	15-8N-6E	283	334 - 959	1000	- 9	0.15
15	Chamblee #1	15-8N-8E	261	593 - 1226	1630 (B-1) 652 (H-1)	+ 4 - 2	0.07
16	Beller Hyde #6-A	6-6N-8E	278	298 - 945	1391 (Br-1) 2174 (H-2)	- 8 - 31	0.08
17	Katy #1	14-5N-7E	287	287 - 613	1674	- 22	0.11
18	County Line Unit #11- 2B	18-1S-3W	284	395 - 1127	587 (EH-11) 1000 (HH-2)	+ 45 - 71	0.20

19	Freeman #5	5-2S-10W	310	457 - 767	1217	+ 2	0.15
20	Hewitt unit #22-4203	22-4S-2W	277	16 - 912	1000	+ 114	0.21

¹Distance in m from the well with conductivity measurements (abbreviations between parentheses refer to the conductivity wells from Table 2). The range is 434 - 3826 m; the average distance between the conductivity well and the porosity well is 1382 ± 30 m. Error is one standard error of the arithmetic mean.

²Stratigraphic offset above (+) or below (-) the conductivity well(s). The range is between -70 m and + 114 m; the average offset is $- 8 \pm 1$ m. Error is one standard error of the arithmetic mean.

Porosity has been determined from density logs (gamma - gamma, compensated densilog) using the matrix densities from conductivity measurements as a constraint. The range of porosities is between 0.02 and 0.21; the average porosity for the 20 wells investigated is 0.12 ± 0.003 .

Fig. A6); the average horizontal distance is 1,382 m.

The "conductivity" and "porosity" wells are not, in general, at the same stratigraphic level. The stratigraphic offset is positive (+) when the "porosity" well is stratigraphically higher than "conductivity" well and is negative (-) when the "porosity" well is stratigraphically lower than "conductivity" well. The stratigraphic offset varies between -70 m (site #2, Fig. A4) and +114 m (site #20, Fig. A40); the average stratigraphic offset of "porosity" wells with respect to "conductivity" wells is -81 m (Table 3). The stratigraphic offset values were used to adjust the porosities of "conductivity" well strata. For each site, porosities determined from density logs were constrained by using matrix densities obtained after thermal conductivity measurements.

The average porosities for the 20 sites studied vary from 0.02 (site #7) to 0.21 (site # 20); the average porosity value for all 20 sites is 0.12. The average porosity for Permian samples is 0.21; for Pennsylvanian samples is 0.11; for Mississippian samples is 0.06; for Devonian sample is 0.04; and for Ordovician samples is 0.01 (Table 4). Porosity decreases with burial depth and depends upon lithology.

Porosity corrections were made using a geometric mean model. *In situ* conductivity (λ_{pr}) was estimated as

$$\lambda_{pr} = (\lambda_T)^{1 - \phi} (\lambda_w)^\phi \quad (3)$$

where λ_T is the estimated matrix conductivity perpendicular to bedding at *in situ* temperature T, λ_w is the estimated conductivity of pore fluid (water) at *in situ* temperature T, and ϕ is the average formation porosity. For the porosity range found in the wells I studied (0.02 - 0.21; average is 0.12), λ_{pr} is decreased by comparison with λ_T by 3% - 23% (average 14%).

TABLE 4
Thermal Conductivities in central Oklahoma

Geologic unit	Lithology	N ¹	In situ conductivity ² (W/m-K)	Matrix conductivity ³ (W/m-K)	Porosity ⁴
Permian	red sandstone	107	1.49±0.03	1.63±0.04	0.21
Pennsylvanian	shale	1369	1.67±0.01	1.84±0.02	0.11
Mississippian	limestone	16	1.62±0.08	1.78±0.08	0.06
Devonian	shale	1	1.47	1.51	0.04
Ordovician	shale	5	1.34±0.07	1.50±0.06	0.01

¹Number of measurements.

²Harmonic mean of measurements after corrections for anisotropy, temperature, and porosity. The error is one standard error of the arithmetic mean.

³Harmonic mean perpendicular to bedding at 22°C. The error is one standard error of the arithmetic mean.

⁴Estimated from density logs and matrix density measurements.

The conductivity of the saturating pore fluid (λ_w) was assumed to be the same as pure water and was calculated after Touloukian et al., 1970 as:

$$\lambda_w(T) = 0.5648 + 1.878 \times 10^{-3}T - 7.231 \times 10^{-6}T^2, \text{ for } 0 \leq T \leq 137 \text{ }^\circ\text{C} \quad (4)$$

For the temperature range found in the wells I studied, λ_w varies between 0.594 W/m-K (for $T = 16.6^\circ\text{C}$) and 0.648 W/m-K (for $T = 56.8^\circ\text{C}$).

3.4. Heat production

Few heat production measurements have been made on basement rocks in Oklahoma, mainly because nearly the whole state is covered by large thicknesses (as much as 12 km in the Anadarko Basin) of sedimentary rocks (Roy et al., 1968; Borel, 1995; Lee et al., 1996). A search of the core library of the Oklahoma Geological Survey has shown that very few cores of Oklahoma basement are available; heat production in the four existing ones were measured by Borel (1995). Therefore, I estimated the heat production of the basement rocks of Oklahoma in an indirect way, using an empirical relationship between gamma ray values, measured in wells that penetrated the basement, and heat generated in those rocks (Bücker and Rybach, 1996):

$$A = 0.0158 (\gamma - 0.8) \quad (5)$$

where A is heat production in $\mu\text{W}/\text{m}^3$ and γ is the gamma ray log reading in API units. The above relationship is considered to be valid for an interval of A ranging 0.03 - 7.0 $\mu\text{W}/\text{m}^3$ within an accuracy of $\pm 10\%$ (Bücker and Rybach, 1996).

3.5. Heat flow

Several methods can be used to combine the temperature and conductivity data to give heat flow. Heat flow estimates in this study were obtained by the so-called "interval method". This procedure may reveal disturbances by water flow and other departures from an equilibrium conductive system. Variations of apparent heat flow due to conductivity sampling errors are also sometimes revealed. In other words, the "interval method" is very powerful for showing the individual characteristics of any data set, for detecting disturbances, or for verifying the quality of measurements (Jessop, 1990).

Heat flow at each site was estimated as follows:

(a) Heat flow intervals (Figures A1d, A3d, A5d, A7d, A9d, A11d, A13d, A15d, A17d, A19d, A21d, A23d, A25d, A27d, A29d, A31d, A33d, A35d, A37d, and A39d) by multiplying thermal gradients (Figures A1b, A3b, A5b, A7b, A9b, A11b, A13b, A15b, A17b, A19b, A21b, A23b, A25b, A27b, A29b, A31b, A33b, A35b, A37b, and A39b) by *in situ* thermal conductivities (Figures A1c, A3c, A5c, A7c, A9c, A11c, A13c, A15c, A17c, A19c, A21c, A23c, A25c, A27c, A29c, A31c, A33c, A35c, A37c, and A39c) (Appendix A) from the same depth interval as for thermal gradients. An example is shown in Figure 5d;

(b) Average heat flow for a site (Table 1), by multiplying the average thermal gradient (obtained by a simple linear regression based on least squares) by harmonic mean of all *in situ* thermal conductivities measured in the "conductivity" well(s). The resulting heat flow values are listed in the last column of Table 1 and are shown in Figure 13.

4. RESULTS

4.1. Thermal gradients

For each site, interval thermal gradients (Figures A1b, A3b, A5b, A7b, A9b, A11b, A13b, A15b, A17b, A19b, A21b, A23b, A25b, A27b, A29b, A31b, A33b, A35b, A37b, and A39b, Appendix A) and an average thermal gradient (Table 1) were calculated as explained in Sec. 3.2. The minimum interval thermal gradient, maximum interval thermal gradient, and average thermal gradient for each site are given in Appendix B.

The mean of 20 average thermal gradients is $30.50^{\circ}\text{C}/\text{km}$. In general, thermal gradients increase from SW ($14.11^{\circ}\text{C}/\text{km}$, site #18) to NE ($42.24^{\circ}\text{C}/\text{km}$, site #11). Other geothermal maps of Oklahoma show the same trend. Thus, Gilarranz (1964) and Schoepel and Gilarranz (1966) indicate a variation of geothermal gradients from $14.4^{\circ}\text{C}/\text{km}$ in SW to $25.5^{\circ}\text{C}/\text{km}$ in NE; Cheung (1978, 1979), and Harrison et al. (1983) show that thermal gradients in Oklahoma vary from $19.9^{\circ}\text{C}/\text{km}$ in SW to $41.5^{\circ}\text{C}/\text{km}$ in NE. On the geothermal gradient map of the conterminous U. S., Nathenson and Guffanti (1988), showed the southwestern part of Oklahoma outlined by the $25^{\circ}\text{C}/\text{km}$ isoline and two other areas (north central and southeastern) delineated by a $35^{\circ}\text{C}/\text{km}$ isoline. Thus, my average value of $30.5^{\circ}\text{C}/\text{km}$ falls between those values.

4.2. Thermal conductivity

Using the method described in Sec. 3.3, I made 1,498 thermal conductivity measurements (Table 1, Table 2, and Table 4). Thermal conductivity variation with depth is shown for each site in Figures A1c, A3c, A5c, A7c, A9c, A11c, A13c, A15c, A17c, A19c, A21c, A23c, A25c, A27c, A29c, A31c, A33c, A35c, A37c, and A39c (Appendix A). Variation of thermal

conductivity with both depth and geologic ages for each site is shown in Figure 7 (for sites #1, #2, #3, and #4), Figure 8 (for sites #5, #6, #7, and #8), Figure 9 (for sites #9, #10, #11, and #12), Figure 10 (for sites #13, #14, #15, and #16) and Figure 11 (for sites #17, #18, #19, and #20).

In order to cover the whole temperature interval, for some sites (#3, #9, #12, #15, #16, and #18) drill cuttings from two wells were used for thermal conductivity measurements. These sites are shown in Figures A5c (for site #3), A11c (for site #6), A17c (for site #9), A23c (for site #12), A29c (for site #15), A31c (for site #16), and A35c (for site #18) by different abbreviations and symbols.

After corrections for anisotropy, temperature, and porosity, the range of 1,498 *in situ* thermal conductivity measurements was 0.90 - 6.10 W/m-K. The average *in situ* thermal conductivity for 1,498 measurements was 1.68 ± 0.07 W/m-K (Table 2). The error specified here and throughout the text is one standard error of the arithmetic mean, unless otherwise specified.

A short presentation of thermal conductivity data for each site is given in Appendix C. Table 4 and Figures 7, 8, 9, 10 and 11 show the thermal conductivity distribution with age for 20 sites studied in central Oklahoma.

107 samples of Permian age, represented mainly by red sandstone and shale, yielded an average *in situ* thermal-conductivity of 1.49 ± 0.03 W/m-K and an average matrix thermal-conductivity of 1.63 ± 0.04 W/m-K.

1369 samples of Pennsylvanian age, represented mainly by shale of different colors (gray, black, red) and small amounts of limestone, yielded an average *in situ* thermal conductivity of 1.67 ± 0.01 W/m-K and an average matrix thermal conductivity of 1.84 ± 0.02 W/m-K.

16 samples of Mississippian age, represented mainly by shale of different colors (gray, black, red) and small amounts of limestone, yielded an

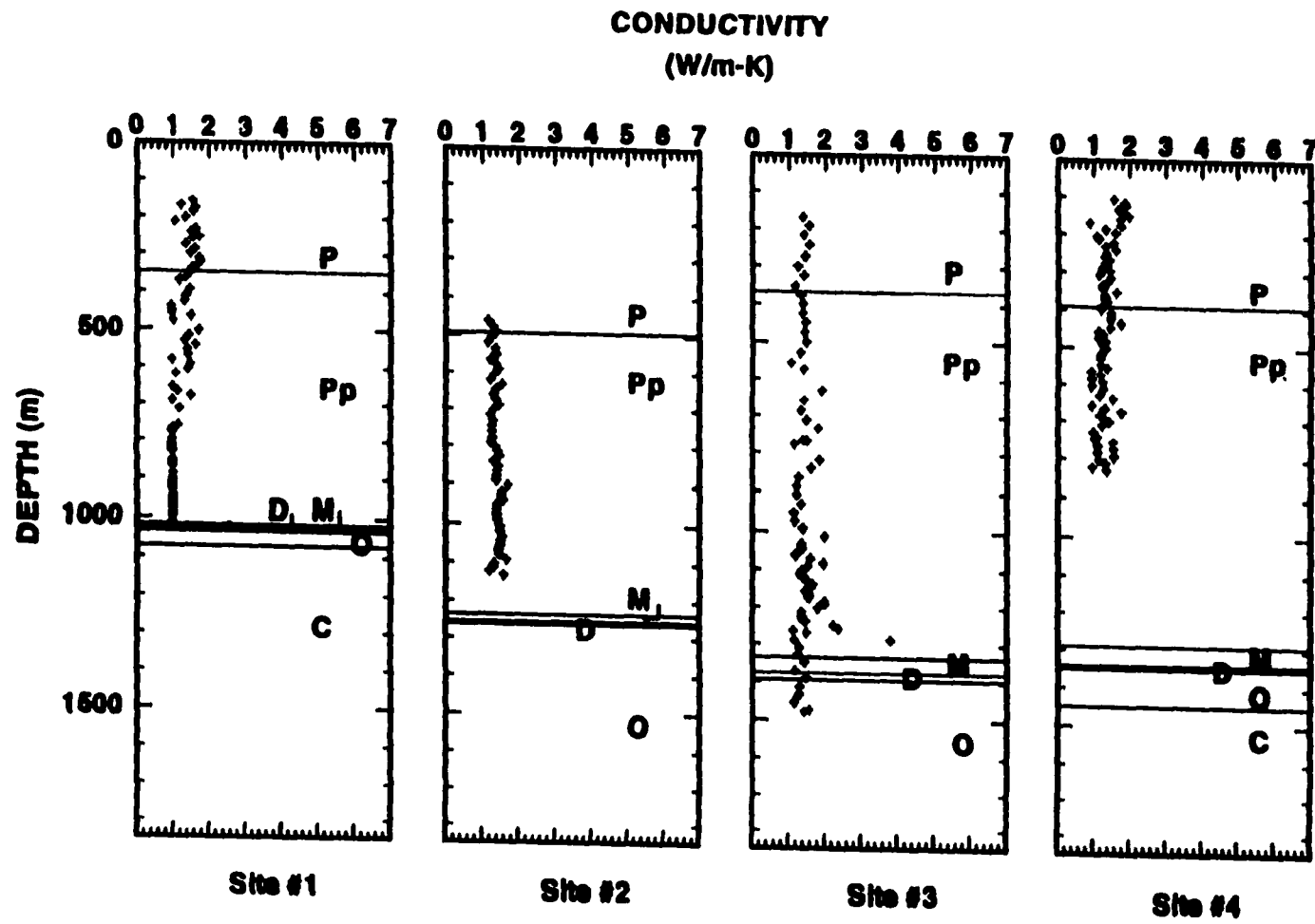


Fig. 7. Thermal conductivity distribution with depth and geologic ages at sites #1, #2, #3, and #4 (for location, see Table 2 and Figures A2, A4, A6, and A8). P - Permian; P_p - Pennsylvanian; M - Mississippian; D - Devonian; S - Silurian; O - Ordovician; C - Cambrian.

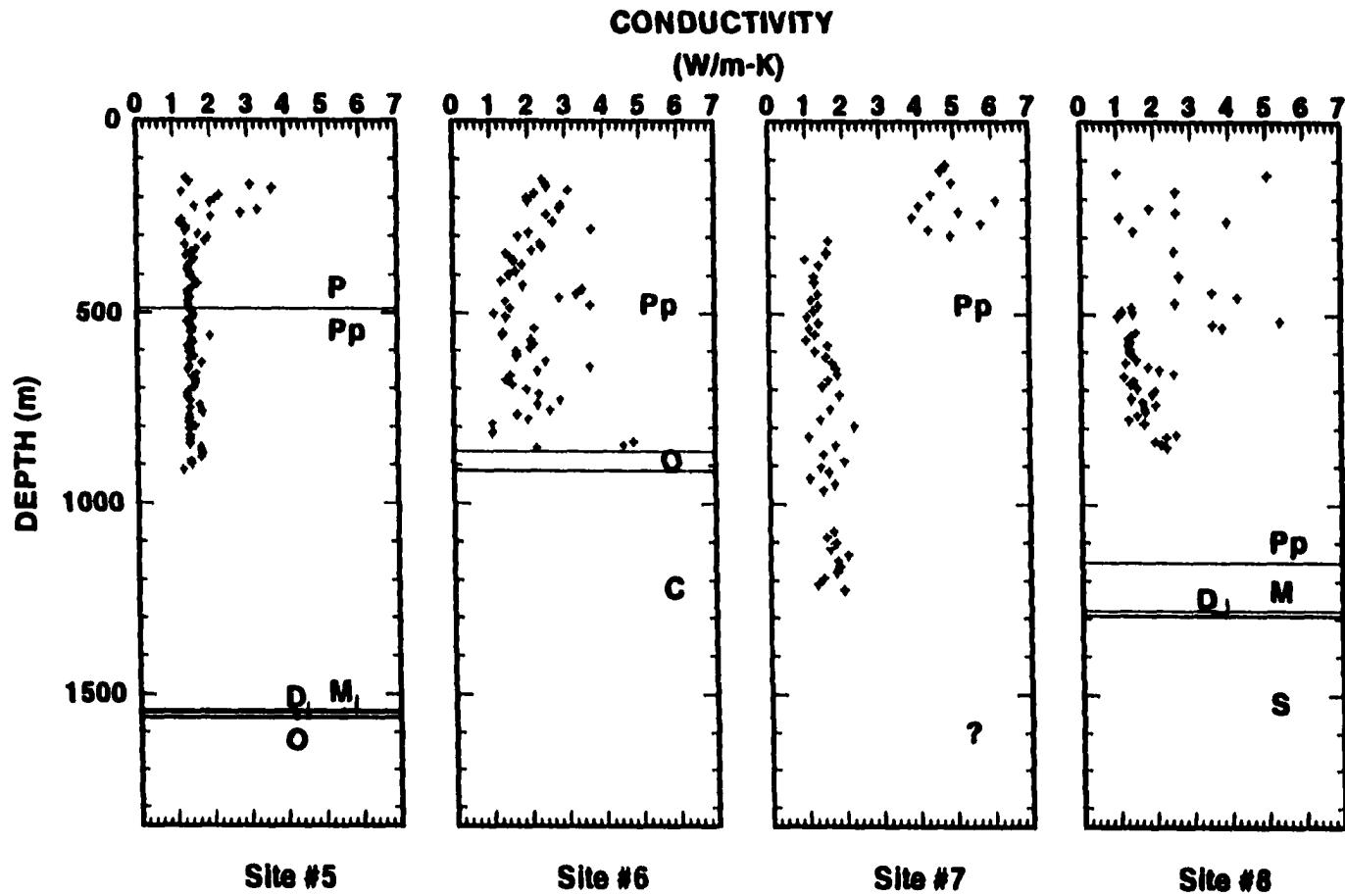


Fig. 8. Thermal conductivity distribution with depth and geologic ages at sites #5, #6, #7, and #8 (for location, see Table 2 and Figures A10, A12, A14, and A16). P - Permian; Pp - Pennsylvanian; M - Mississippian; D - Devonian; S - Silurian; O - Ordovician; C - Cambrian.

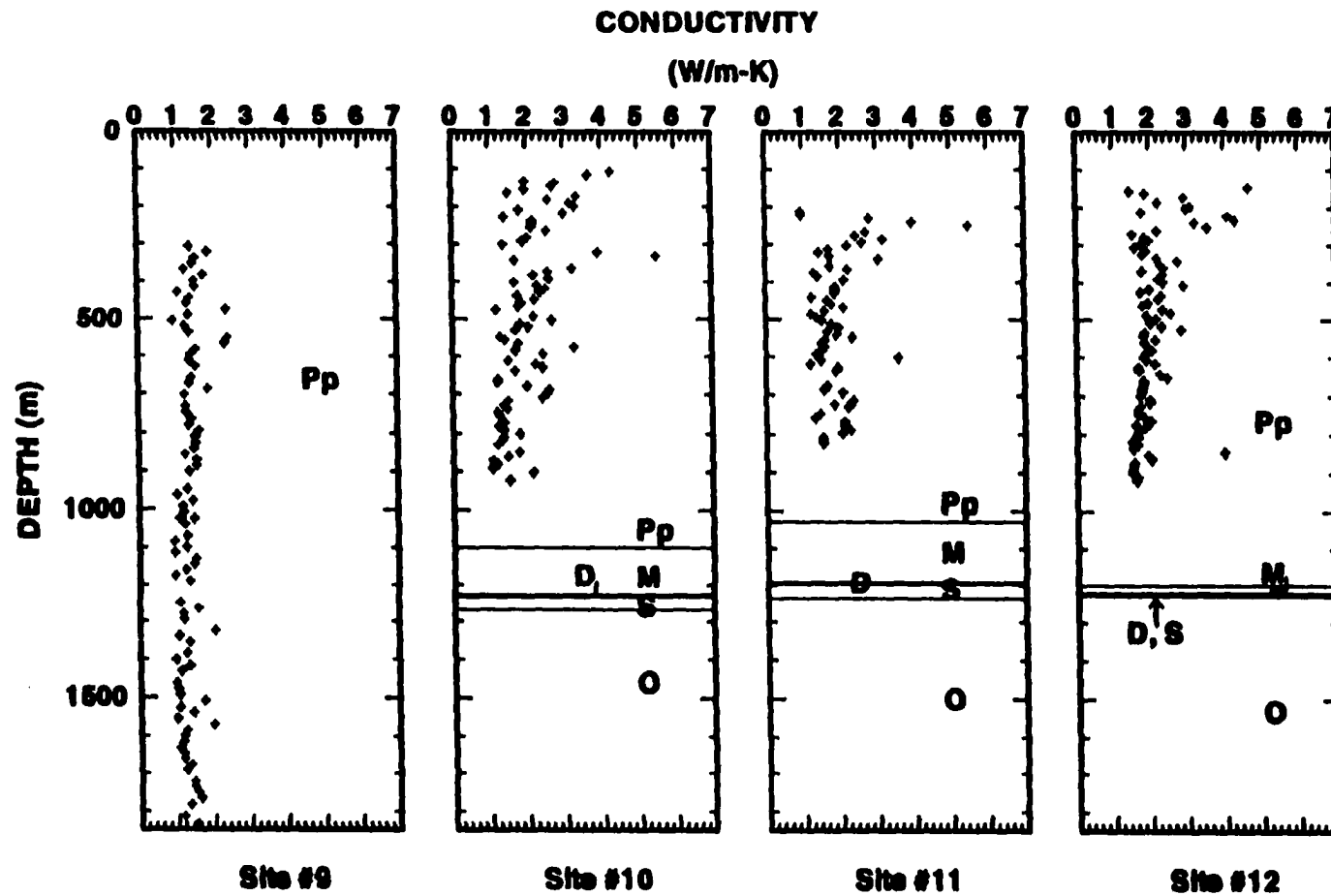


Fig. 9. Thermal conductivity distribution with depth and geologic ages at sites #9, #10, #11, and #12 (for location, see Table 2 and Figures A18, A20, A22, and A24). Pp - Pennsylvanian; M - Mississippian; D - Devonian; S - Silurian; O - Ordovician.

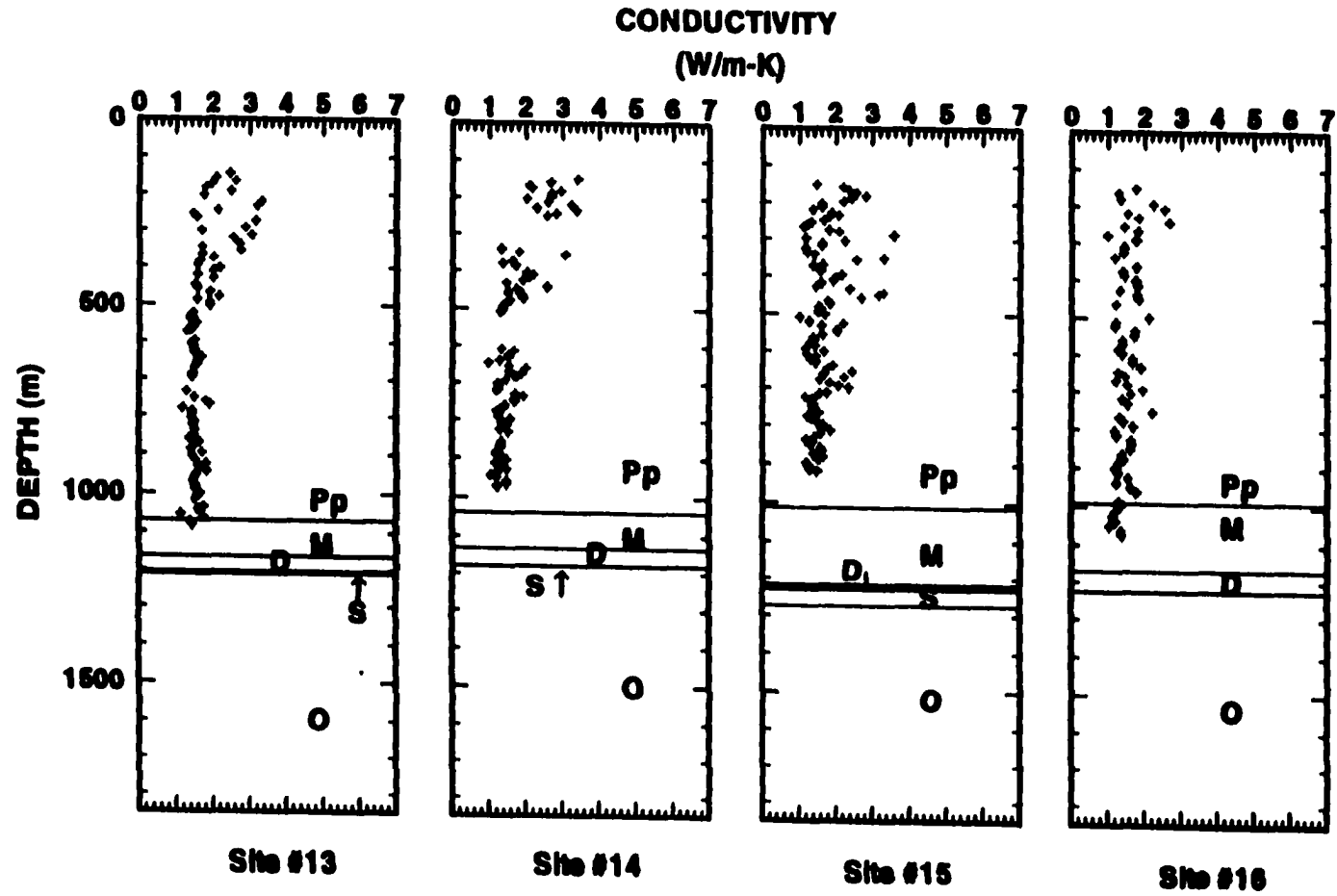


Fig. 10. Thermal conductivity distribution with depth and geologic ages at sites #13, #14, #15, and #16 (for location, see Table 2 and Figures A26, A28, A30, and A32). Pp - Pennsylvanian; M - Mississippian; D - Devonian; S - Silurian; O - Ordovician.

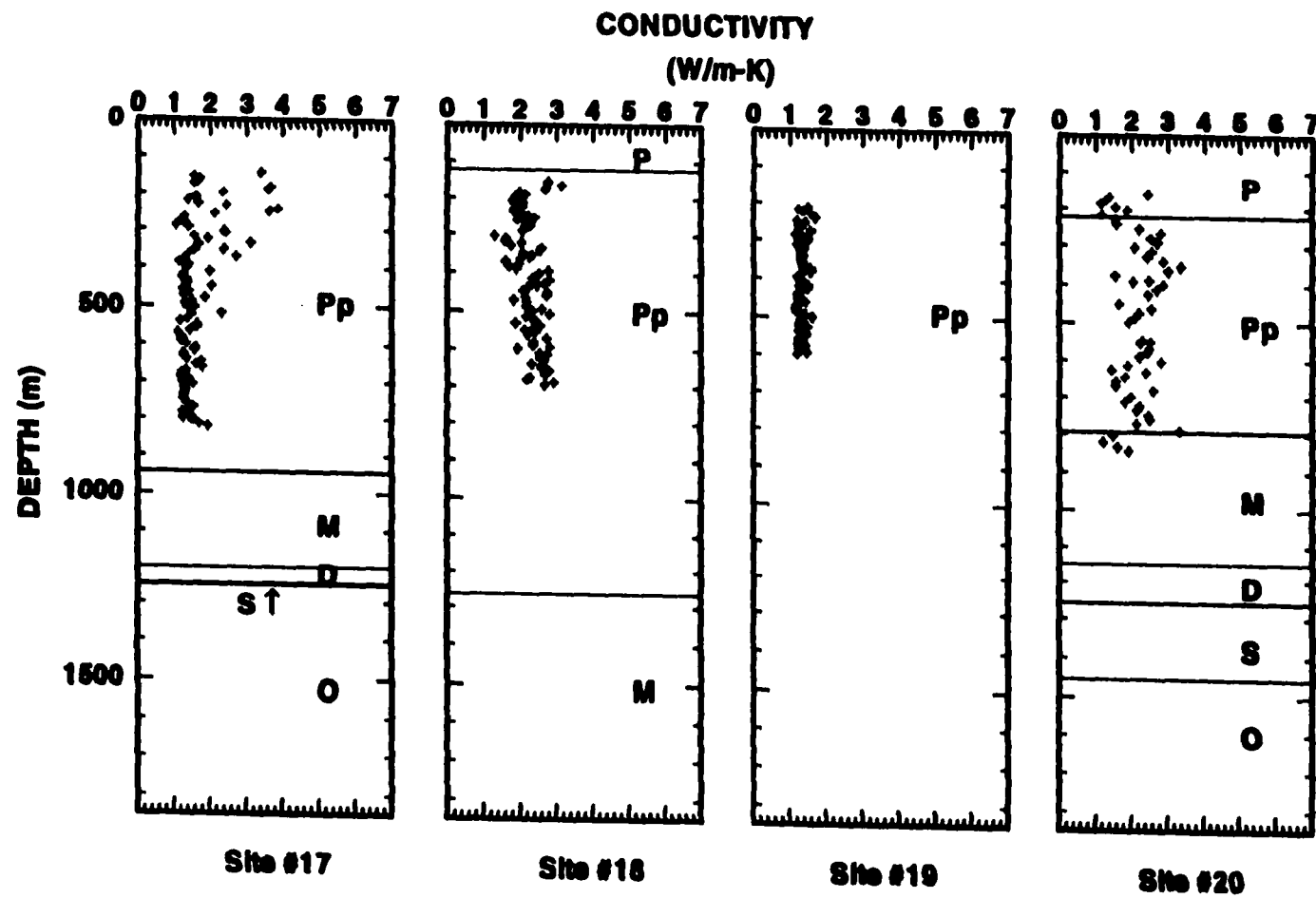


Fig. 11. Thermal conductivity distribution with depth and geologic ages at sites #17, #18, #19, and #20 (for location, see Table 2 and Figures A34, A36, A38, and A40). P - Permian; Pp - Pennsylvanian; M - Mississippian; D - Devonian; S - Silurian; O - Ordovician.

average *in situ* thermal conductivity of 1.62 ± 0.08 W/m-K and an average matrix thermal conductivity of 1.78 ± 0.08 W/m-K.

There is only one sample of Devonian age, a piece of (probably) Woodford shale, that has an *in situ* thermal conductivity of 1.47 W/m-K and a matrix thermal conductivity of 1.51 W/m-K.

5 samples of Ordovician age, mainly represented by shale, yielded an average *in situ* thermal conductivity of 1.34 ± 0.07 W/m-K and an average matrix thermal conductivity of 1.50 ± 0.06 W/m-K.

In general, the depth intervals used to determine heat flow values in this study were shallow (see Figures A1a, A3a, A5a, A7a, A9a, A11a, A13a, A15a, A17a, A19a, A21a, A23a, A25a, A27a, A29a, A31a, A33a, A35a, A37a, and A39a, Appendix A), around 1,000 m or less. Therefore, Pennsylvanian and Permian ages are oversampled, while Mississippian, Devonian, and Ordovician ages are undersampled. The relatively low thermal conductivities reflect the dominance of shale in the lithologic units.

A systematic study of 843 samples from the Arkoma Basin (Lee et al., 1996) showed similar thermal conductivity values for different geologic ages (except the Ordovician samples). In their study, Pennsylvanian rocks (shales, sandstones, and limestones) displayed the following matrix thermal conductivity values: Savanna Formation - 2.05 W/m-K; McAlester Formation - 1.84 W/m-K; Hartshorne Formation - 2.28 W/m-K; Atoka Formation - 1.71 W/m-K; Morrowan Formation - 1.49 W/m-K. The Mississippian - Devonian rocks (shale, limestone), measured by Lee et al. (1996) have a matrix conductivity of 1.73 W/m-K, Devonian - Silurian rocks (limestone, shale) showed an average matrix conductivity of 1.97 W/m-K, and the Ordovician rocks (limestone, shale, sandstone) have an average matrix conductivity of 2.40 W/m-K. The last value differs from the value I

found in this study (1.50 W/m-K), probably because there are fewer Ordovician age samples in my study (5 vs. 55).

4.3. Heat production

Based on the procedure described in Sec. 3.4., I made 27 new determinations of heat production of basement rocks using gamma-ray logs from various parts of Oklahoma (Table 5 and Fig. 12). The average value was 2.51 ± 0.09 , the range of values is from $1.1 \mu\text{W}/\text{m}^3$ to $3.5 \mu\text{W}/\text{m}^3$. The average heat production of the basement rocks of Oklahoma, as determined from 49 estimates, including 22 previously published by Roy et al. (1968), Borel (1995), and Lee et al. (1996), is $2.48 \pm 0.08 \mu\text{W}/\text{m}^3$. The age of basement rocks in Oklahoma is Middle Proterozoic (1,300 - 1,500 m.y. ago, Denison et al., 1984). According to Vitorello and Pollack (1980), the worldwide average heat production rates of basement rocks of Early Proterozoic (2,500 - 1,600 m.y. ago) and Late Proterozoic age (900 - 570 m.y. ago) are 1.9 ± 0.0 and $2.4 \pm 1.2 \mu\text{W}/\text{m}^3$, respectively (the error range indicates ± 1 standard deviation). The average values found for my 27 measurements ($2.51 \pm 0.09 \mu\text{W}/\text{m}^3$) and for the entire state of Oklahoma, based on 49 measurements ($2.48 \pm 0.08 \mu\text{W}/\text{m}^3$) seem to be slightly higher than average for continental rocks of similar age.

A comparison between heat generation rates measured on cores and using gamma ray logs shows no great difference between data: a core from 897 m depth measured at 36.28°N and 96.47°W yielded a value of $2.4 \mu\text{W}/\text{m}^3$ (Borel, 1995); a determination made using a gamma ray log in a basement found at 796 m at 36.31°N and 96.51°W produced a value of $2.5 \mu\text{W}/\text{m}^3$ (Lee et al., 1996). The distance between the two sites is about 4.8 km. Another core measurement of heat production from a depth of 2974 m at 34.63°N and 98.10°W yielded a value of $1.8 \mu\text{W}/\text{m}^3$ (Borel, 1995). A determination using

TABLE 5
Heat Production Estimates

Section, Township and Range	Latitude (°N)	Longitude (°W)	Heat Production ¹ ($\mu\text{W}/\text{m}^3$)	Depth to basement (m)	Sampling interval below the top of basement (m)	Geologic unit ²
2-1N-9W	34.58	98.12	1.9	1049	65	CR
2-1N-9W	34.58	98.11	2.2	1070	163	CR
19-2N-10W	34.63	98.28	2.3	333	89	CR
20-2N-10W	34.62	98.26	3.5	273	57	CR
20-2N-10W	34.61	98.25	2.5	298	21	CR
14-4N-21W	34.83	99.40	2.6	350	37	WP
32-4N-21W	34.78	99.42	1.8	152	777	WP
4-5N-24W	34.93	99.74	2.1	1036	207	R
12-5N-24W	34.92	99.68	2.4	914	76	R
16-7N-21W	35.08	99.42	1.7	382	67	CR
21-7N-1W	35.05	97.25	2.5	298	21	MG
25-8N-26W	35.13	99.90	1.9	1049	65	CR
7-25N-4W	36.63	97.60	3.3	2264	21	MG
10-26N-2W	36.74	97.40	2.6	1949	25	MG
1-26N-22W	36.75	99.60	3.1	2612	253	?
1-27N-10W	36.84	98.22	2.2	2207	18	?
27-27N-21W	36.79	99.45	3.6	2688	70	?
13-2N-5E	34.64	96.73	2.2	1372	30	MG
4-1N-22EC	36.57	100.69	2.8	3334	18	?
10-2N-7EC	36.74	102.40	2.9	2101	29	R
9-2S-2E	34.39	97.10	2.4	488	1759	MG
13-2S-7E	34.37	96.51	2.6	2371	84	MG
35-3S-10E	34.26	96.27	1.6	2417	35	MG
15-5S-8E	34.10	96.44	1.1	3139	683	TG

45

1-3S-19W	34.33	99.15	1.7	2210	63	M
22-6S-5W	34.02	97.70	1.7	2087	46	CR
5-6S-8W	34.06	98.05	2.2	1265	12	CR

¹Estimated from gamma ray logs as explained in text, average of 27 estimates is $2.51 \pm 0.09 \mu\text{W}/\text{m}^3$

²MG - Mesozonal granite; CR - Carlton rhyolite; R - Rhyolite; WP - Wichita province (granite, rhyolite, gabbro); TG - Tishomingo granite; M - Metamorphic rocks, after Denison et al., 1984. These rocks formed in the interval 1,300 - 1,500 m.y. ago (Denison et al., 1984)

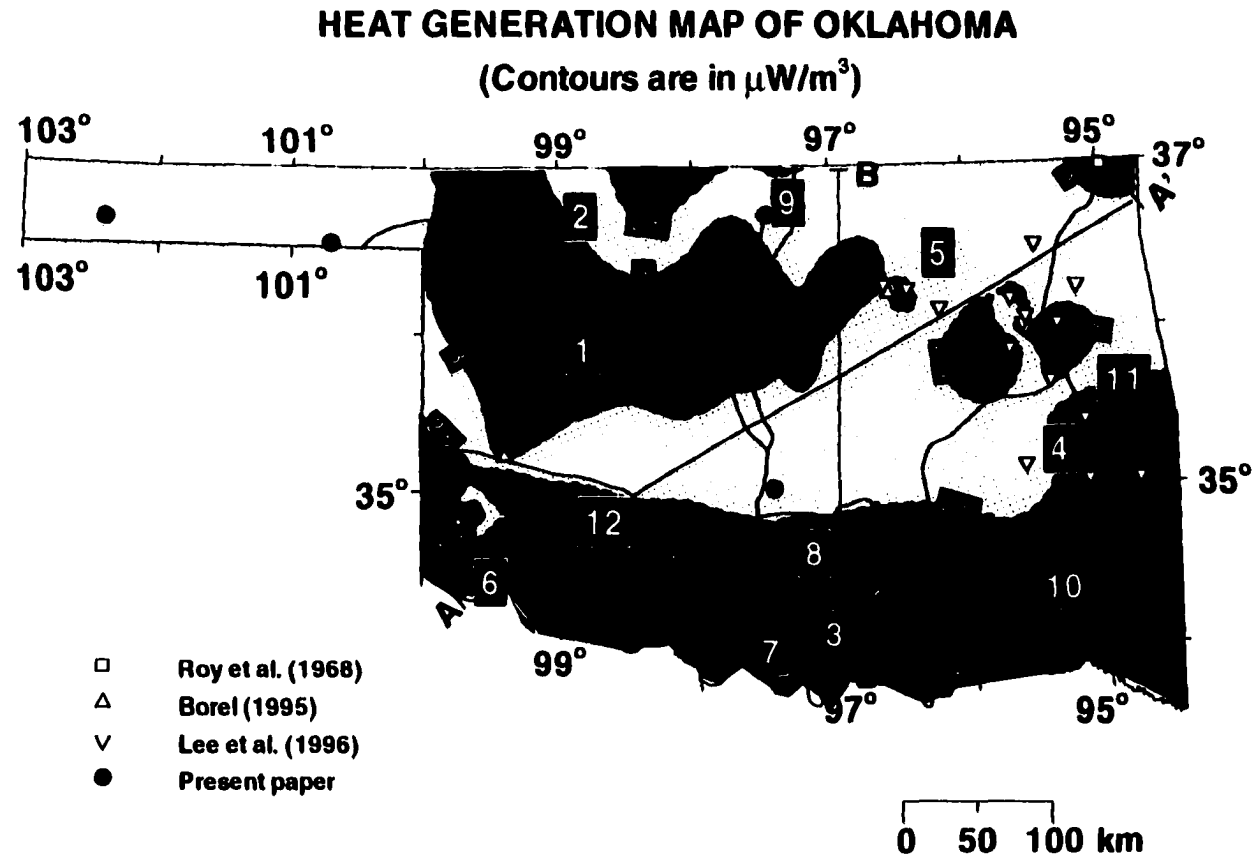


Fig. 12. Heat Generation Map of Oklahoma. Big numbers represent geologic provinces of Oklahoma, according to Fig. 1.

gamma ray logs, made in vicinity of the previous one (34.58°N, 98.12°W, 1049 m basement depth) produced a value of $1.9 \mu\text{W}/\text{m}^3$. The distance between the two sites is about 5.8 km.

Using the geologic map of basement rocks of Oklahoma, as it was defined by Denison et al. (1984), I plotted the heat production estimates defined for each type of basement rock (Fig. 3) as follows: Carlton Rhyolite: $2.2 \pm 0.06 \mu\text{W}/\text{m}^3$; Wichita province (Cambrian rocks): $2.2 \pm 0.2 \mu\text{W}/\text{m}^3$; Rhyolite: $2.5 \pm 0.13 \mu\text{W}/\text{m}^3$; Mesozonal granite: $2.5 \pm 0.07 \mu\text{W}/\text{m}^3$; Metamorphic rocks (mostly metasedimentary, grade variable, mostly low to medium): $1.7 \mu\text{W}/\text{m}^3$; Epizonal granite (Lee et al., 1996): $2.8 \pm 0.05 \mu\text{W}/\text{m}^3$.

The heat generation map of Oklahoma (Fig. 12), which is the first map of this type ever compiled for Oklahoma, represents one of the main results of the present study. It comprises 27 new heat production estimates and 22 more values previously published by Roy et al. (1968) (one value), Borel (1995) (four values), and Lee et al. (1996) (seventeen values). The method used for interpolating heat generation data was kriging on a grid of 500 x 500 cells (Davis, 1986).

There is a trend of increasing heat production rates from SW and S (values $< 2 \mu\text{W}/\text{m}^3$) toward NE and N (values $> 3 \mu\text{W}/\text{m}^3$), respectively (Fig. 12). Profiles A - A' (Fig. 14) and B - B' (Fig. 15) show the distribution of individual heat generation estimates along SW - NE and N- S directions, respectively. The scatter of data does not allow the inference of a definite trend, but seems to indicate a distribution of weak radioactive heat sources in the SW and S, and stronger sources in the NE and N.

The area with the lowest heat production ($< 1.5 \mu\text{W}/\text{m}^3$), according to Fig. 12, lies in the southeastern parts of the Ardmore Basin and the Arbuckle Uplift. Areas with the highest heat production ($> 3 \mu\text{W}/\text{m}^3$, Fig. 12) occupy

the northcentral part of the Anadarko Basin, the southern part of the Anadarko Shelf, a small part of the western Cherokee Uplift, and isolated patches on the Ozark Uplift and northeastern corner of the state. A comparison with Figure 3 provides a possible explanation relating the trend of heat generation to the composition of basement rocks: metamorphic rocks, Carlton rhyolite, and mafic rocks (basalts, gabbros) of the Wichita Province have heat generation rates of 1.7, 2.2, and 2.2 $\mu\text{W}/\text{m}^3$, respectively, whereas mesozonal granites, epizonal granites, and northeastern rhyolites have heat generation rates of 2.5, 2.8, and 2.5 $\mu\text{W}/\text{m}^3$, respectively. The heterogeneous composition of the basement rocks of Oklahoma is supported by both magnetic (Jones and Lyons, 1964; Committee, 1987) and gravimetric (Kruger and Keller, 1986; Robbins and Keller, 1992) maps. Large positive anomalies on the gravimetric and magnetic maps are usually associated with a more mafic basement (with less heat generation), while lower gravimetric and magnetic anomalies are considered produced by a granitic basement (with more heat generation). For example, basement rocks under the northern shelf, the northern edge of the Anadarko Basin, and the Cimarron Arch are considered to be cratonic granites (Ham et al, 1964; Ham, 1969; Denison et al., 1984). They appear as relative lows on both gravimetric and magnetic maps. In contrast, basement rocks with a mafic composition (gabbro, basalt), underlying the southwestern part of Oklahoma, are indicated by relative high magnetic and gravimetric anomalies.

In the heat generation map of Oklahoma (Fig. 12) there are inherent uncertainties due to the lack of uniformly distributed values, the lack of heat produced by sediments, especially shales, and ambiguities inherent in the kriging (interpolation) procedure. The Anadarko Basin, for example, is partly shown as an area of high heat production while, in fact, only basement rocks

on the margins of the basin were sampled. The Anadarko Basin basement is covered by sedimentary rocks with thicknesses up to 12 km, and wells rarely penetrate it. Caution should therefore be used in interpreting the extent of anomalous high or low heat-generation areas inferred from the extrapolation of a few measurements.

4.4. Heat flow

The average near-surface heat flow values for each site (Table 1) range from 22 ± 4 mW/m² (site # 19) to 86 ± 17 mW/m² (site #8); the average is 50 mW/m². The distribution of heat flow intervals for each site is shown in Appendix D. Compared to the continental average heat flow value of 65 mW/m² (Pollack et al., 1993), the heat flow regime of Oklahoma can be characterized as rather low, with only one northeastern area on the Cherokee Platform (Fig. 13) that exhibits values greater than 65 mW/m².

Another main result of this study is the Heat Flow Map of Oklahoma (Fig. 13). An earlier version of this map was presented elsewhere (Cranganu and Deming, 1997). This map compiles 40 previously published heat flow values and 20 new heat flow values reported in this study. The margins of this map were constrained by using 191 published and unpublished heat flow values distributed within 30°N - 40°N, 90°W - 105°W area. Published values are taken from Blackwell et al. (1994); unpublished values were kindly provided by D. D. Blackwell (pers. comm., Blackwell, 1996) and Föster and Merriam (1996) (used by permission). The heat flow map was interpolated using a kriging procedure on a grid of 500 x 500 cells (Davis, 1986).

The heat flow map of Oklahoma (Fig. 13) exhibits a relatively low heat flow area in the SW (values < 30 mW/m²), covering the northern parts of the Marietta and Hollis Basins and the Wichita Uplift, and a relatively high heat

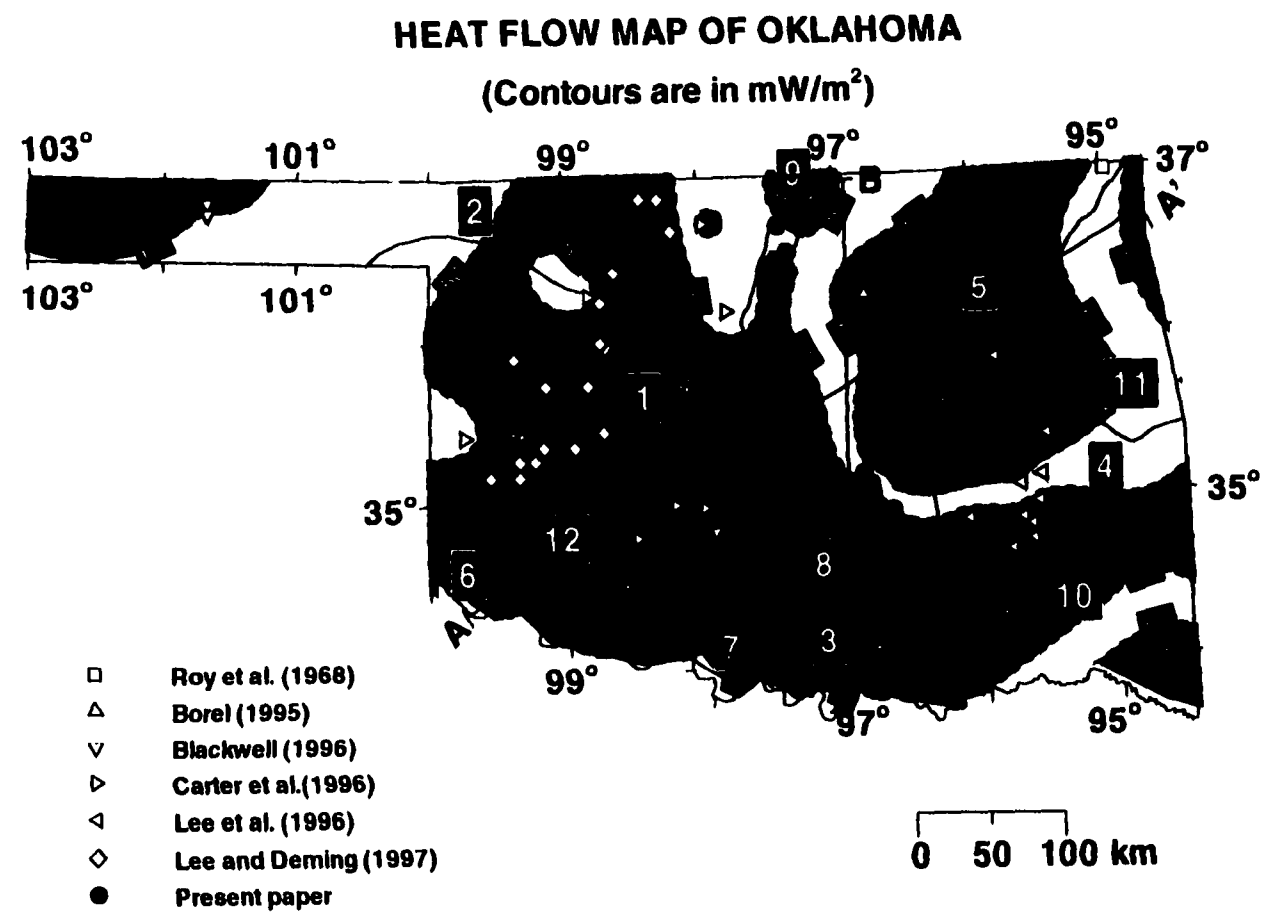


Fig. 13. Heat Flow Map of Oklahoma. Big numbers represent geologic provinces of Oklahoma, according to Fig. 1.

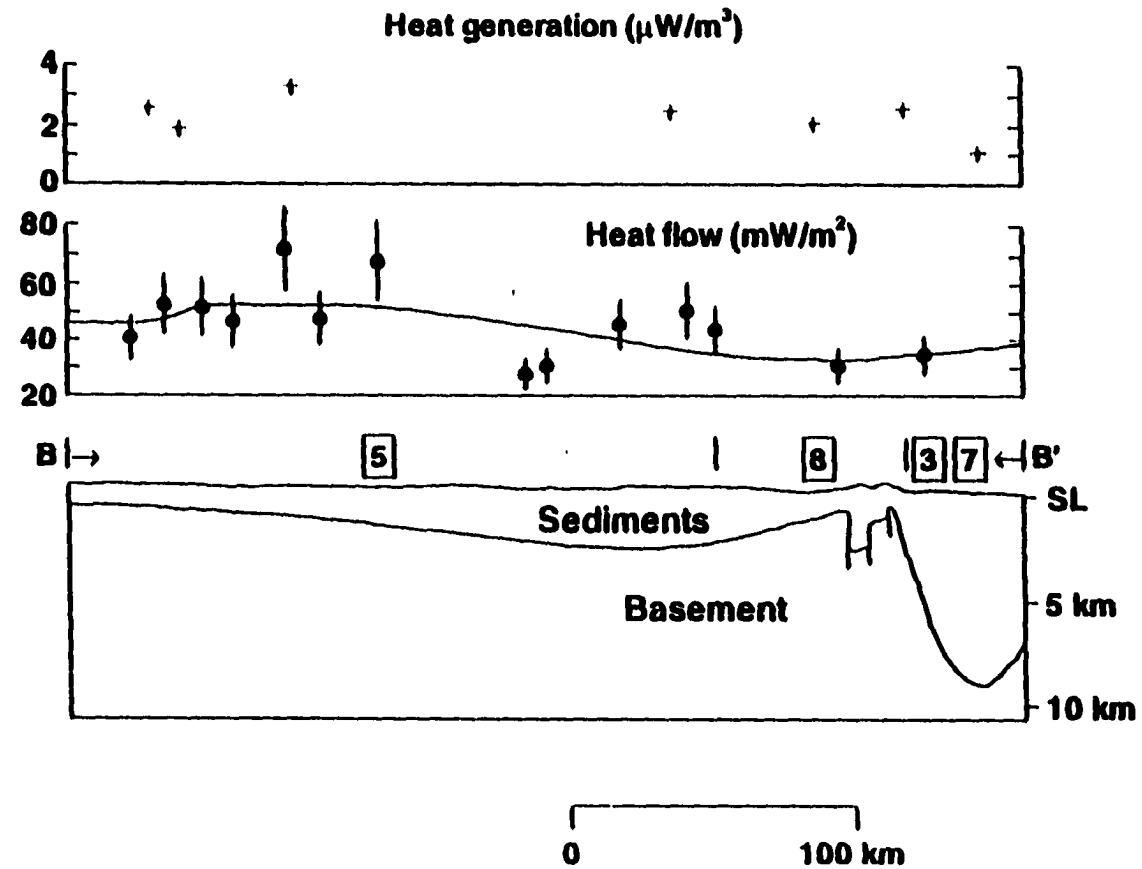


Fig. 15. Geologic cross-section B - B' (after Johnson et al., 1972) with heat generation and heat flow distribution. Numbers on line B - B' represent geologic provinces of Oklahoma according to Fig. 1.

flow area (values $> 70 \text{ mW/m}^2$), in the northeastern part of the Cherokee Platform. Between these two areas there is a large area of low-to-intermediate heat flow values ($30 - 50 \text{ mW/m}^2$) covering parts of the Hollis, Ardmore, Marietta, and Anadarko Basins as well as parts of the Arbuckle, Wichita, and Ouachita Uplifts, and an area of intermediate-to-high heat flow values ($50 - 70 \text{ mW/m}^2$), covering parts of the Cherokee Platform, Ozark and Ouachita Mountains Uplifts, Anadarko Shelf, and Arkoma Basin.

The heat flow and heat generation distributions along profiles A - A' and B - B' from Figures 12 and 13 are shown in Figures 14 and 15, respectively, along with the geologic structure of the upper crust. The individual heat flow values are shown as filled circles with error bars. In general, there is a trend of increasing of heat flow values from SW ($\sim 30 \text{ mW/m}^2$) to NE ($\sim 80 \text{ mW/m}^2$) in Figure 14 and from N ($\sim 70 \text{ mW/m}^2$) to S ($\sim 30 \text{ mW/m}^2$) in Figure 15 which seems to be controlled by the depth of basement or thickness of sediments.

5. ERROR ANALYSIS

5.1. Temperature data

The intention of the American Petroleum Institute in collecting temperature data I used in this study was to obtain "absolutely reliable measurements" (Heald, 1930, p. 2). Van Orstrand (1930) documented the instruments and methodology used in the API study. He estimated the accuracy of individual temperature determinations as $\pm 0.3^{\circ}\text{F}$ ($\pm 0.17^{\circ}\text{C}$) (Van Orstrand, 1930, p. 15) and the probable depth error as 1 foot in 1000 ft (0.3 m per 305 m) (Van Orstrand, 1930, p. 15). The API researchers recognized the problem of drilling disturbances, and they carefully noted the amount of time wells had been idle before temperature logging. They also made checks to ensure that recorded temperatures, extrapolated to mean annual ground surface temperatures, did not exceed observed mean annual air temperatures by more than 2 or 3 $^{\circ}\text{F}$ (1.1 - 1.7 $^{\circ}\text{C}$). A stem correction for thermometers was applied, which removed the errors introduced by reading the position of the constriction in the capillary in two different environments (the warmer borehole and the cooler ground surface).

Guffanti and Nathenson (1981, p. 2) noted that "the API data have had limited utility in heat flow studies because core samples were not available". However, they also noted that Birch (1954), Benfield (1947), Joyner (1960), and Blackwell (1967) had used these temperature data for heat flow estimates by estimating thermal conductivities from core sample or outcrop samples.

In conclusion, I believe that the temperature data set I am using for my heat flow study in Oklahoma can be regarded in general as providing high quality, accurate estimates of rock temperatures.

5.2. Thermal gradients

Error in estimating thermal gradients depends upon errors in measuring subsurface temperature and depths. The accuracy of individual temperature determination was estimated by Van Orstrand (1930, p. 10) to be ± 0.17 °C and the probable depth error as 0.3 m per 305 m (1 foot/1,000 ft). To estimate the error in determining the average thermal gradients I used the propagation of error techniques for uncorrelated random variables (Barry, 1978, p. 75) as shown in equation (6):

$$E_{\text{product}} = \pm ABC \dots N \sqrt{(E_A/A)^2 + (E_B/B)^2 + (E_C/C)^2 + \dots (E_N/N)^2} \quad (6)$$

where E_{product} is the total error of a product; A, B, C, ..., N - individual values of the product; $E_A, E_B, E_C, \dots, E_N$ - individual error of values A, B, C, ..., N. Using equation (6), I estimated the error in determining average thermal gradients to be $\pm 2\%$.

5.3. Thermal conductivity

Estimating *in situ* thermal conductivity involves several possible types of errors: (1) sampling errors; (2) systematic errors in measuring devices, and (3) errors introduced by the corrections applied to measured data (anisotropy, temperature, and porosity corrections).

5.3.1. Sampling error. This error is due to the bias inherently present in any sampling strategy (inadequate lateral or vertical sampling). Devising a sampling strategy is not an easy task because every strategy is likely to be unique. The basic procedure followed during sampling was to sample every 20 - 30 ft thickness of sediments. When one well was not enough (because of

gaps in lithologic column or depths not covered), an additional well was used (sites # 3, 6, 9, 12, 15, 16, and 18) to cover the entire depth of the temperature measurements.

In order to constrain sampling errors due to lateral variation in lithology and to vertical offsets between temperature and conductivity wells, I constructed stratigraphic maps for each site (Figures A2, A4, A6, A8, A10, A12, A14, A16, A18, A20, A22, A24, A26, A28, A30, A32, A34, A36, A38, and A40, Appendix A) based on stratigraphic data provided by scout cards on file at the University of Oklahoma Geology Library and Core Library in Norman, as well as by other sources (e. g., Weinzierl, 1922; Johnson et al., 1988; Arbenz, 1989; Johnson and Cardott, 1992).

For each temperature well I tried to find the closest well(s) with drilling cuttings to reduce at maximum the errors due to lateral lithologic variability.

An analysis of error introduced by lateral variability of lithology was carried out for two clusters of sites: (1) site #3 and site #4, separated by a distance of 5.5 km showed a difference between *in situ* thermal conductivity measured at the same stratigraphic level of 15%; (2) site #13 and site #14, separated by a distance of ~8 km, showed difference between *in situ* thermal conductivity measured at the same stratigraphic level of 2.5%. An average value of $\pm 10\%$ was estimated for error introduced by lateral variability of lithology. Having sufficient measurements for each site would greatly reduce such errors.

5.3.2 Measurement error. The apparatus I used to make thermal conductivity measurements was a divided bar device. The calibration of this apparatus was made with disks of fused silica. The values used for calibration were those provided by Ratcliffe (1959). Every day, before measurements, the

calibration values were checked using three out of six available calibration disks of different thickness, selected randomly. Individual sample holders (cells) were calibrated using the known thermal conductivity of water as a function of temperature. The probable inaccuracy produced by systematic errors in the divided bar and cell technique is around $\pm 5\%$ or less (Borel, 1995; Lee et al., 1996). In addition to systematic errors inherent in the measurement apparatus itself (divided bar), some other errors may arise from the cell technique that is based upon a mixing model (Sass et al., 1971). However, using the same apparatus, Lee et al. (1996) have found that the conductivity of an isotropic crushed aggregate of fused silica estimated with the cell technique was within $\pm 1 - 2\%$ of the value used to calibrate the divided bar. Therefore, I consider that using a geometric mean mixing model (Equation 3) may introduce negligible errors, at least when working with isotropic materials.

5.3.3. Correction errors. The error introduced by the anisotropy correction is difficult to estimate because the correction formula I used here (Deming and Borel, 1995) was derived from measurements made on samples of Pennsylvanian age from north central Oklahoma. I estimate that the overall error introduced by this correction is $\pm 10\%$, but I do not have a definitive basis for quantifying the uncertainties introduced in thermal conductivity measurements by anisotropic effects.

It is also difficult to precisely estimate the errors introduced by using the temperature correction. The literature dedicated to this subject is extensive (e. g., Birch and Clark, 1940; Sugawara and Yoshizawa, 1961; Kawada, 1964, 1966; Anand et al., 1973; Kappelmayer and Haenel, 1974; Sibbit et al., 1979; Roy et al., 1981; Cermák and Rybach, 1982; Mongelli et al., 1982; Robertson, 1988; Seipold, 1990; Funnell et al., 1996). However, because the

temperature interval used in this study is relatively small (16.6°C - 56.8°C) the average error introduced by Sekiguchi's formula (2) is estimated to be $\pm 2\%$.

There is an error due to uncertainty in the determination of porosity using geophysical logs. For example, for an estimated average porosity of 0.12 (see Table 3), an estimation error in porosity of $\pm 20\%$ will lead to an error *in situ* conductivity estimation of $\pm 5\%$.

An average of standard errors of the mean, associated with thermal conductivity measurements (Table 1) was estimated to be $\pm 7\%$. Using standard techniques (Barry, 1978; see eq. 6) for propagating the above uncorrelated error sources, I estimate a total error in determining thermal conductivity of $\pm 17\%$.

5.4. Heat production error

Basement heat production errors can be caused by the procedure of heat production estimates from gamma ray logs and by uncertainty introduced by shale heat generation. The validity of equation (5) relies on "standard" Th/U and K/U ratios and, even though it was calibrated for a variety of rock types in numerous research wells, it is possible that it may not be valid for basement rocks from Oklahoma. Bückner and Rybach (1996) estimated the accuracy of equation (5) to be $\pm 10\%$. One additional possible source of error is represented by an unknown amount of alteration due to paleoweathering to which basement rocks used in my determinations may have been subjected. However, since no other sources for determining heat production of the basement rocks were available, the relation (5) provided the only possibility for this type of determination.

Among other sedimentary rocks found in Oklahoma (sandstones, carbonates), shales are by far the most important heat generator due to their

high ^{40}K content. Using formula (5), I estimated the heat production of shale sections in the 27 wells used in this study to be in the range $1.6 - 1.8 \mu\text{W}/\text{m}^3$. Rybach (1986, p. 314, ; 1988, p. 136) indicated an average value of $1.8 \mu\text{W}/\text{m}^3$ for shales. Calculating the average thickness of shale deposits in Oklahoma, based on published data (e.g., Johnson et al., 1988), I found that the Viola shale, Woodford Shale, Mississippian shales, and Pennsylvanian shales sum up to 1,450 - 2,000 m in the aulacogen, and 50 - 1,400 m in the shelf area. Multiplying the average thicknesses of shale by their average heat production ($1.7 \mu\text{W}/\text{m}^3$), I obtained a heat flow contribution from shales of $2.3 - 3.6 \text{ mW}/\text{m}^2$ in aulacogen, and $0.08 - 2.52 \text{ mW}/\text{m}^2$ in the shelf area. Compared to the average heat flow in Oklahoma ($50 \text{ mW}/\text{m}^2$), the influence of shale heat production on the total heat flow in Oklahoma represents 4 - 7% in the aulacogen, and 0.2 - 5% in the shelf areas. In other words, the uncertainty of heat production of shales that might affect heat flow values in Oklahoma is estimated to be $\pm 5\%$. The overall error of heat production estimation is considered to be $\pm 11\%$.

5.5. Heat flow error

Using eq. (6), when thermal gradient error is $\pm 2\%$ and thermal conductivity error is $\pm 17\%$, I found an estimated error in heat flow determinations of $\pm 17\%$. Taking into consideration the various uncertainties involved in estimating the magnitude of errors, I considered it useful to round the estimated error level of heat flow determinations off to a uniform $\pm 20\%$.

6. INTERPRETATION OF RESULTS AND DISCUSSION

6.1. Introduction

The geothermal regime of any area is governed by the following general equation which relates temperature and the processes that generate, transport, and store heat in the crust:

$$-\nabla \cdot \hat{q} = -A + \rho'c'\beta \cdot \nabla T + \rho c \frac{\partial T}{\partial t} \quad (7)$$

where \hat{q} is the conductive flux vector and T is the temperature. A denotes the rate of heat generation per unit volume; it could represent the effects of radioactive decay, frictional heating phase changes, or chemical reactions. ρ and c are the density and heat capacity of material at any point, and ρ' and c' are the corresponding properties for material (usually water or magma) moving with velocity β . In general, all the parameters in (7), including β , are functions of spatial coordinates x , y , and z , and some can significantly depend upon temperature and pressure.

Equation (7) describes a 3-D variation of the geothermal regime; however, in many situations it is more useful to adopt a simpler interpretation that requires a one-dimensional model. In this case, all parameters in (7) vary only with depth (z) beneath the Earth surface. We can also adopt a customary definition of "heat flow" q as the upward component of conductive flux with the reversed sign and thus we obtain the well-known Fourier's law:

$$q \equiv \lambda_{pr} \frac{\partial T}{\partial z} \quad (8)$$

Now, equation (7) can be reduced, for the 1-D case, to (Cranganu and Deming, 1996):

$$\frac{\partial q}{\partial z} = \rho'c'\mu \frac{\partial T}{\partial z} + \rho c \frac{\partial T}{\partial t} - A \quad (9)$$

where q is the upward conductive heat flow, μ is the upward volume flux of material with volumetric heat capacity $\rho'c'$, and ρc is the corresponding quantity in any stationary element.

Interpretations of the crustal thermal regime generally represent attempts to integrate (9) with simplifications believed to be appropriate for a specific province. The first term on the right side of eq. (9) describes effects of relative vertical movement of crustal (and upper mantle) masses; these may be solid blocks moving along faults (as during an earthquake, generating heat by friction) or magmatic and aqueous fluids moving through fractures created by faulting or through pore spaces (Lachenbruch and Sass, 1977). Since these movements are generally intermittent or, sometimes, short-lived, they represent, along with depositional/erosional processes and climatic changes, the transient thermal disturbances denoted by the second term on the right side of eq. (9).

Terrestrial heat flow, normally estimated in the upper 1% of the crust, provides only a boundary condition for eq. (9). We can use this to estimate the variation of heat flow through the entire crust, i.e., to characterize the thermal regime of the crust in a specific area. In order to do this, it is necessary to appropriately characterize the processes described by the right side terms of eq. (9). These processes may have both shallow causes (geometric effects of topographic relief, transient effects of sedimentary processes, climatic changes) and deep causes (effects of distribution of sources associated with the decay of

radioactive elements, thermal refraction, phase changes, convective heat transfer, and recent tectonic/volcanic activity).

6.2. Transient effects of sedimentary processes and metamorphic/igneous activity

Two sedimentary processes, deposition and erosion of sediments, have opposite effects. When sediments are deposited in a basin the thermal gradient and heat flow are reduced. During erosion, warmer underlying material is exposed, increasing the thermal gradient. Thus, there is a tendency for rapid sedimentary processes to cause heat flow to become anomalously high in eroded areas and low in accumulation areas (Langseth et al., 1965; De Bremaecker, 1983; Hutchison, 1985; Cranganu and Deming, 1996). However, erosion also leads to a loss of radioactive heat-generating elements from the upper crust with a concomitant decrease of the surface heat flow (Vitorello and Pollack, 1980).

During Late Paleozoic time (333 - 245 m.y. ago), Oklahoma experienced intense sedimentation and subsidence in the existing Proterozoic depositional provinces. At the same time, tectonic movements produced folding and thrusting of the Ouachita Foldbelt as well as the rising of the Wichita, Criner, Arbuckle, Nemaha, and Ozark uplifts (Ham and Wilson, 1967; Johnson et al., 1988). Since deposition of Permian strata (~245 m.y. ago), erosion has been the primary sedimentary activity throughout almost all of Oklahoma (Johnson and Cardott, 1992). In the eastern part of Oklahoma, Permian beds are not found, suggesting that erosion started even earlier (~310 m.y. ago), during Atokan time (Houseknecht, 1986). The total sediment thickness is as high as 12,000 - 13,000 m in the Anadarko basin, but the rate of sedimentation was very low (~29 m/m.y.) during Precambrian - Mississippian time (523 - 333

m.y. ago), and increased to ~107 m/m.y. during Pennsylvanian - Permian time (333 - 245 m.y. ago. Erosion occurred for the last ~245 m.y. at an average rate of ~8m/m.y. (Gilbert, 1992). The present surface heat flow in Oklahoma is likely not depressed by sedimentation because the thermal time constant of the continental lithosphere (~50 m.y., Pollack and Chapman, 1977) is less than time elapsed since erosion and any transient depression of heat flow should have long since dissipated. Although erosion has been the predominant process for the last ~250 m.y., erosion rates tend to decrease exponentially with increasing time (Vitorello and Pollack, 1980). Therefore, it is unlikely that present-day heat flow has been significantly elevated by erosion. In fact, the loss of radioactive heat-generating elements by erosion, coupled with the decay of transient thermal perturbations of poorly understood origin may produce a heat flow decrease of about 30 mW/m² over 300 m.y. (Vitorello and Pollack, 1980). In conclusion, the thermal state of Oklahoma has changed over time due to transient effects of sedimentary processes, but these effects do not significantly influence the present-day heat flow regime of Oklahoma because there has been no significant tectonic activity in Oklahoma for at least 250 m.y. (Johnson et al., 1988).

Oklahoma has not experienced recent metamorphic or igneous activity for the last ~ 500 m.y. (Johnson et al., 1988). This is suggested by the absence of earthquakes with magnitudes greater than 2.5 - 2.7 (Luza and Lawson, Jr., 1983), absence of ash in sediments (Johnson et al., 1988) and absence of high amplitude short wavelength magnetic anomalies (Jones and Lyons, 1964; Committee, 1987). Thus, it seems unlikely that the observed variation of the surface heat flow values in Oklahoma can be associated with a variable distribution of volcanic sources or frictional heating due to tectonic movements.

6.3. Climatic effects

Calculating the effects of climatic changes in the past 120,000 years, Beck (1977) found that, for latitudes between 20°N - 40°N (Oklahoma's latitude range) and for thermal conductivities ranging from 1.26 W/m-K to 6.28 W/m-K, required corrections needed are less than 0.2 - 0.3 mW/m² for depths between 150 m - 2,000 m. In conclusion, the present day thermal regime of Oklahoma is not significantly influenced by past climatic changes.

6.4. Effects of variable distribution of heat generation sources

If we integrate eq. (9) over an interval $\Delta z = z_2 - z_1$, and assume that A does not vary with depth, we get

$$\Delta q = \int_{z_1}^{z_2} \frac{\partial q}{\partial z} \Delta z \quad (10a)$$

$$\Delta q = \rho'c'\mu\Delta T + \rho c \frac{\partial T}{\partial t} \Delta z + A\Delta z \quad (10b)$$

where the parameters in (10b) are taken as appropriate average values and ΔT is the temperature difference across the layer of thickness Δz .

If we consider only the contribution of heat generation sources from the crust with thickness h and constant heat production A , then that contribution can be expressed as:

$$\Delta q \text{ (mW/m}^2\text{)} = h \text{ (km)} A \text{ (\mu W/m}^3\text{)} \quad (11)$$

Taking an average crustal thickness in Oklahoma $h = 46$ km (Mitchell and Landisman, 1970) and an average value $A = 2.51 \mu\text{W}/\text{m}^3$ (Table 4), crustal heat generation alone would account for all surface heat flow in Oklahoma. However, heat generation estimated close to the top of basement (Table 5) is not constant throughout the crust. Therefore, the distribution $A(z)$ is important to an understanding of the crustal thermal regime, and has been the subject of considerable study (Lachenbruch, 1970; Lachenbruch and Sass, 1977). The vertical variation of A is not known in Oklahoma, due to the lack of measurements. Data presented in Table 5 represent heat production estimated very close to the basement surface (the sampling interval was, in most cases, less than 100 m below the top of the basement). However, the lateral variation of heat generation sources at the upper basement surface can be estimated and is shown in Figures 3 and 12. As can be seen from Figure 3, the basement rocks of Oklahoma have variable composition (granites, basalts, rhyolites, gabbros, metasedimentary rocks) with variable heat production (ranging from $1.1 \mu\text{W}/\text{m}^3$ to $3.5 \mu\text{W}/\text{m}^3$).

A comparison between the heat flow map of Oklahoma (Fig. 13) and the heat generation map of Oklahoma (Fig. 12), as well as the two cross-sections A - A' and B - B' (Figures 14 and 15), shows the following: (1) the relatively lowest heat flow area ($< 30 \text{ mW}/\text{m}^2$), covering the southwestern part of the state (Fig. 13), corresponds to a relatively intermediate heat production ($2.0 - 2.5 \mu\text{W}/\text{m}^3$) area in Figure 12; (2) a large area with relatively low heat flow ($30 - 50 \text{ mW}/\text{m}^2$), covering the central western and southeastern parts of Oklahoma (Fig. 13), corresponds to areas with relatively intermediate to high heat production rates ($2 - 3 \mu\text{W}/\text{m}^3$) in Figure 12; (3) an area with relatively intermediate heat flow ($50 - 70 \text{ mW}/\text{m}^2$), covering the Oklahoma Panhandle, the northeastern part, and the southeastern corner of

the state (Fig. 13), corresponds to areas with relatively intermediate to high heat generation rates ($2 - 3 \mu\text{W}/\text{m}^3$) in Figure 12; (4) an area with the relatively highest heat flow values ($> 70 \text{ mW}/\text{m}^2$), covering the southwestern part of the Cherokee Platform (Fig. 13), corresponds to an area with intermediate heat generation rates ($2.5 \mu\text{W}/\text{m}^3$).

A large area, such as the northern half of the Anadarko Basin, is shown on Figure 12 as being underlain by a high heat-production crust, while the same area displays in Figure 13 only low-to-intermediate surface heat flow. Similarly, the far northeastern corner of the state displays a high-heat production area (Fig. 12), while the heat flow map (Fig. 13) shows values between 50 and 60 mW/m^2 . One possible interpretation that might explain these discrepancies is the inherent uncertainties introduced in the heat production map (Fig. 12) and heat flow map (Fig. 13) by the lack of enough data. Variations in the background heat flow (the heat flow produced by subcrustal sources) might be another possibility.

As a conclusion, the relatively lowest and highest heat flow areas do not correspond to the relatively lowest and highest heat production areas, respectively, suggesting that other causes (e.g., groundwater movement) are probably involved. However, as can be seen from the two cross-sections, A-A' (Fig. 14) and B-B' (Fig. 15), there is some correlation between the variation of surface heat flow and the distribution of heat production values, suggesting that heat generated in the basement may make a significant contribution to the thermal regime of Oklahoma.

The relationship between the surface heat flow and heat generated by radioactive decay of U, Th, and K was found to be of the form

$$q = q^* + bA_0 \quad (12)$$

for many localities in the United States (Birch et al., 1968; Roy et al., 1968; Lachenbruch, 1970). Here, q and A_0 are heat flow and heat generation near the surface ($z = 0$) and q^* and b are intercept and slope parameters that define a heat flow province (Roy et al., 1968).

Applying eq. (12) to the heat flow and heat generation data from Oklahoma, I obtained the results shown in Figure 16. The intercept is negative ($- 30.4 \text{ mW/m}^2$) and the slope (30.8 km) represents a value comparable to the average crustal thickness. The coefficient of correlation is 0.51. Both parameters are in contradiction with usual values (7 - 10 km for slope and 16 - 58 mW/m^2 for intercept: Vitorello and Pollack, 1980). The explanation for this situation may be related to the errors due to different data distributions and methods used in estimating the two input parameters, surface heat flow and heat production. It should be emphasized that locations of heat flow and heat production estimates do not coincide: for each heat production site, I interpolated a heat flow value using the map from Figure 13. Therefore, it is possible that errors due to estimating heat flow through a map interpolation procedure along with errors in heat production estimates, may have led to unrealistic estimates of the slope and intercept on the heat flow - heat production plot (Fig. 16).

Another possible explanation is that a linear relationship between heat flow and heat generation data has no significance for Oklahoma, i.e., Oklahoma is not a heat flow province as defined by Roy et al. (1968). Also, it is possible that the linear relationship (13) is an artifact or pseudo-linear (Furlong and Chapman, 1987; Bachu, 1993) because it is related not to a vertical distribution of heat sources in a one-dimensional model, but rather to effects of multi-dimensional heat transfer in a heterogeneous crust. In

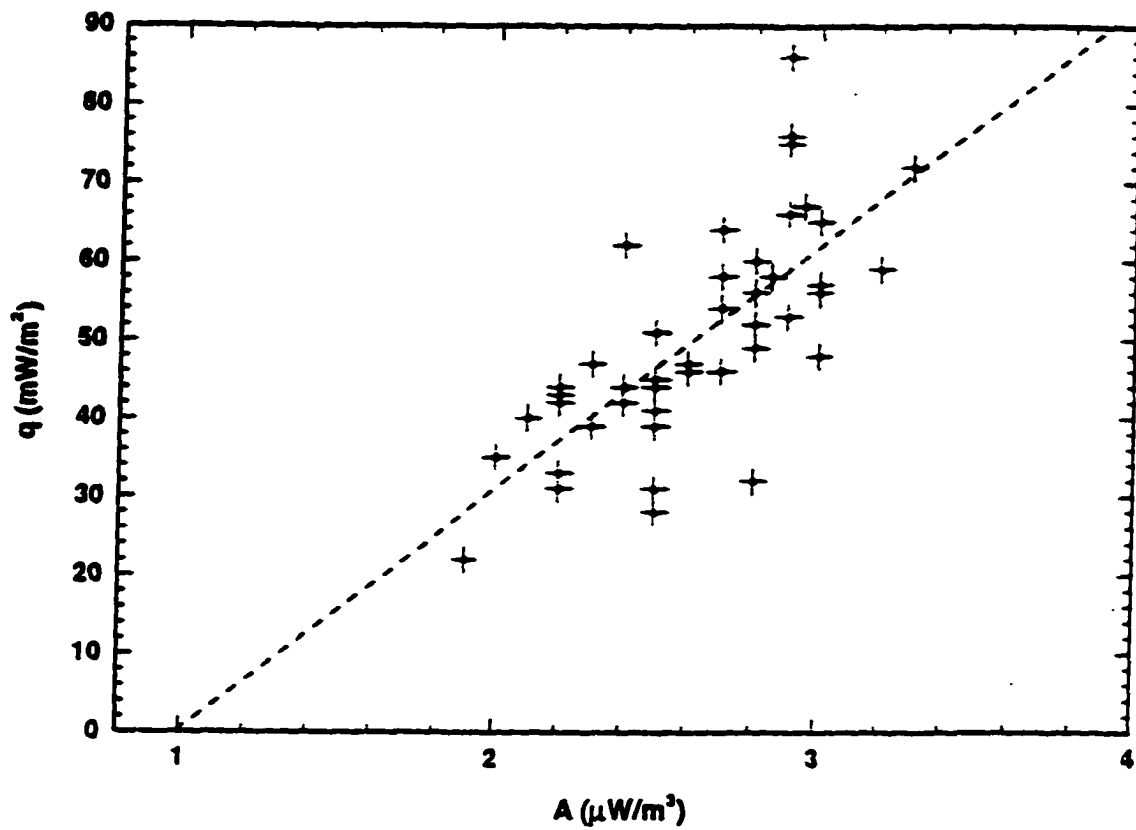


Fig. 16. Heat generation (A) - heat flow (q) relationship for Oklahoma. The intercept is - 30.4 mW/m² and the slope is 30.8 km. The coefficient of correlation is 0.51.

other words, the coupling of effects produced by variability in distribution of heat sources and by heterogeneities in crustal thermal conductivity may lead to a non-linear relationship between surface heat flow and heat generation.

The heat flow values estimated on the margins of the Anadarko and Arkoma Basins may be influenced by the thermal refraction (see next section). Finally, it is possible that the heat flow is disturbed by 3-dimensional effects of groundwater movement, such as low heat flow values belong to a recharge area, while high heat flow values occur in a discharge area.

In conclusion, I have found that the linear relationship between surface heat flow and surface radioactivity does not apply in Oklahoma. For the linear relation to hold, crustal contributions to surface heat flow should be exclusively from radioactivity, and the mantle flux should be uniform. These two conditions are probably violated in Oklahoma by one or more of the causes previously discussed. On the other hand, even though the heat flow - heat generation relationship fails to define a heat flow province in Oklahoma as defined by Roy et al. (1968), it must be said that radioactive heat generated in the basement rocks of Oklahoma is an important contributor to the thermal regime of the state and probably controls, to a large extent, this regime.

6.5. Effects due to contrasts in thermal conductivity

When rocks with different thermal conductivities meet along steeply dipping contacts, heat flows preferentially along the least resistant path, i.e., from less conductive rocks into more conductive rocks. This phenomenon, called thermal refraction, produces heat-flow contrasts because temperature is continuous across the contact, but thermal conductivity is not. The magnitude of the perturbation from the regional value is a function of

position, conductivity ratio, and the geometrical configuration of the two media. This perturbation cannot exceed the ratio of conductivities of the two rock types (Lachenbruch and Marshall, 1966).

Due to the contrast between low thermal conductivity of sedimentary rocks of the Arkoma Basin (~ 1.6 W/m-K) and the higher conductivity of the basement in the same basin (~ 3 W/m-K), the heat flow varies about 5 - 10 mW/m², from higher values in the northern part to lower values in the southern part of the Arkoma Basin (Lee et al., 1996). Carter et al. (1996) considered two situations for estimating thermal refraction in the Anadarko Basin: (1) the contrast between low thermal conductivity gabbros with low heat generation and high thermal-conductivity carbonates with low heat generation at the southern edge of the basin, and (2) the contrast between the high conductivity Pennsylvanian "granite wash" section in the south and the low conductivity Pennsylvanian shale section to the north. The modeled heat flow for the southern part of the Anadarko Basin is slightly perturbed (38 mW/m² calculated, 39 mW/m² measured); for the northern part of the Anadarko Basin the calculated heat flow is 48 to 51 mW/m², slightly lower than the observed heat flow data (55 - 64 mW/m²) for this area. The magnitude of refraction for the Anadarko Basin, according to Carter et al., (1996), varies between 2 and 3 mW/m².

In conclusion, the contrast between higher conductive basement rocks and lower conductive sedimentary rocks controls to a moderate to low extent the distribution of heat flow values in the Arkoma and Anadarko Basins, respectively.

6.6. Effects due to groundwater movement

The first right-side term of eq. (9) represents the upward convective

component of the surface heat flow. The most frequently encountered upward mass movements are magma rising and groundwater circulation. Since Oklahoma has not experienced volcanic activity for the last ~500 m.y. (Johnson et al., 1988), rising magma can be ruled out.

Groundwater circulation has been considered an important contributor to the heat flow regime in many areas, such as the Western Canadian Sedimentary Basin (Majorowicz and Jessop, 1981); the Uinta Basin in Utah (Chapman et al., 1984); the North Slope Basin in Alaska (Deming et al., 1992, 1996); the Williston Basin (Bachu and Hitchon, 1996) and the Northern Alberta Basin in Canada (Bachu, 1997). Heat flow is elevated in discharge areas and depressed in recharge areas. Moreover, regional fluid flow is a geologic process that has implications for various phenomena, including hydrocarbon maturation and migration, ore formation, and diagenesis.

Temperature distribution in a given basinal area is affected by the intrinsic properties of the medium and contained fluid: thermal diffusivity of the solid-fluid complex and the hydraulic conductivity, the water-table configuration and the ratio of basin depth to basin length (Domenico and Palciauskas, 1973). The extent to which basin hydrodynamics affect the thermal history of sediments and petroleum generation in a basin is primarily dependent on the magnitude of convective heat transfer. Convective heat transfer can vary considerably in sedimentary basins due to the differences in groundwater flow rates, the thickness of the sedimentary column, and the thermal conductivity of porous medium (Bredehoeft and Papadopoulos, 1965).

Jorgensen (1989, 1993) defined two regional aquifer systems and three regional groundwater flow systems in the south-central U. S. (Fig. 17). The Western Interior Plains aquifer extends from Nebraska in the north and

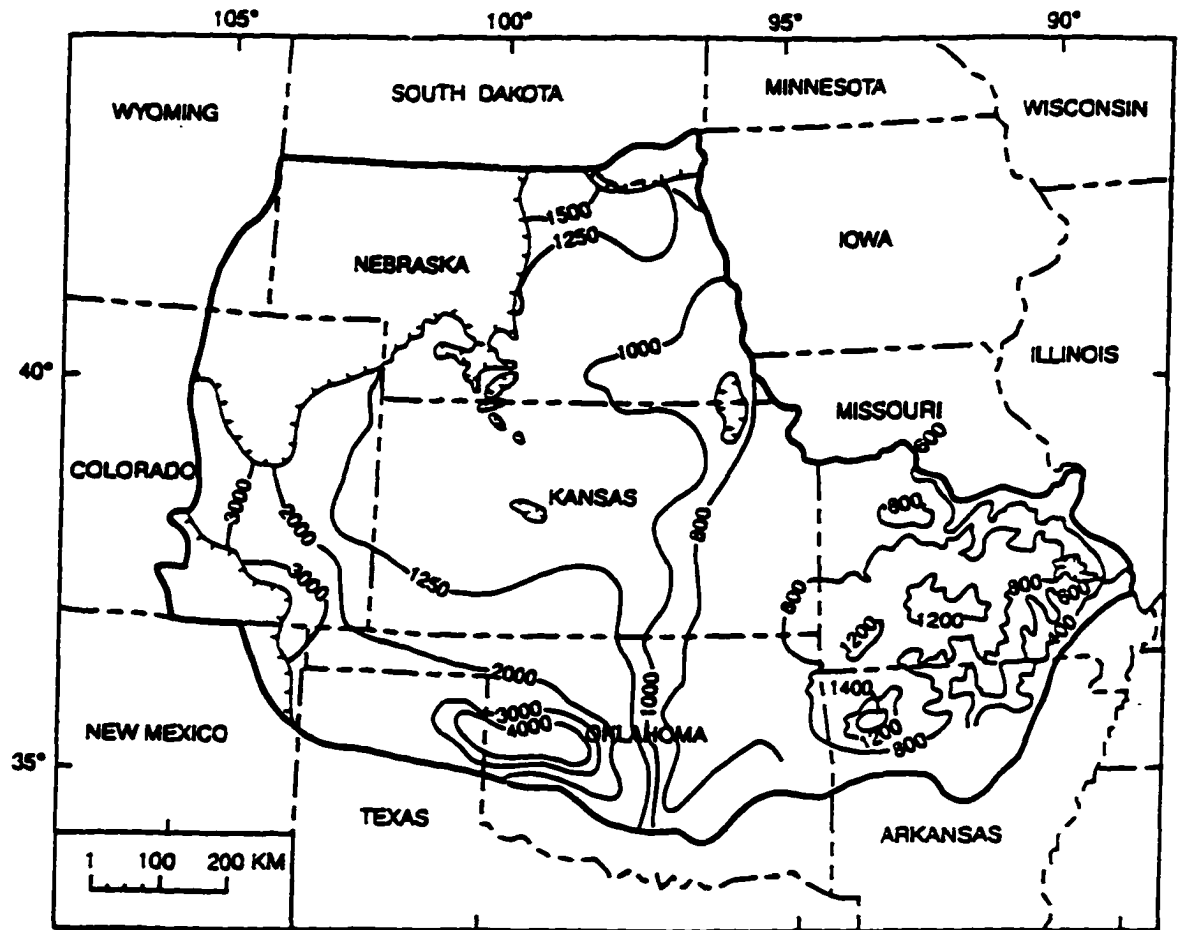


Fig. 17. Equivalent freshwater head, in ft (1 ft = 0.30 m), in Cambrian and Ordovician rocks of the Central United States (modified from Jorgensen, 1989). Hatchured lines represent western limit of Cambrian and Ordovician rocks.

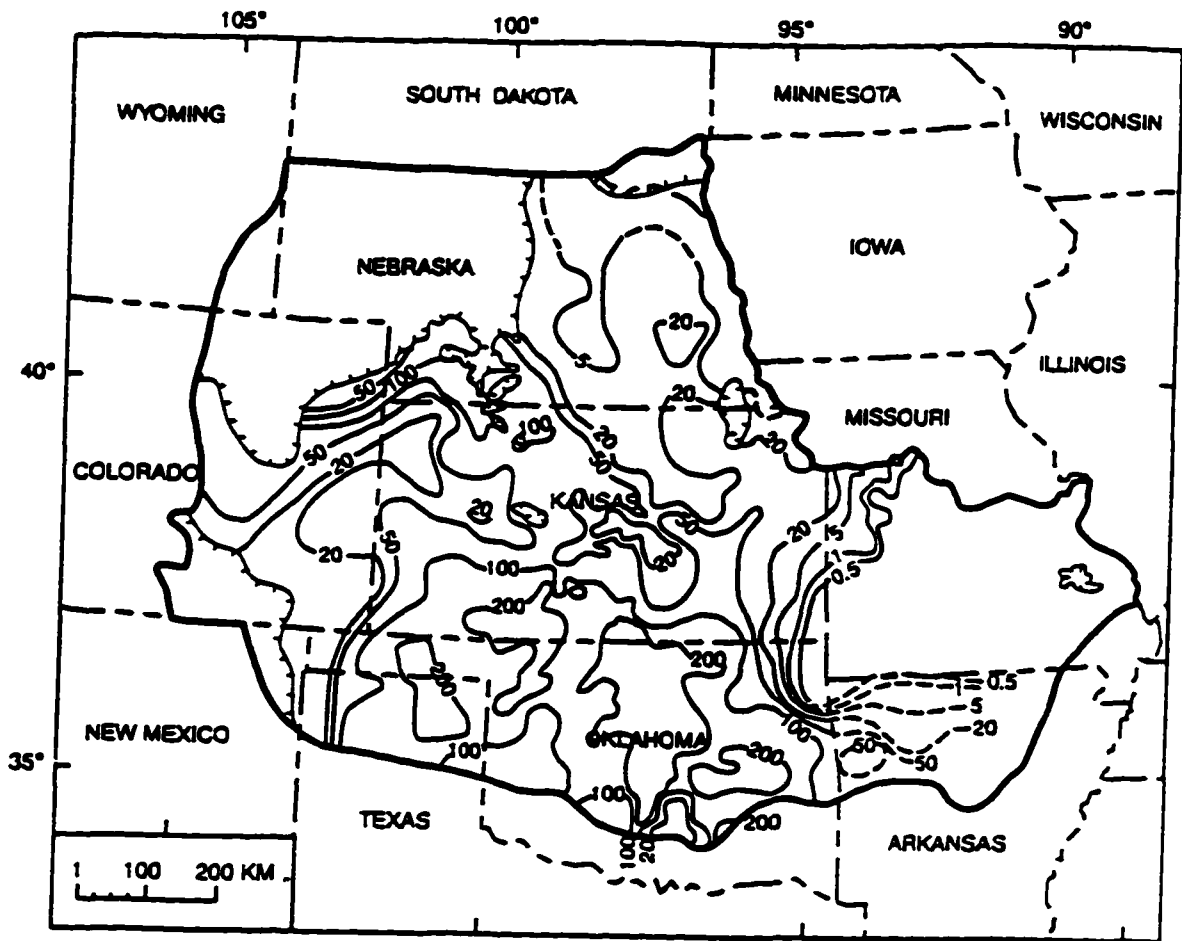


Fig. 18. Concentration of total dissolved solids (mg/liter) in groundwater from Cambrian and Ordovician rocks of the Central United States (modified from Jorgensen, 1989). Hatchured lines represent western limit of Cambrian and Ordovician rocks.

Colorado in the west, to Oklahoma in the south and westernmost Missouri and Arkansas in the east (Fig. 17). The Ozark Dome aquifer system extends through most of the southern half of Missouri and part of northern Arkansas (Fig. 17). The rocks composing the Western Interior Plains system area mainly represented by Cambrian - Mississippian dolostones, limestones, and sandstones. The Ozark Dome system is composed mainly of Cambrian - Ordovician dolostones, limestones, and sandstones.

The three regional flow paths in the Western Interior Plains and Ozark Dome aquifer systems can be traced from measurements of hydraulic heads (Fig. 17), formation water salinities (Fig. 18), and geochemical analyses (e.g., Banner et al., 1989). An eastward, topographically-driven flow path is defined by head decreases from 3000 feet (914 m) in Colorado to 800 feet (244 m) in northeastern Oklahoma and southeastern Kansas (Fig. 17). A westward flow path off the Ozark Dome is outlined by head decreasing from 1200 feet (366 m) in the center of the Ozark Dome in the south-central Missouri, to 800 feet (244 m) in northeastern Oklahoma and southeastern Kansas (Fig. 17). The third flow path originates from the overpressure zone of the Anadarko Basin (southwestern Oklahoma), where the head reaches a value of 4000 feet (1219 m) and spreads radially outward from the center of the Anadarko Basin (Fig. 17).

Geochemical analysis is another way of defining groundwater flow paths. For example, using isotopic and trace element analyses, Banner et al. (1989) concluded that saline groundwaters discharging from springs and artesian wells in central Missouri, north of the Ozark Dome, could have originated as meteoric recharge in the Front Range of Colorado. Another indication of groundwater circulation is related to total dissolved solutes (TDS) or solute content in groundwater. In general, TDS is relatively low in

active topographically-driven flow and is relatively high in areas with stagnant conditions. Jorgensen (1989, 1993) reported very low TDS levels (< 1 mg/liter) throughout most of the Ozark Dome that increase radially outward (Fig. 18), suggesting that there exists an active flow outward from the high elevations of the Ozark Dome into surrounding areas. The eastward groundwater flow path from Colorado is not clearly underlined by TDS decreasing. This might be explained by a slower topographically-driven flow through the West Interior Plains system than through the Ozark Dome system or perhaps a greater addition of solute from fluid-rock interactions caused by longer flow path. TDS increases from values of 20 - 50 mg/liter in central and northern Kansas, to values generally in the range of 100 - 200 mg/liter in south Kansas and most of Oklahoma.

An important parameter controlling groundwater circulation is permeability. Unfortunately, published permeability data of rocks in Oklahoma are rare. However, based on consideration of burial diagenesis, Jorgensen et al. (1993) estimated indirectly a range of permeability of lower units of the Western Interior Plains aquifer system (sandstones, dolostones, limestones) in Oklahoma from 10^{-16} m² in SW to 10^{-12} m² in NE. They also estimated the aquifers in the Ozark region to be most permeable, those in Kansas, Nebraska, and Colorado to be of intermediate permeability, and those in Oklahoma to be least permeable. These interpretations, together with the relatively high concentration of TDS in most Oklahoma rocks, suggest that most eastward flow through the Western Interior Plains system preferentially follows higher permeability pathways through Kansas rocks, bypassing Oklahoma. Although hydraulic head in the Anadarko Basin is as high as 4,000 feet (1,219 m, Fig. 17), the total amount of leakage from this overpressured basin is likely to be very small, or overpressure would not be

preserved (Deming, 1994c; Bredehoeft et al., 1994). Jorgensen (1989) described the amount of fluid escaping from the Anadarko Basin as "trivial". It is therefore unlikely that regional flow velocities from the Anadarko Basin are high enough to be an efficient heat transport mechanism and significantly influence the thermal regime of Oklahoma.

On the Anadarko shelf, permeability increases toward north and east, primarily due to weathering during Early Paleozoic erosion (Jorgensen, 1989). A slow rate of groundwater flow has been observed, generally from west to east, through the Arbuckle Group in Kansas (Carr et al., 1986) and northern Oklahoma (Jorgensen, 1989; Musgrove and Banner, 1993). Fairchild et al. (1982, 1990) and Fairchild and Davis (1983), studying groundwater movement in the Arbuckle Mountains in south-central Oklahoma, reported that in the eastern part of the area, the groundwater gradient is generally eastward and ranges 20 - 60 feet/mile (3.81 - 11.43 m/km). The flow direction indicated above is opposite to the flow direction coming off of the Ozark Dome in the northeastern corner of Oklahoma. The two flow systems meet in northeastern Oklahoma and their intersection must be marked by upwelling groundwater and elevated thermal gradients. Relatively high heat flow (70 - 80 mW/m²) in the northeastern part of the state (Fig. 13) may be related to upwelling groundwater where these two flow systems meet.

Conservation of energy requires that convective heat losses in groundwater recharge areas are balanced by convective heat gains in discharge areas. The geothermal gradient increases with increasing depth in recharge areas, decreases with increasing depth in discharge areas, and is unperturbed at the hinge line separating areas of recharge and discharge. If pure conduction is the dominating heat transfer mechanism in Oklahoma, then the vertical variations of q are relatively small and entirely due to heat

production. A convective component may be present if q varies significantly with depth. An upward convective component, suggesting a possible discharge area, means that heat flow near the top of the borehole is higher than the heat flow near the bottom of the well; conversely, a downward convective component yields the opposite.

An area of interest for studying the possible influence of groundwater movement on surface heat flow is the northeastern part of Oklahoma (Fig. 13), where heat flow estimates are higher than 70 mW/m^2 . These relatively high heat flow values are not fully explained by heat generation from the crust because, according to Figure 12, the area is not underlined by a high heat production crust. Moreover, two sites situated in this area (site #8, Fig. A15 and site #10, Fig. A19) show an apparent decrease of heat flow with depth, suggesting the presence of a discharge area. As said earlier, this area might represent the meeting place of upward movement of groundwater flowing off of the Ozark Dome and the groundwater flowing toward northeast from the Arbuckle Mountains.

According to Darcy's law, fluid flow is expected between any two points with a finite permeability and non-zero potential energy gradient. The topographic gradient (~ 0.001) from the Arbuckle Mountains toward northeast is non-zero, permeability is finite, and thus there must exist some topographically driven fluid flow from southwest to northeast with concomitant heat transport.

Intense experimental and research work has been done on the Arbuckle-Simpson aquifer in the Arbuckle Mountains (Fairchild et al., 1982, 1990; Fairchild and Davis, 1983; Barthel, 1985; Hanson and Cates, 1994). These rocks are of Late Cambrian to Middle Ordovician age and are composed of dolomites, limestones and sandstones with thickness ranging from 1,500 m to

2,700 m. These rocks were subjected to intensive folding and faulting related to major uplift of the area during Early to Late Pennsylvanian time. Associated with the major fault zones are numerous faults and joints that occur in the more dense beds, such as the Arbuckle carbonate rocks. Geologic structure is of significance because fractures caused by folding and faulting provide channels for groundwater movement. Acid water enters the fractures, joints and bedding planes and enlarges them by solution. The result is an irregular network of openings of all sizes and shapes, extending both vertically and horizontally, and thus favoring groundwater circulation. Recharge to/discharge from the aquifer is estimated at about 4.7 inches/year (3.78×10^{-9} m/s). Almost 100 springs discharge water from the Arbuckle-Simpson aquifer to streams that drain the Arbuckle Mountains area (Fairchild et al., 1982, 1990).

The relatively high heat flow area from the northeastern part of Oklahoma (Fig. 13), not fully explained by radiogenic heat produced in the crust, may be caused partly by upward groundwater movement, traveling about 125 km from the Arbuckle Mountains area under a head drop $\Delta h \approx 139$ m, similar to the elevation drop across that distance.

The ratio between convective and conductive heat flow in an area (Peclet number, Pe) can be used to estimate the influence of groundwater movement on the surface heat flow distribution. Considering the Arbuckle Mountains area (#8 on Fig. 13) as a recharge area (Johnson, 1991), where surface heat flow varies between 30 and 40 mW/m^2 , and the area situated at northeast from the Arbuckle Mountains, where surface heat flow ranges 70 - 80 mW/m^2 , as a discharge area, along with the average surface heat flow in Oklahoma (50 mW/m^2), it appears that the ratio of convective to conductive heat flow (Peclet number) is about 1. When groundwater flow is in a steady-

state regime, in a idealized, two-dimensional basin, with homogeneous and isotropic properties, Peclet number (Pe) can also be defined as (Domenico and Palciuskas, 1973):

$$Pe = \frac{\Delta h k \Delta z \rho^2 g C}{2 \mu \lambda_{pr} L} \quad (13)$$

where Δh is the total head drop across a basin of length L and depth Δz , k is permeability, ρ is fluid density, C is fluid specific heat, g is the acceleration due to gravity, μ is fluid dynamic viscosity, and λ_{pr} is the thermal conductivity of a porous rock (matrix and fluid). If we consider the head drop to be equal to the elevation drop across a distance L from the Arbuckle Mountains to the northeast site with highest surface heat flow, $\Delta h/L = 139 \text{ m}/125,000 \text{ m}$. Taking $\Delta z = 2,000 \text{ m}$, $\rho = 1,000 \text{ kg/m}^3$, $g = 9.8 \text{ m/s}^2$, $C = 4,200 \text{ J/kg-K}$, $\lambda_{pr} = 1.68 \text{ W/m-K}$, $\mu = 6 \times 10^{-4} \text{ kg/m.s}$ (pure water at 40°C), a Peclet number $Pe = 1$ will yield an average permeability k of $2.2 \times 10^{-14} \text{ m}^2$.

The permeability k can be estimated independently using hydraulic conductivity K , fluid dynamic viscosity μ , acceleration due to gravity g , and fluid density ρ , according to relation:

$$k = \frac{K \mu}{\rho g} \quad (14)$$

With $K = 5 \times 10^{-6} \text{ m/s}$ ("the highest hydraulic conductivity", as indicated by Hanson and Cates, 1994, p. 52), the highest permeability in the Arbuckle - Simpson aquifer is $3 \times 10^{-13} \text{ m}^2$, which is one order of magnitude greater than permeability constrained by heat flow distribution. This difference comes from the fact that measurements made to estimate the highest hydraulic

conductivity were performed on superficial rocks (the average depth of wells used in pumping experiments was less than 100 m), where intensive folding and fracturing associated with major uplift of the area during Early to Late Pennsylvanian time have created an extensive network of fractures, thus increasing hydraulic conductivity. In other words, the hydraulic conductivity of the deep Arbuckle-Simpson aquifer is likely to be one order of magnitude less than the highest value found using pumping tests. Jorgensen et al. (1993) estimated indirectly the permeability of Upper Cambrian through Upper Mississippian age rocks in and near the Arbuckle Mountains area to be in the range 10^{-14} - 10^{-15} m².

The groundwater is moving with a Darcy velocity v given by the following relation:

$$v = K \frac{\Delta h}{L} \quad (15)$$

Using the previous data, the relatively high heat flow estimates in the northeastern Oklahoma can be explained by groundwater movement through the Arbuckle-Simpson aquifer with a Darcy velocity of about 3.6×10^{-10} m/s or ~ 1 cm/yr.

In conclusion, effects of groundwater movement on heat flow regime of Oklahoma may be important, at least for the Arbuckle Mountains area. More data about permeability would provide a more complete picture of these effects.

7. SUMMARY AND CONCLUSIONS

A heat flow map of Oklahoma was constructed using 40 previously published data-sets and 20 new heat flow data-sets, as well as other 191 constraining values distributed within 30° - 40°N, 90° - 105°W area. The 20 new heat flow data were estimated by using discrete temperature measurements made by American Petroleum Institute researchers from 1926 through 1929 and 1,498 thermal conductivity measurements on drilling cuttings using the cell technique. Every thermal conductivity value was corrected for anisotropy, *in situ* temperature, and porosity.

The mean of 20 average thermal gradients was 30.50°C/km. In general, thermal gradients increase from SW (14.11°C/km) to NE (42.24°C/km). The range of 1,498 *in situ* thermal conductivity measurements was 0.9 - 6.1 W/m-K; the average was 1.68±0.07 W/m-K. Thermal conductivity varies slightly with geologic age and lithology as follows: Permian age samples have an average matrix conductivity of 1.63±0.04 W/m-K; Pennsylvanian age samples have an average matrix thermal conductivity of 1.84±0.02 W/m-K; Mississippian age samples have an average matrix thermal conductivity of 1.78±0.08 W/m-K; the one Devonian age sample has a matrix conductivity of 1.51 W/m-K, and Ordovician age samples have an average matrix thermal conductivity of 1.50 W/m-K.

The average heat flow for 20 new sites in Oklahoma varies between 22±4 mW/m² (in SW) and 86±17 mW/m² (in NE); the mean is 50 mW/m². The surface heat flow distribution in Oklahoma exhibits a relatively low heat flow area (< 30 mW/m²) in SW (covering parts of the Marietta Basin, Hollis Basin, and Wichita Uplift) and a relatively high heat flow area (> 70 mW/m²) in the northeastern part of the Cherokee Platform. Between these two areas, there is an area of low-to-intermediate heat flow (30 - 50 mW/m²) with a

large extent (it covers parts of the Hollis, Ardmore, Marietta, and Anadarko Basins as well as parts of the Arbuckle, Wichita, and Ouachita Uplifts) and an area of intermediate-to-low heat flow (50 - 70 mW/m²), covering parts of the Cherokee Platform, Ozark Uplift, Anadarko Shelf, and Arkoma Basin.

A heat generation map of Oklahoma was constructed using 22 previously published values and 27 new data. The new heat production estimates of basement rocks in Oklahoma were made using gamma-ray logs and a relationship between gamma-ray values and heat production rates.

The 27 new heat generation determinations range from 1.1 to 3.5 $\mu\text{W}/\text{m}^3$, with an average of 2.51 $\mu\text{W}/\text{m}^3$. The heat production estimations varies with the type of basement rocks as follows: Carlton rhyolite - 2.2 \pm 0.06 $\mu\text{W}/\text{m}^3$; Mesozonal granite - 2.5 \pm 0.07 $\mu\text{W}/\text{m}^3$; Wichita province - 2.2 \pm 0.2 $\mu\text{W}/\text{m}^3$; Rhyolite - 2.5 \pm 0.13 $\mu\text{W}/\text{m}^3$, and metamorphic rocks - 1.7 $\mu\text{W}/\text{m}^3$. There is a trend of increasing of heat production rates from SW (values < 2 $\mu\text{W}/\text{m}^3$) to NE (values > 3 $\mu\text{W}/\text{m}^3$). The area with the lowest heat production (< 1.5 $\mu\text{W}/\text{m}^3$) lies in the southeastern parts of the Arkoma Basin and the Arbuckle Uplift. Areas with the highest heat production (> 3 $\mu\text{W}/\text{m}^3$) occupy the north central part of the Anadarko Basin, the northern part of the Anadarko Shelf, a small portion of the western Cherokee Platform, and isolated patches on the Ozark Uplift and the northeastern corner of the state. The heat generation map of Oklahoma contains inherent uncertainties due to the lack of uniformly distributed values and ambiguities inherent in the kriging procedure used to interpolate individual values.

A detailed error analysis was performed on temperature data, thermal gradients, thermal conductivity measurements (sampling error, measurement error, correction error), heat production, and heat flow. Using the propagation of error technique for uncorrelated random variables, the

final heat flow error was estimated to be $\pm 17\%$. However, considering various uncertainties involved in estimating the magnitude of errors, a rounded heat flow error of $\pm 20\%$ was used for the final heat flow estimates.

Several causes were analyzed in relation with surface heat flow regime of Oklahoma. Transient effects of sedimentary processes and metamorphic /igneous activity do not significantly influence this regime because sedimentation ceased ~ 250 m.y. ago and erosion decreased exponentially with increasing time. Moreover, Oklahoma has not experienced metamorphic or igneous activity for the last ~ 500 m.y. Also, past climatic changes have no significant influence on the present day heat flow regime of Oklahoma.

Thermal refraction, due to contrasts between basement rocks, with higher thermal conductivity, and sedimentary rocks, with lower thermal conductivity, controls in a low-to-moderate way the distribution of surface heat flow values in the Anadarko and Arkoma Basins.

Heat flow regime of Oklahoma appears to be conductive-controlled by the variable distribution of heat generation sources. A comparison between the heat flow map and the heat generation map of Oklahoma, as well as the two cross-sections (N-S and NE-SW), shows many concordances between heat flow values and heat production rates. However, heat flow - heat generation relationship fails to define Oklahoma as a simple heat flow province. There are some discrepancies revealed by this comparison (the relatively lowest and highest heat flow areas do not correspond to the relatively lowest and highest heat productions, respectively), suggesting that the conductive heat flow is probably perturbed by groundwater movement.

As an example, the groundwater circulation through the Arbuckle-Simpson aquifer from the Arbuckle Mountains to NE is analyzed. Constrained by the surface heat flow distribution, the ratio of convective to

conductive heat flow (Peclet number) equal to 1 yields a regional permeability of $\sim 10^{-14}$ m² and a Darcy velocity of groundwater movement in the Arbuckle-Simpson aquifer of ~ 1 cm/yr.

APPENDIX A

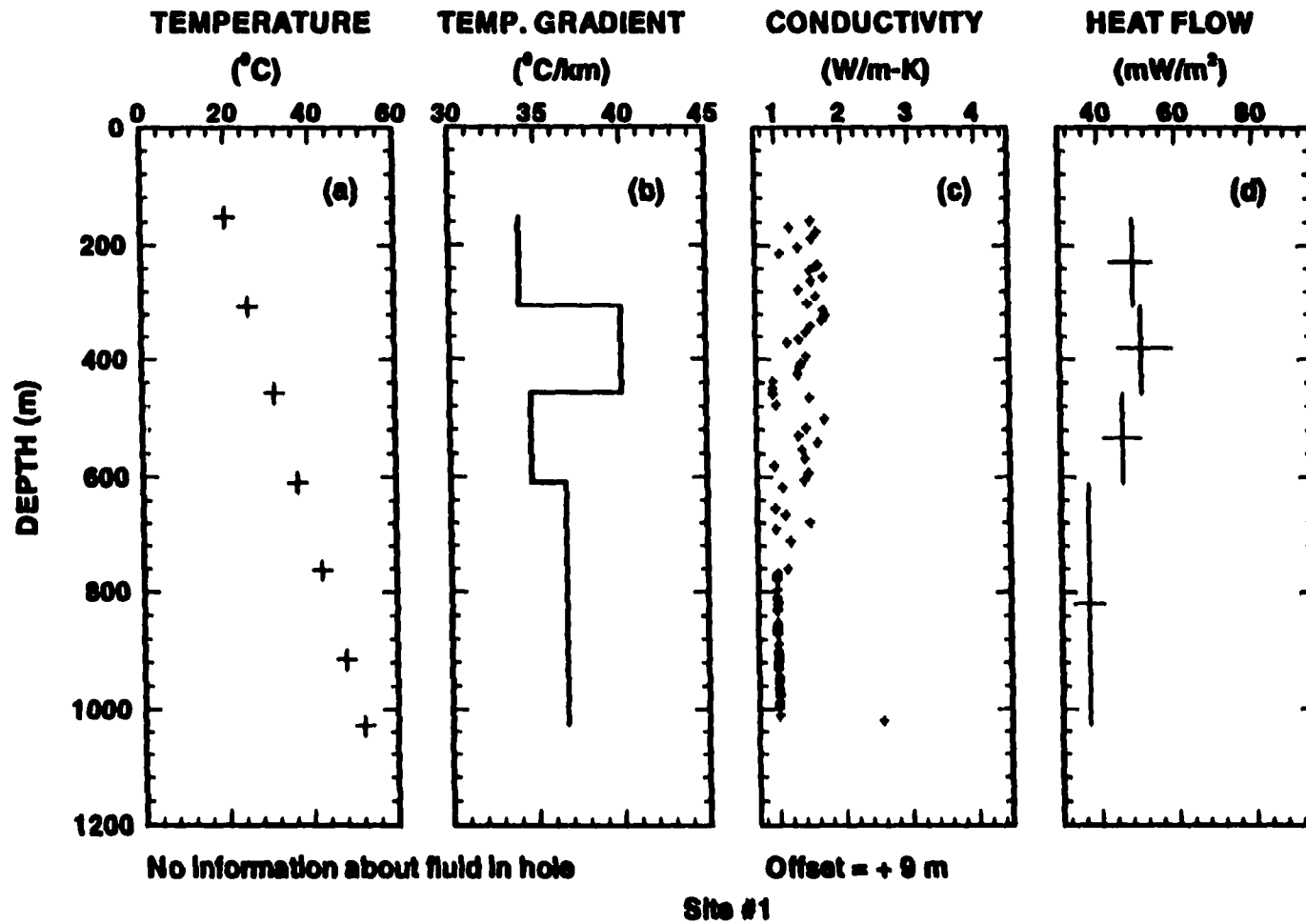


Fig. A1. Temperature (a), thermal gradient (b), thermal conductivity (c), and heat flow (d) distribution with depth at site #1 (for location, see Table 1 and Fig. A2)

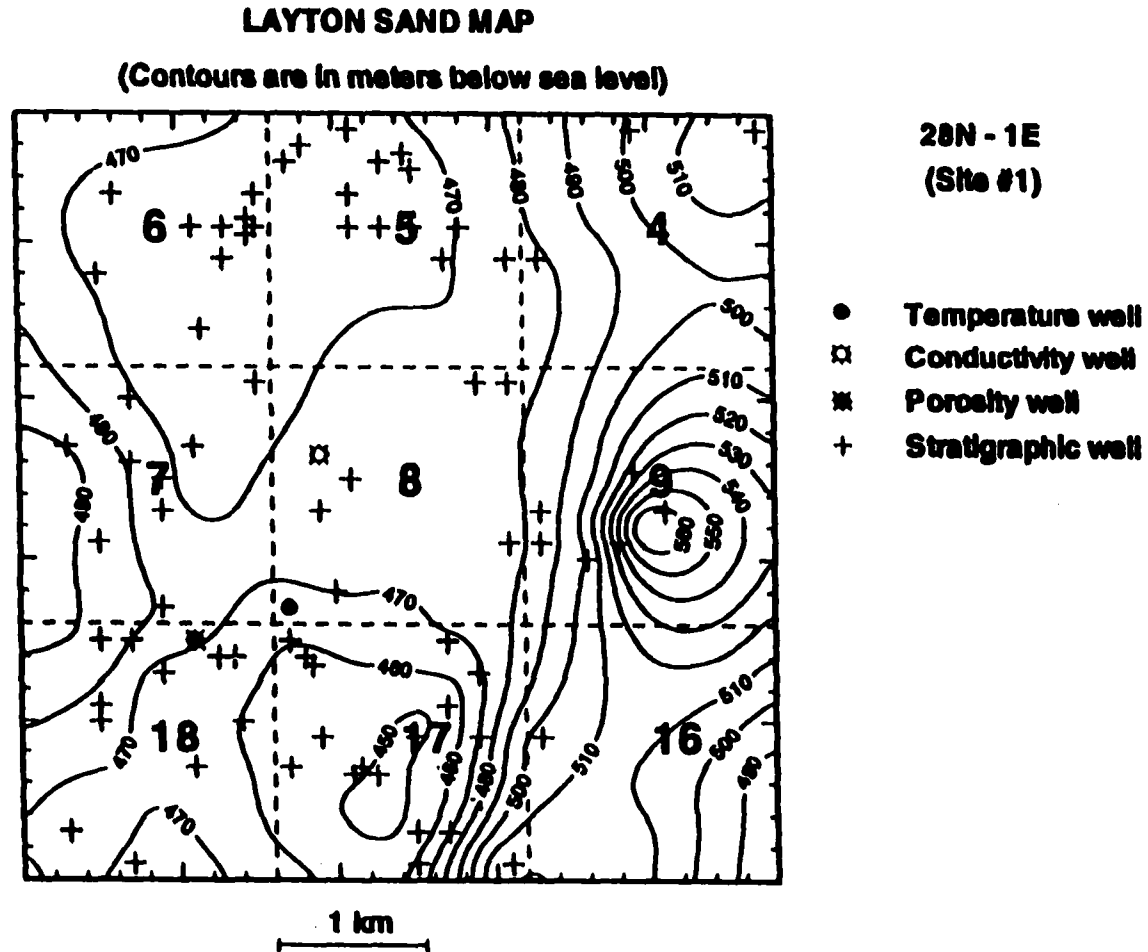


Fig. A2. Stratigraphic map of Layton sand at site #1. The bold numbers in the center of dashed squares represent section numbers of the township and range indicated on the top right side of the figure.

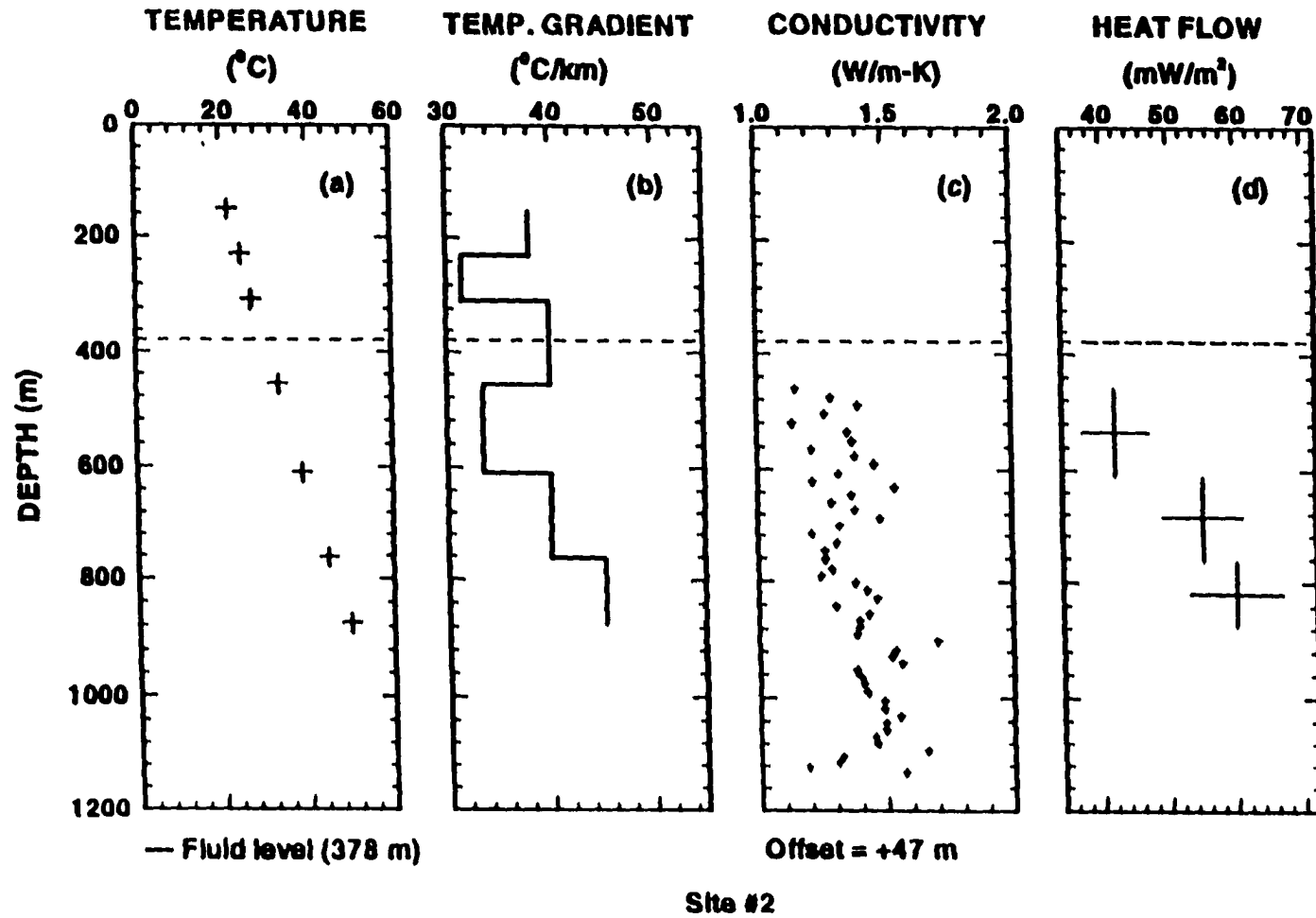


Fig. A3. Temperature (a), thermal gradient (b), thermal conductivity (c), and heat flow (d) distribution with depth at site #2 (for location, see Table 1 and Fig. A4)

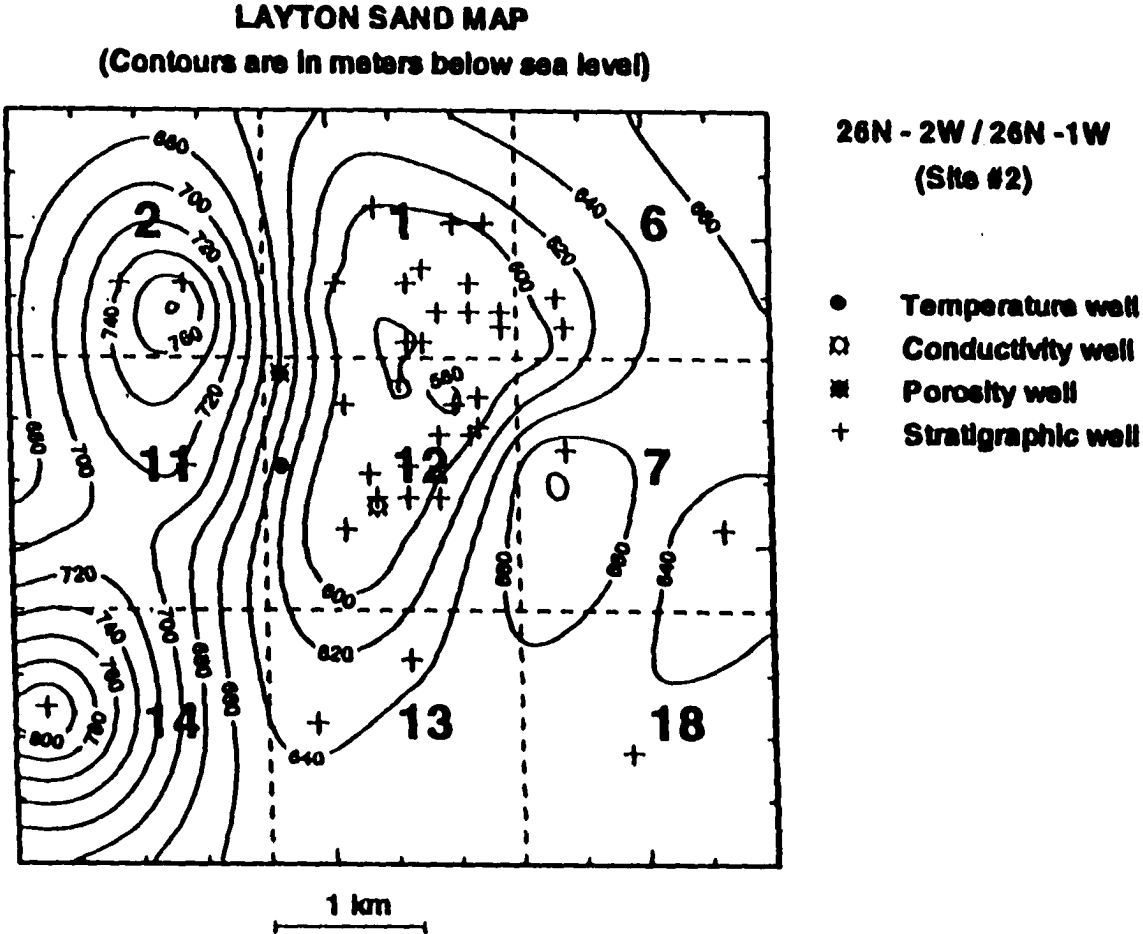


Fig. A4. Stratigraphic map of Layton sand at site #2. The bold numbers in the center of dashed squares represent section numbers of the township and range indicated on the top right side of the figure.

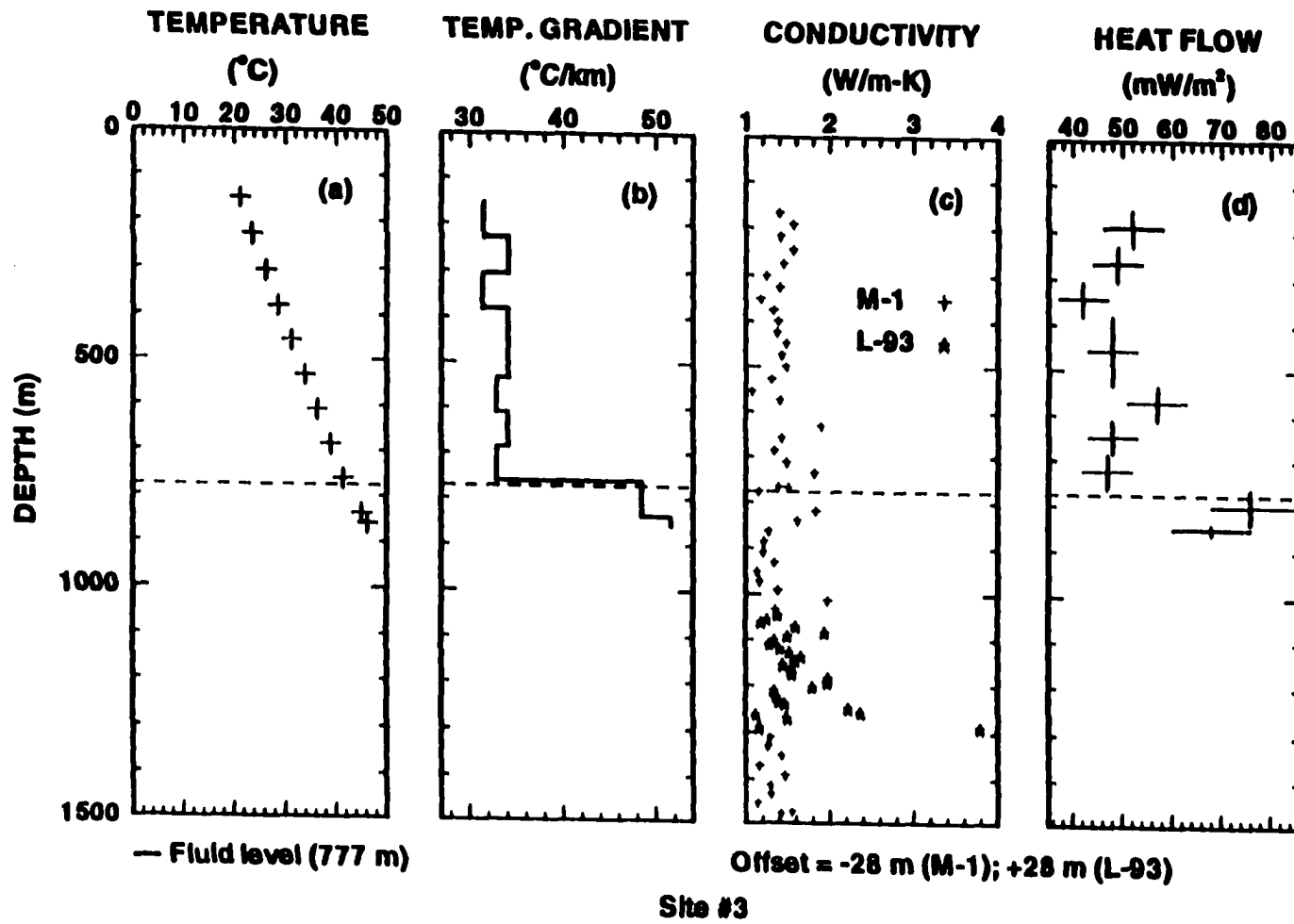


Fig. A5. Temperature (a), thermal gradient (b), thermal conductivity (c), and heat flow (d) distribution with depth at site #3 (for location, see Table 1 and Fig. A6)

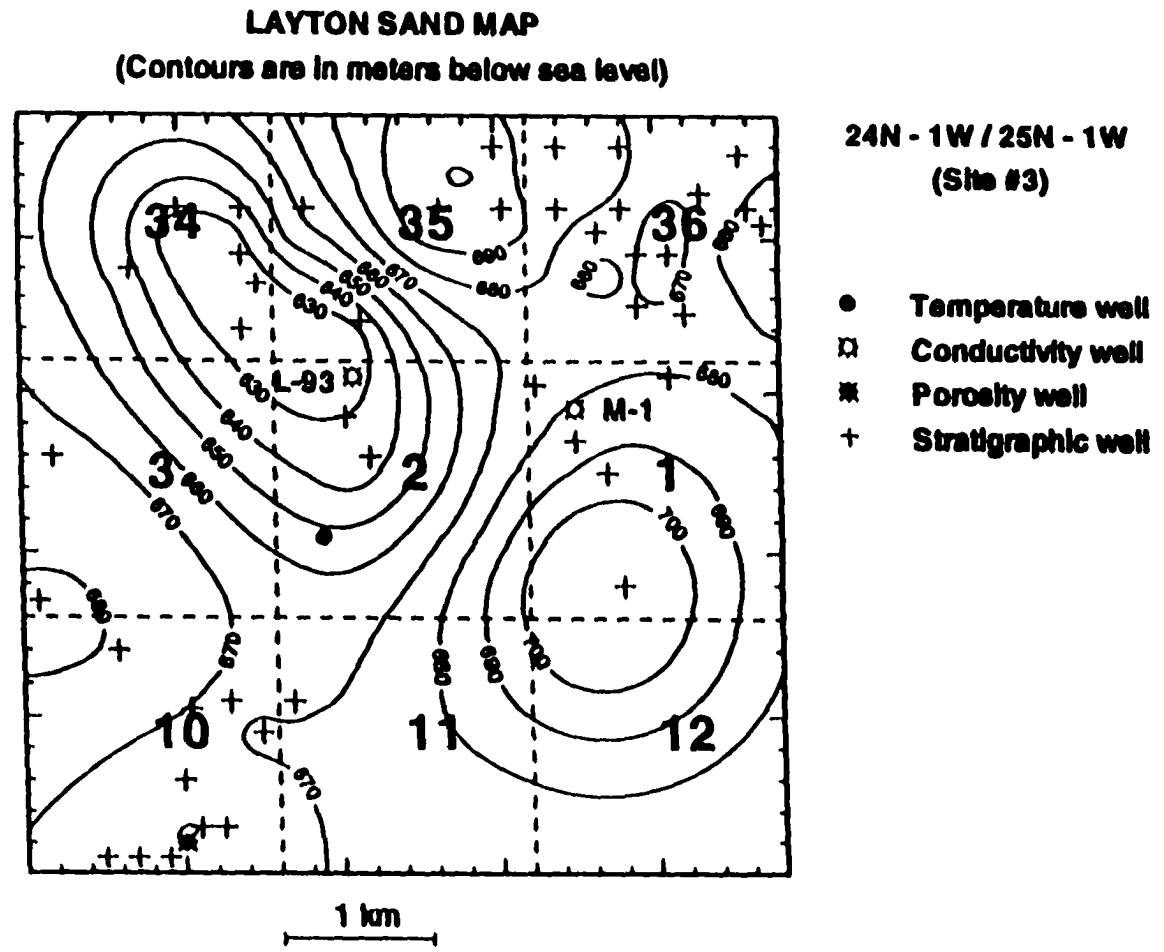


Fig. A6. Stratigraphic map of Layton sand at site #3. The bold numbers in the center of dashed squares represent section numbers of the township and range indicated on the top right side of the figure.

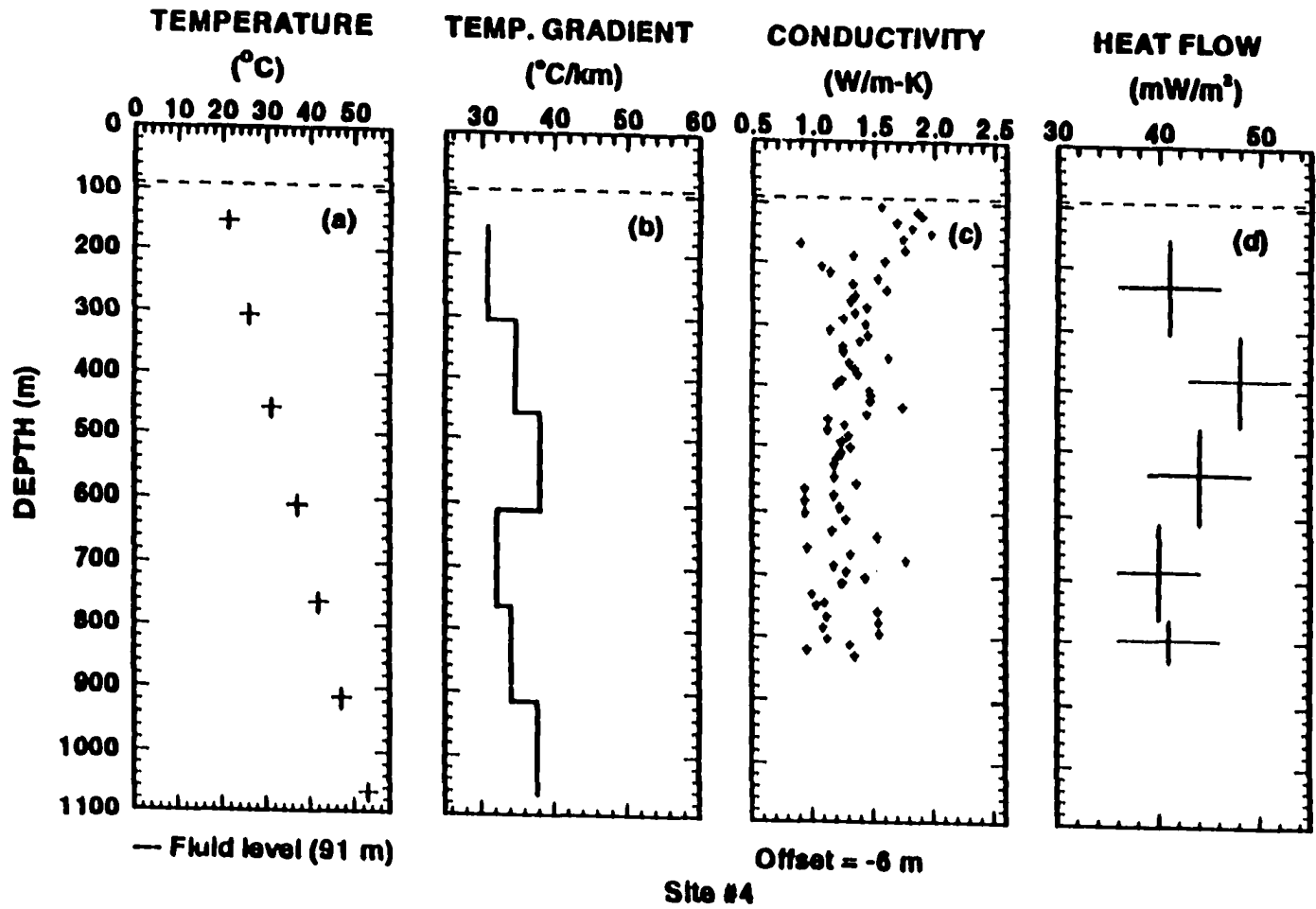


Fig. A7. Temperature (a), thermal gradient (b), thermal conductivity (c), and heat flow (d) distribution with depth at site #4 (for location, see Table 1 and Fig. A8)

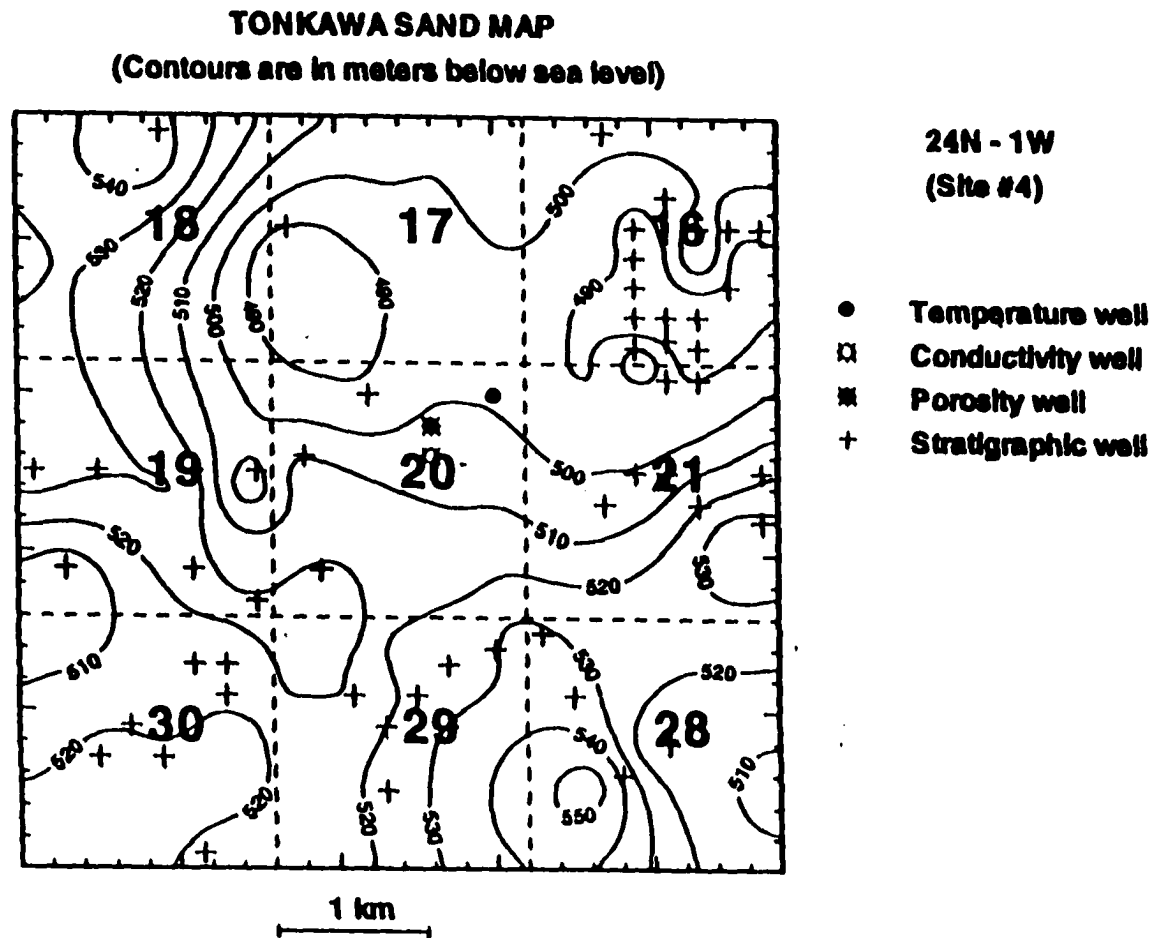


Fig. A8. Stratigraphic map of Tonkawa sand at site #4. The bold numbers in the center of dashed squares represent section numbers of the township and range indicated on the top right side of the figure.

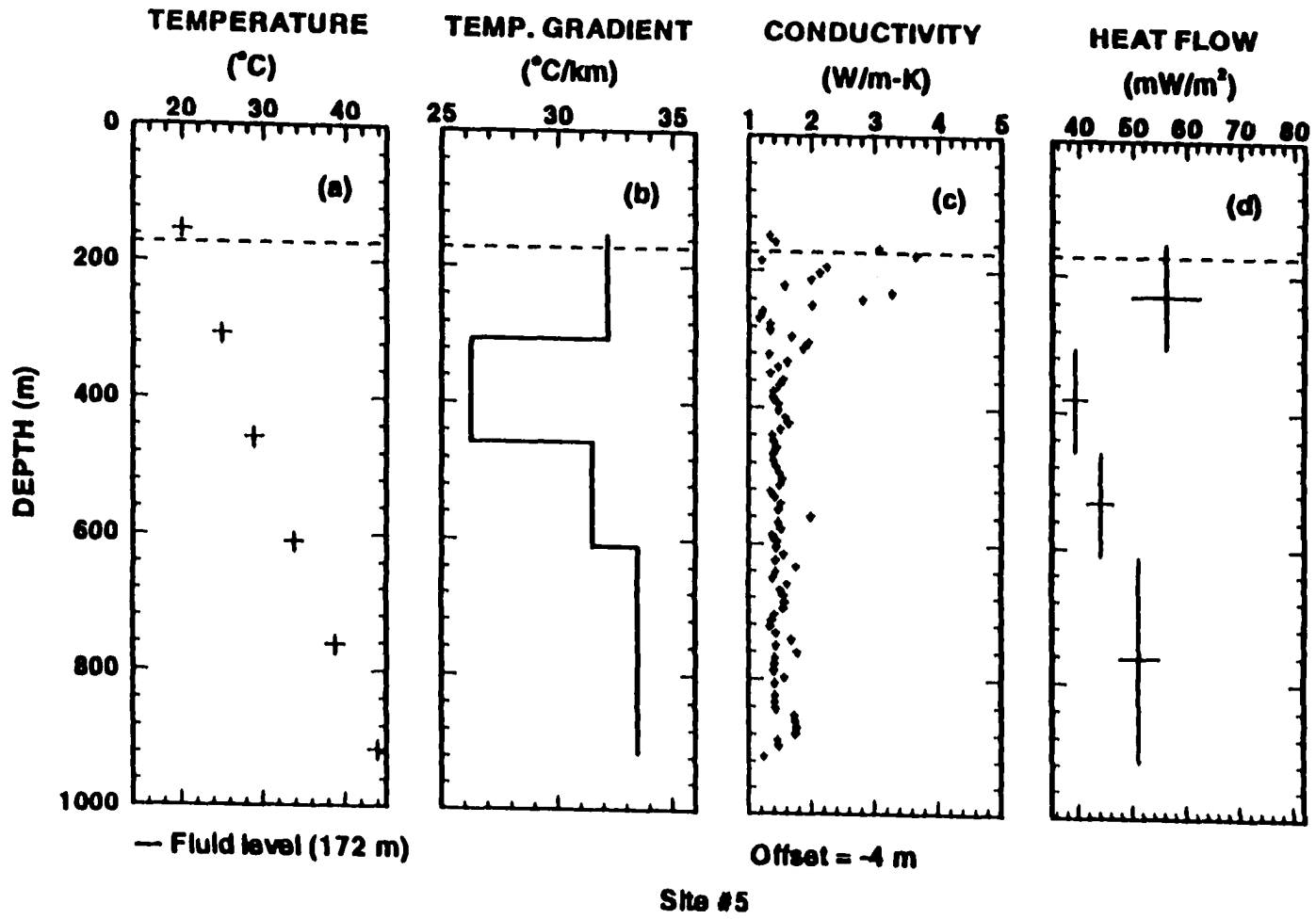


Fig. A9. Temperature (a), thermal gradient (b), thermal conductivity (c), and heat flow (d) distribution with depth at site #5 (for location, see Table 1 and Fig. A10)

OREAD LIMESTONE MAP
 (Contours are in meters below sea level)

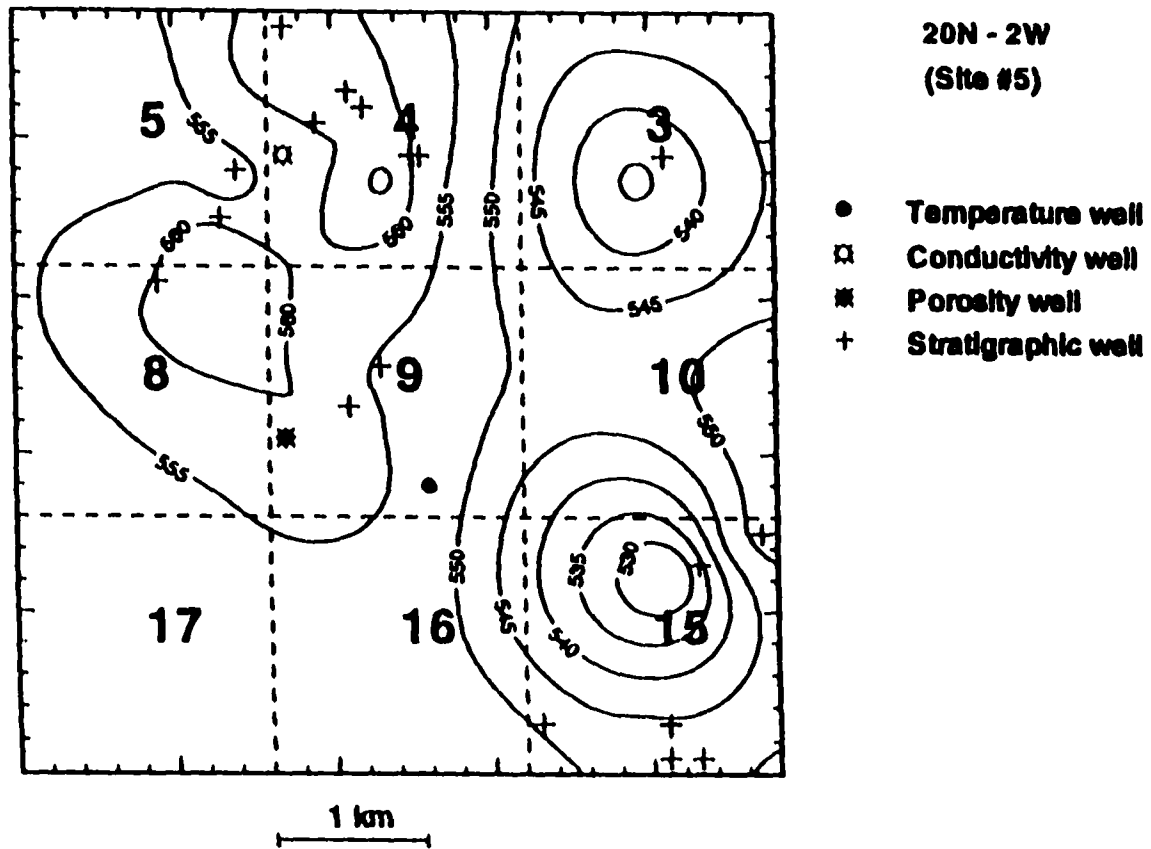


Fig. A10. Stratigraphic map of Oread limestone at site #5. The bold numbers in the center of dashed squares represent section numbers of the township and range indicated on the top right side of the figure.

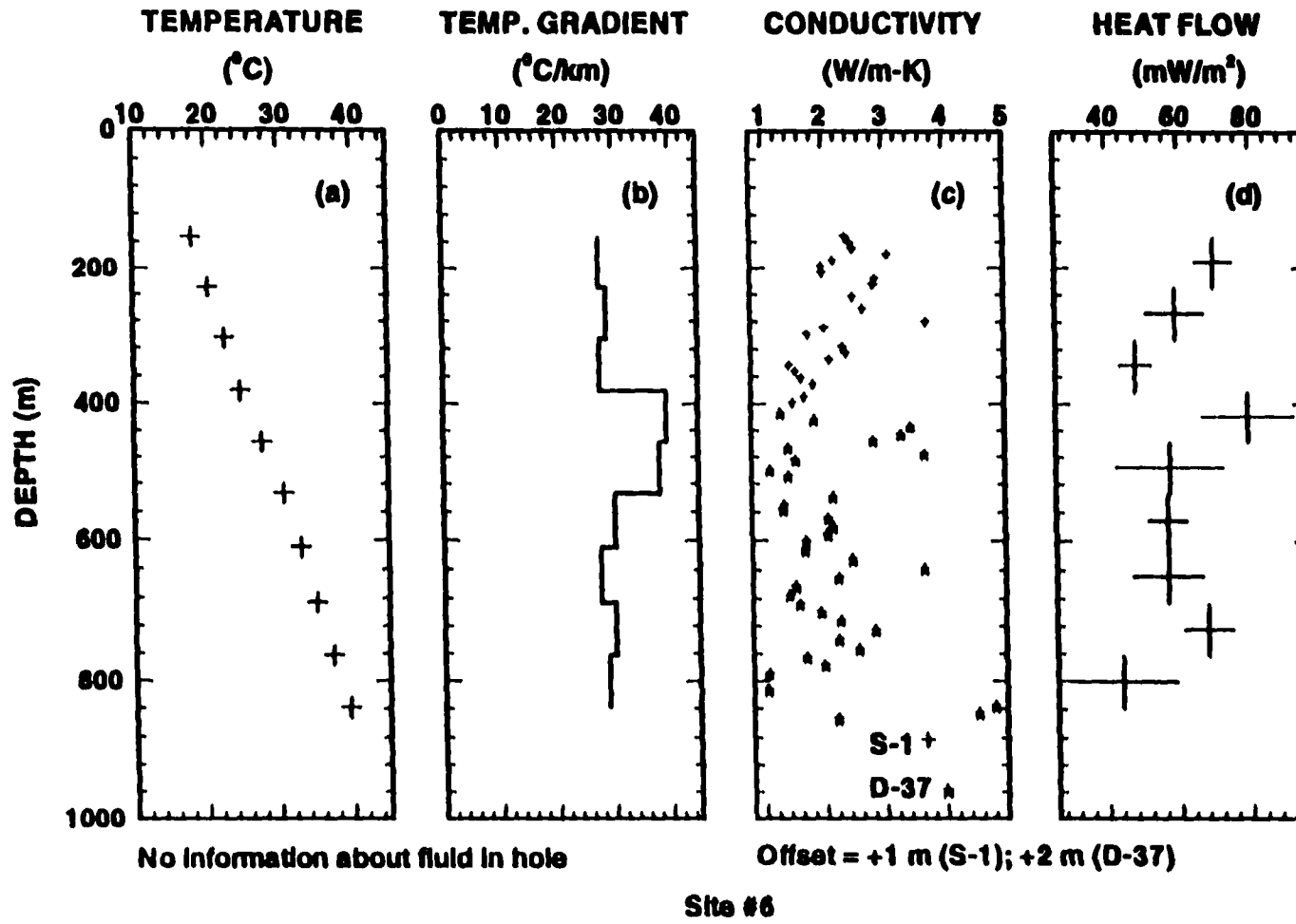


Fig. A11. Temperature (a), thermal gradient (b), thermal conductivity (c), and heat flow (d) distribution with depth at site #6 (for location, see Table 1 and Fig. A12)

LAYTON SAND MAP
 (Contours are in meters below sea level)

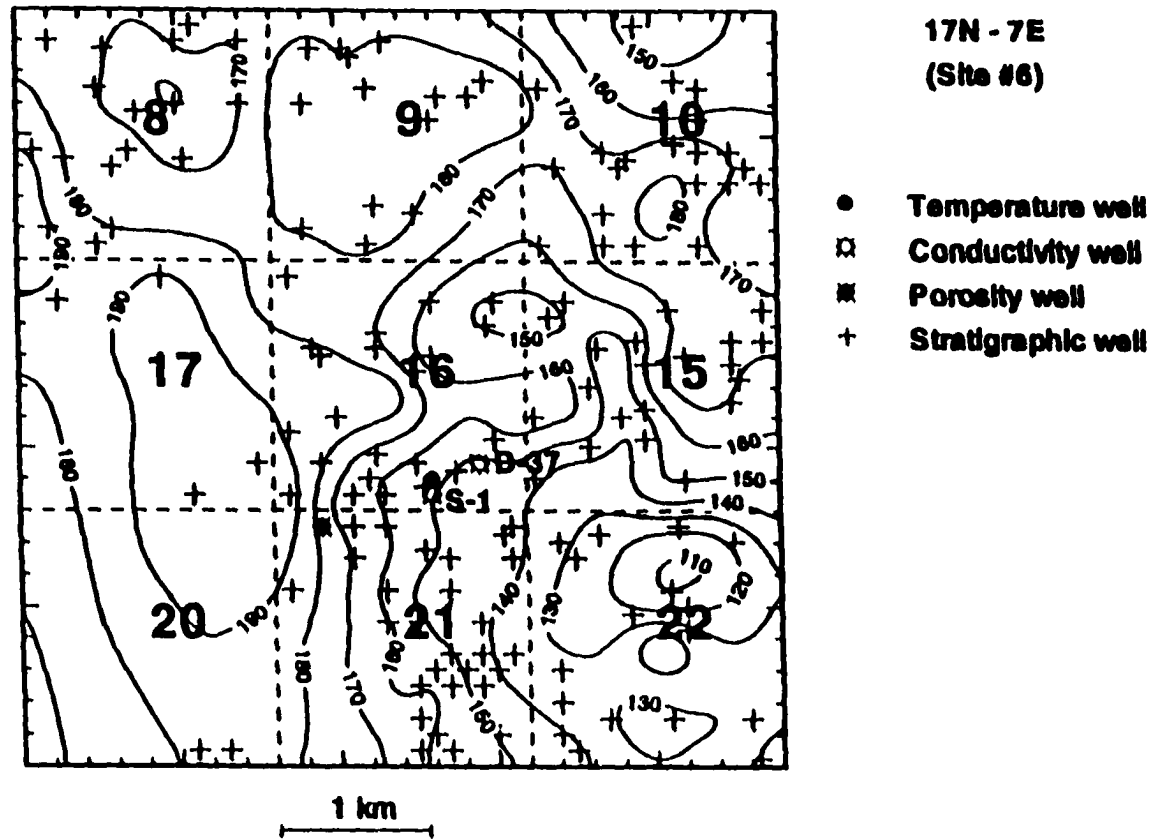


Fig. A12. Stratigraphic map of Layton sand at site #6. The bold numbers in the center of dashed squares represent section numbers of the township and range indicated on the top right side of the figure.

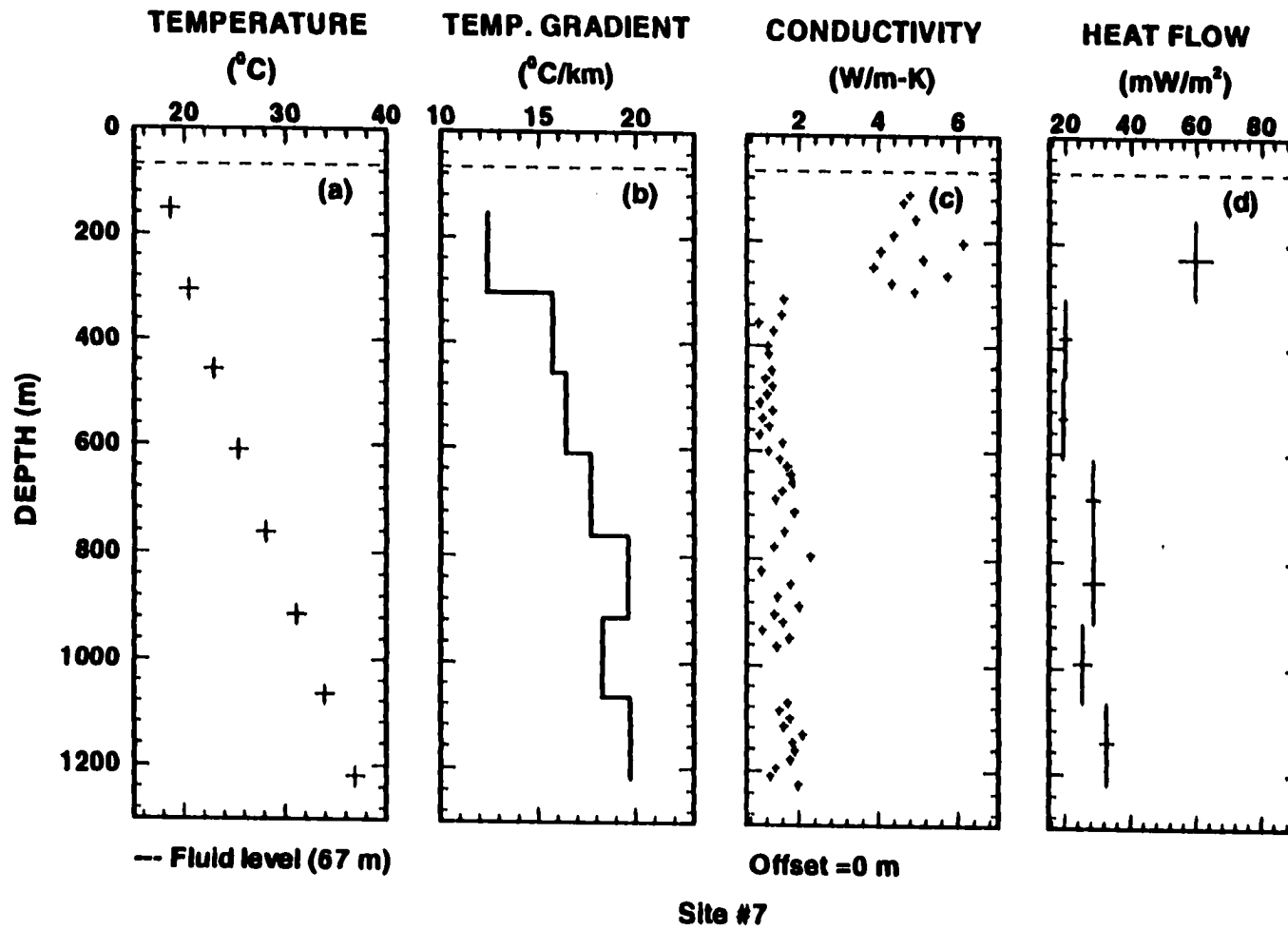


Fig. A13. Temperature (a), thermal gradient (b), thermal conductivity (c), and heat flow (d) distribution with depth at site #7 (for location, see Table 1 and Fig. A14)

LAYTON SAND MAP
 (Contours are in meters below sea level)

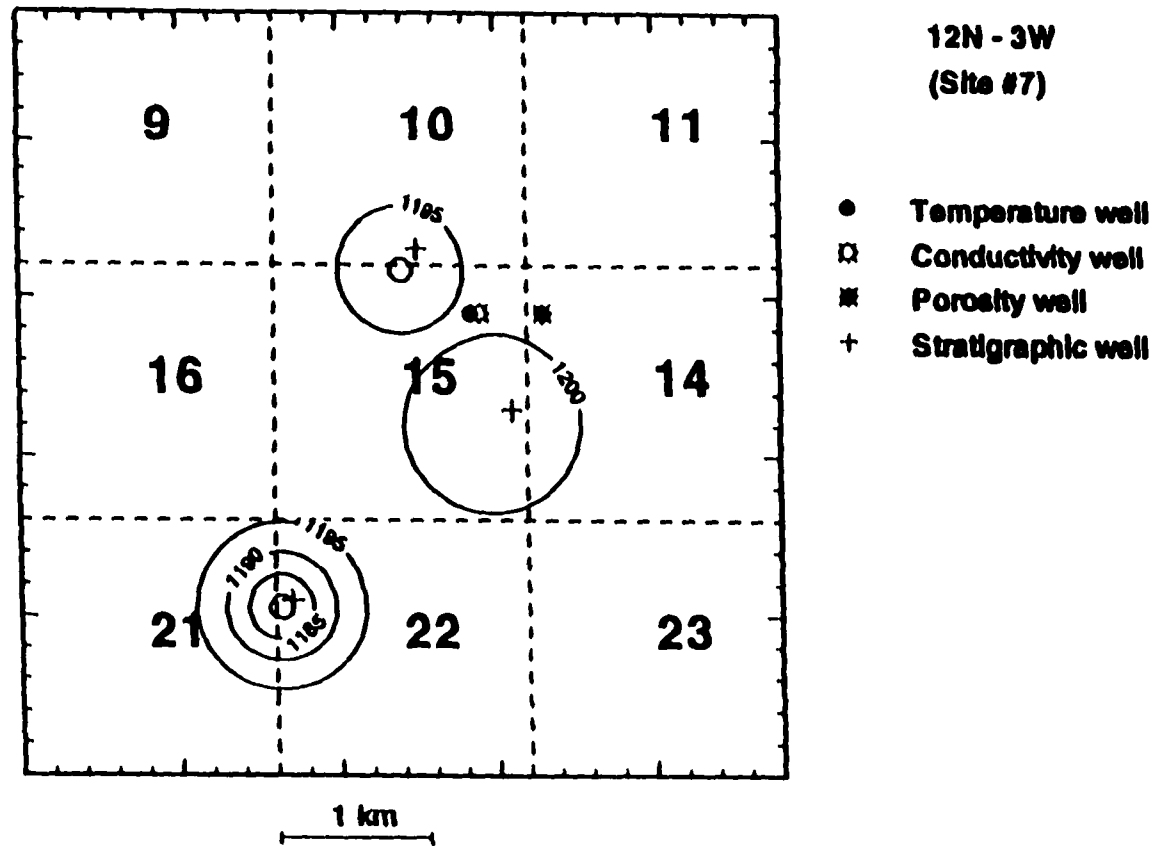


Fig. A14. Stratigraphic map of Layton sand at site #7. The bold numbers in the center of dashed squares represent section numbers of the township and range indicated on the top right side of the figure.

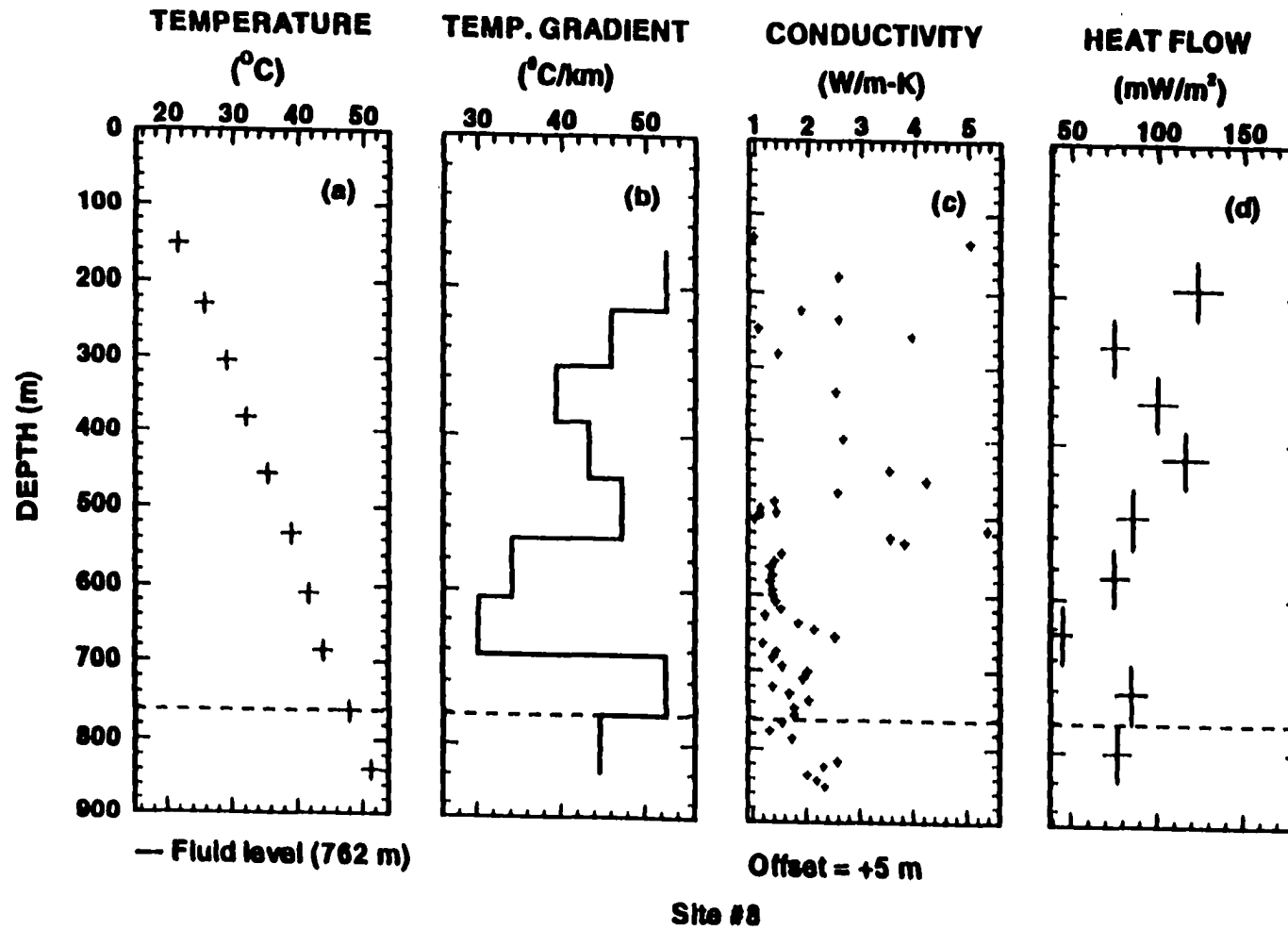
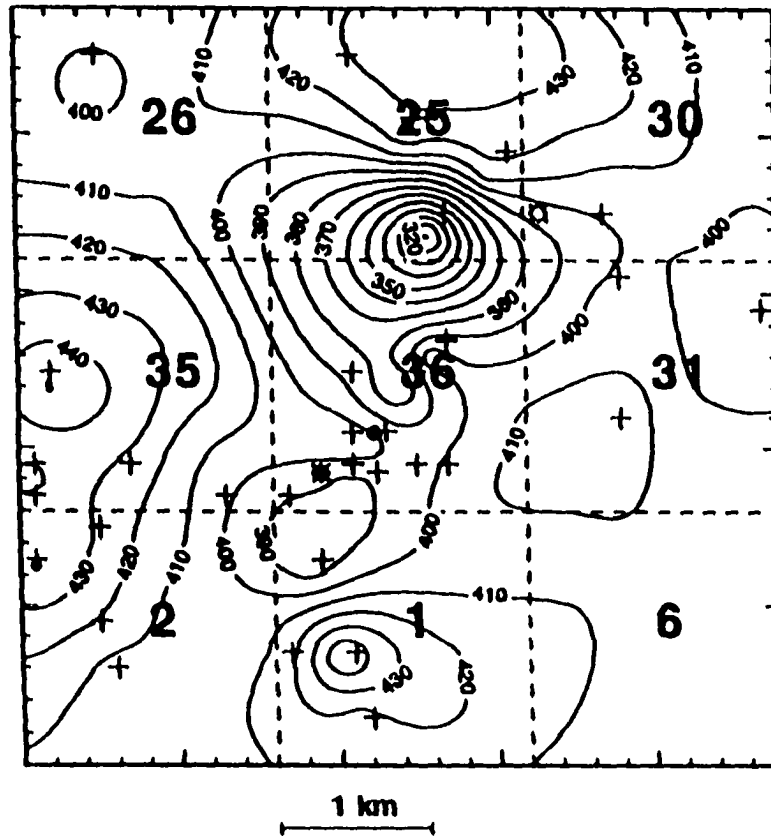


Fig. A15. Temperature (a), thermal gradient (b), thermal conductivity (c), and heat flow (d) distribution with depth at site #8 (for location, see Table 1 and Fig. A16)

BARTLESVILLE SAND MAP
 (Contours are in meters below sea level)



11N - 10E / 12N - 10E
 11N - 11E / 12N - 11E
 (Site #8)

- Temperature well
- ⊠ Conductivity well
- ⊞ Porosity well
- + Stratigraphic well

Fig. A16. Stratigraphic map of Bartlesville sand at site #8. The bold numbers in the center of dashed squares represent section numbers of the township and range indicated on the top right side of the figure.

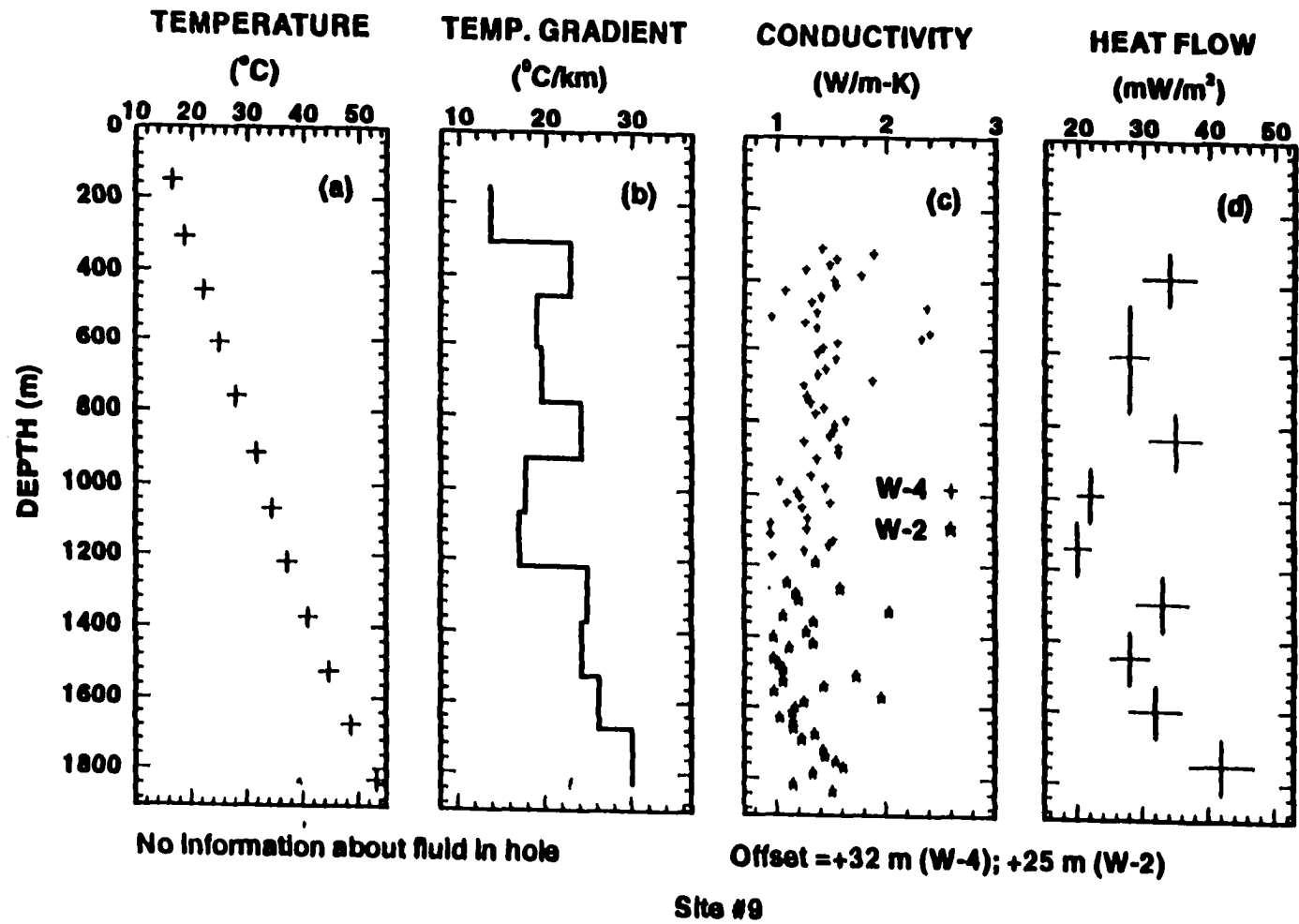


Fig. A17. Temperature (a), thermal gradient (b), thermal conductivity (c), and heat flow (d) distribution with depth at site #9 (for location, see Table 1 and Fig. A18)

LAYTON SAND MAP
 (Contours are in meters below sea level)

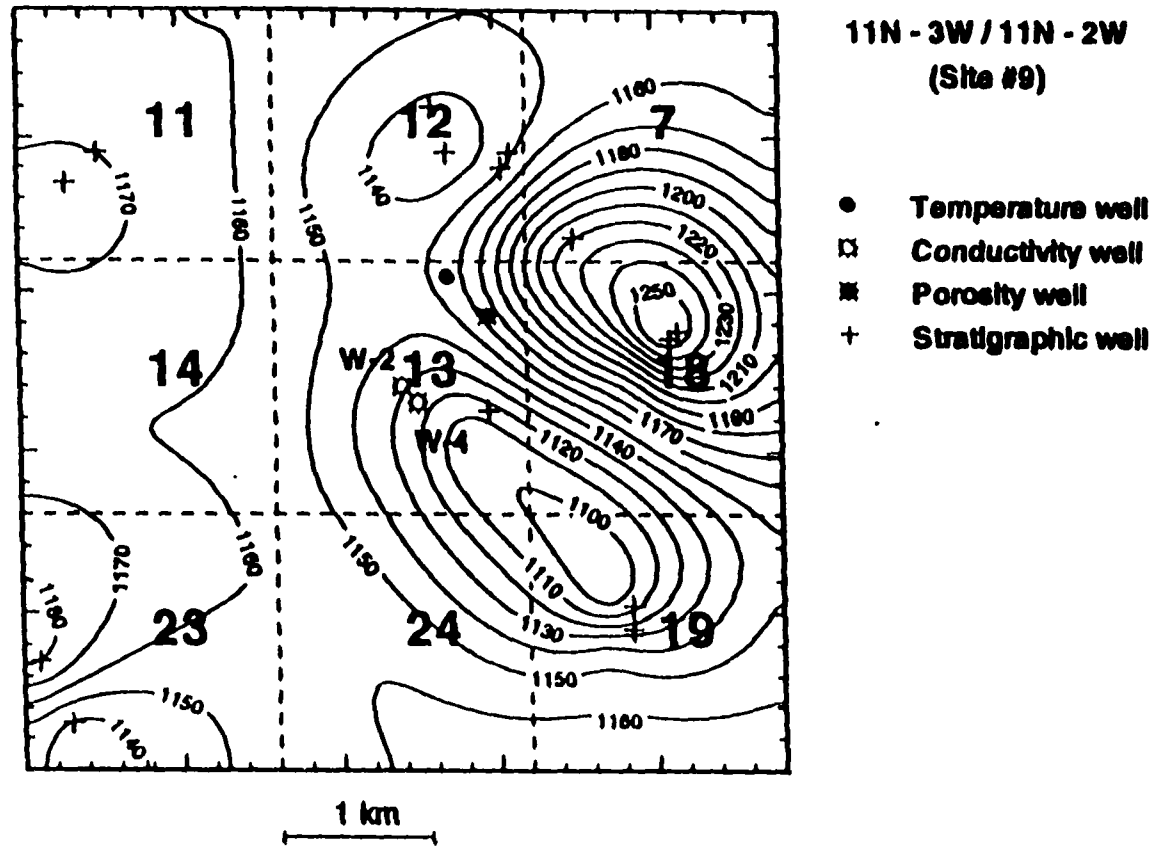


Fig. A18. Stratigraphic map of Layton sand at site #9. The bold numbers in the center of dashed squares represent section numbers of the township and range indicated on the top right side of the figure.

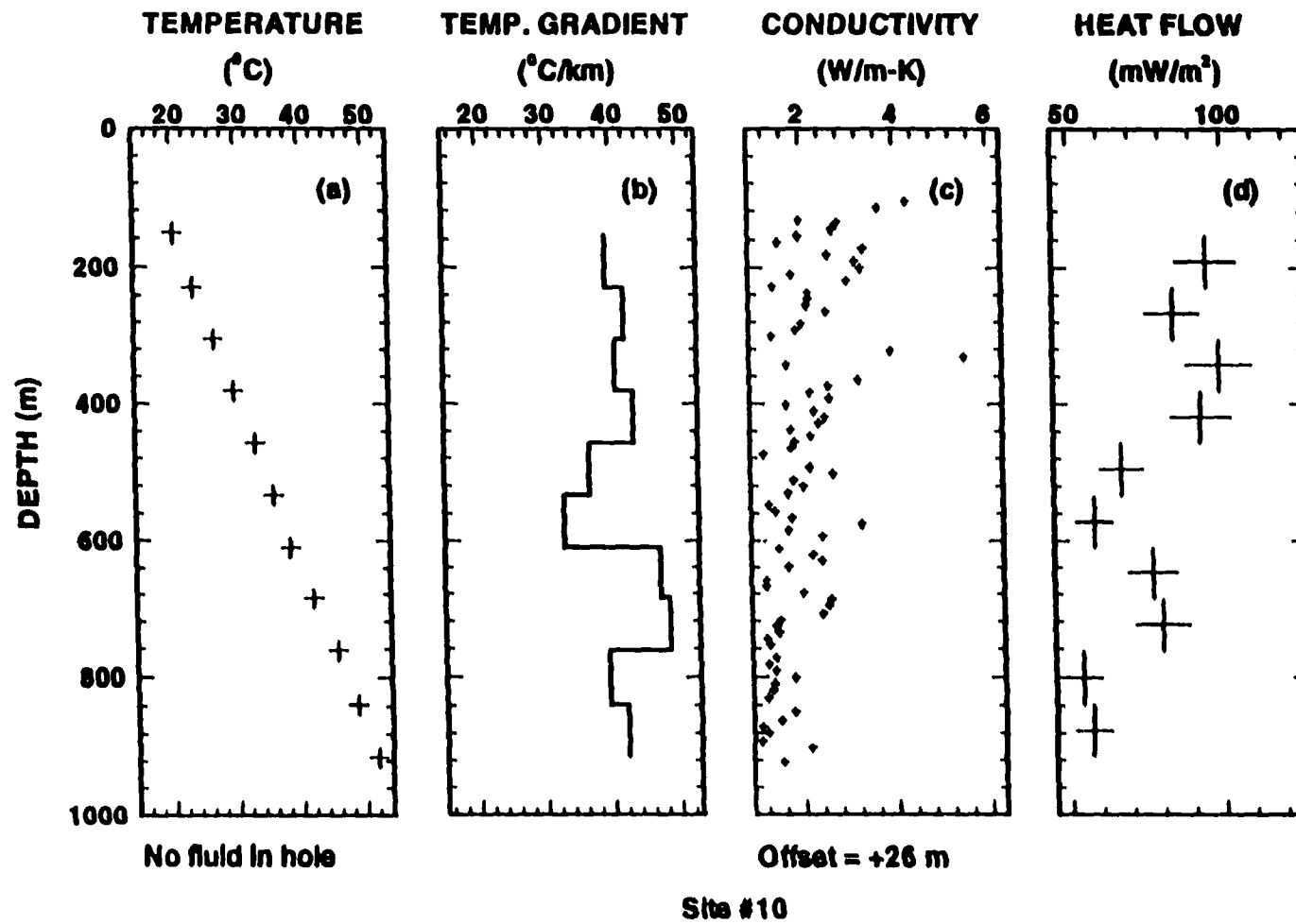
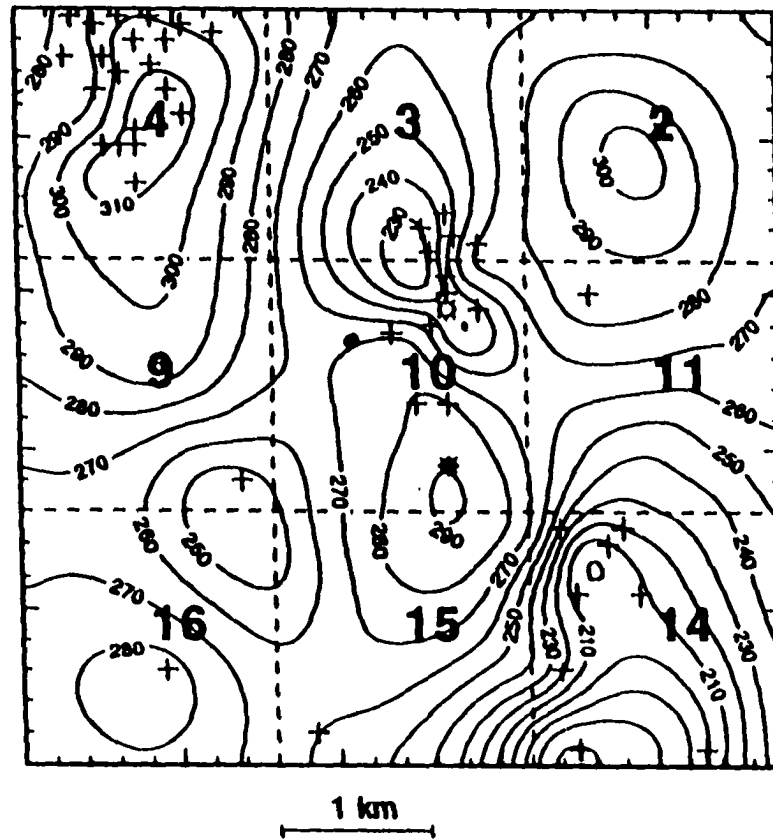


Fig. A19. Temperature (a), thermal gradient (b), thermal conductivity (c), and heat flow (d) distribution with depth at site #10 (for location, see Table 1 and Fig. A20)

CALVIN SAND MAP
 (Contours are in meters below sea level)



10N - 8E
(Site #10)

- Temperature well
- ⊠ Conductivity well
- ⊞ Porosity well
- + Stratigraphic well

Fig. A20. Stratigraphic map of Calvin sand at site #10. The bold numbers in the center of dashed squares represent section numbers of the township and range indicated on the top right side of the figure.

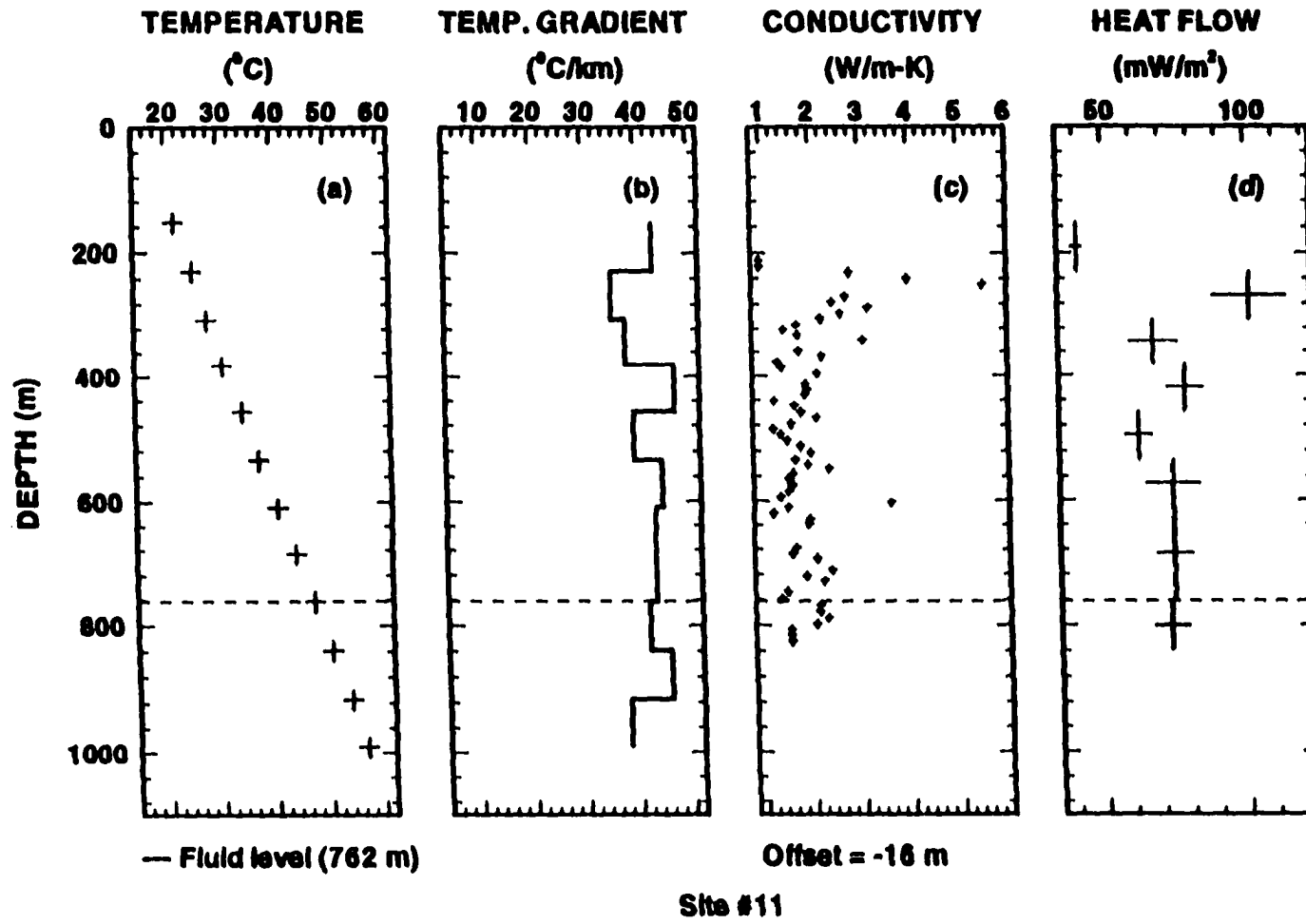


Fig. A21. Temperature (a), thermal gradient (b), thermal conductivity (c), and heat flow (d) distribution with depth at site #11 (for location, see Table 1 and Fig. A22)

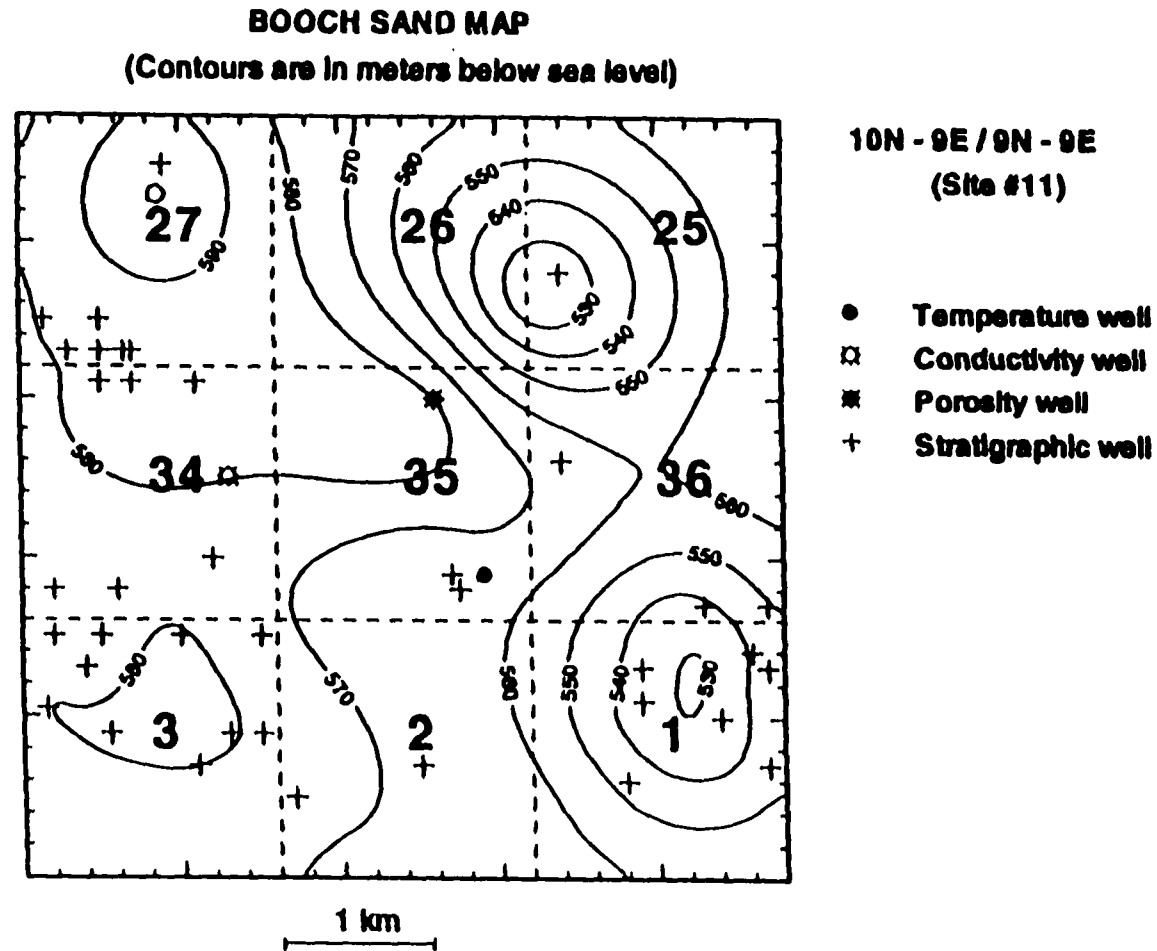


Fig. A22. Stratigraphic map of Booch sand at site #11. The bold numbers in the center of dashed squares represent section numbers of the township and range indicated on the top right side of the figure.

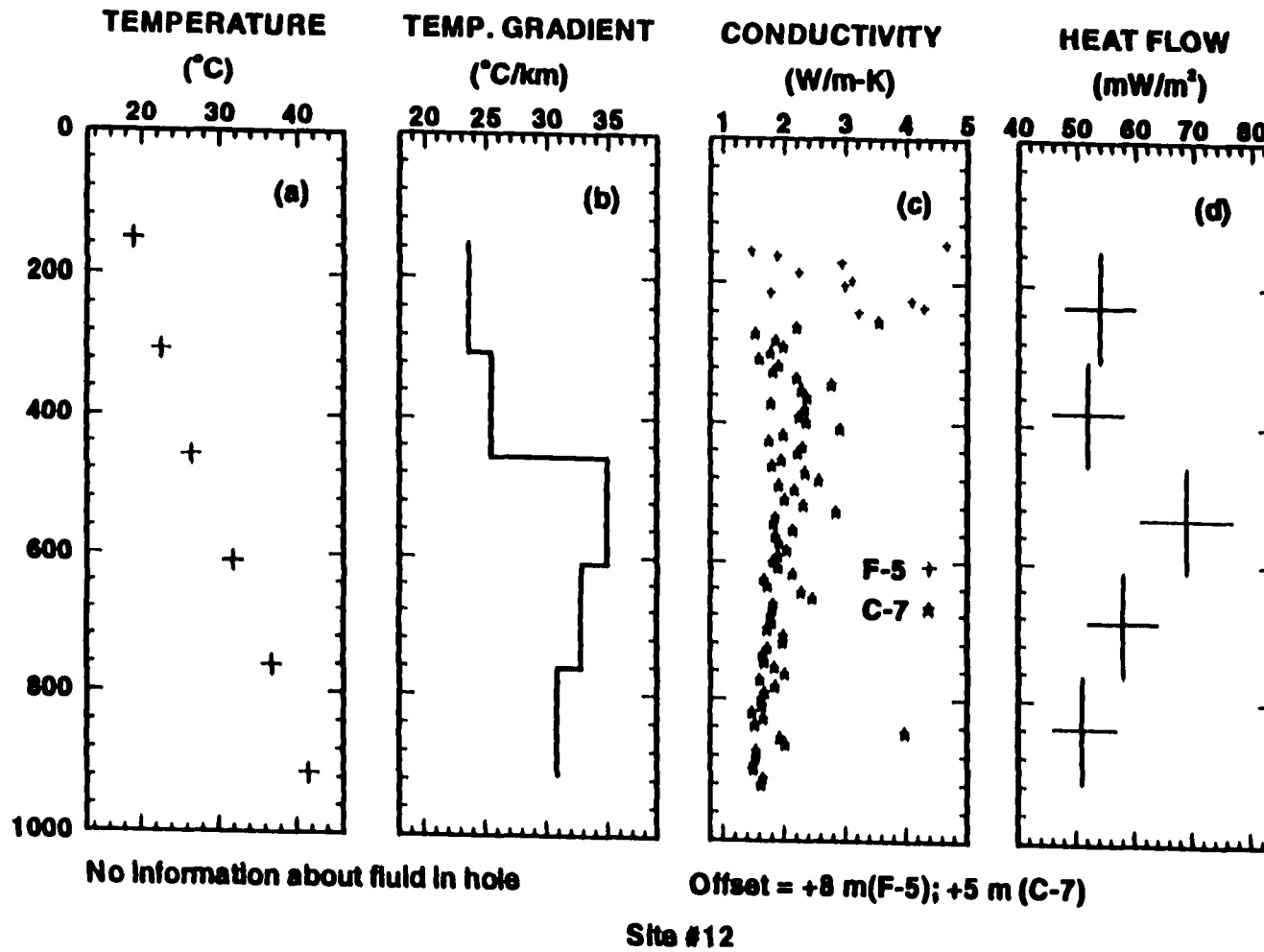


Fig. A23. Temperature (a), thermal gradient (b), thermal conductivity (c), and heat flow (d) distribution with depth at site #12 (for location, see Table 1 and Fig. A24)

CHECKERBOARD MARL MAP
 (Contours are in meters below sea level)

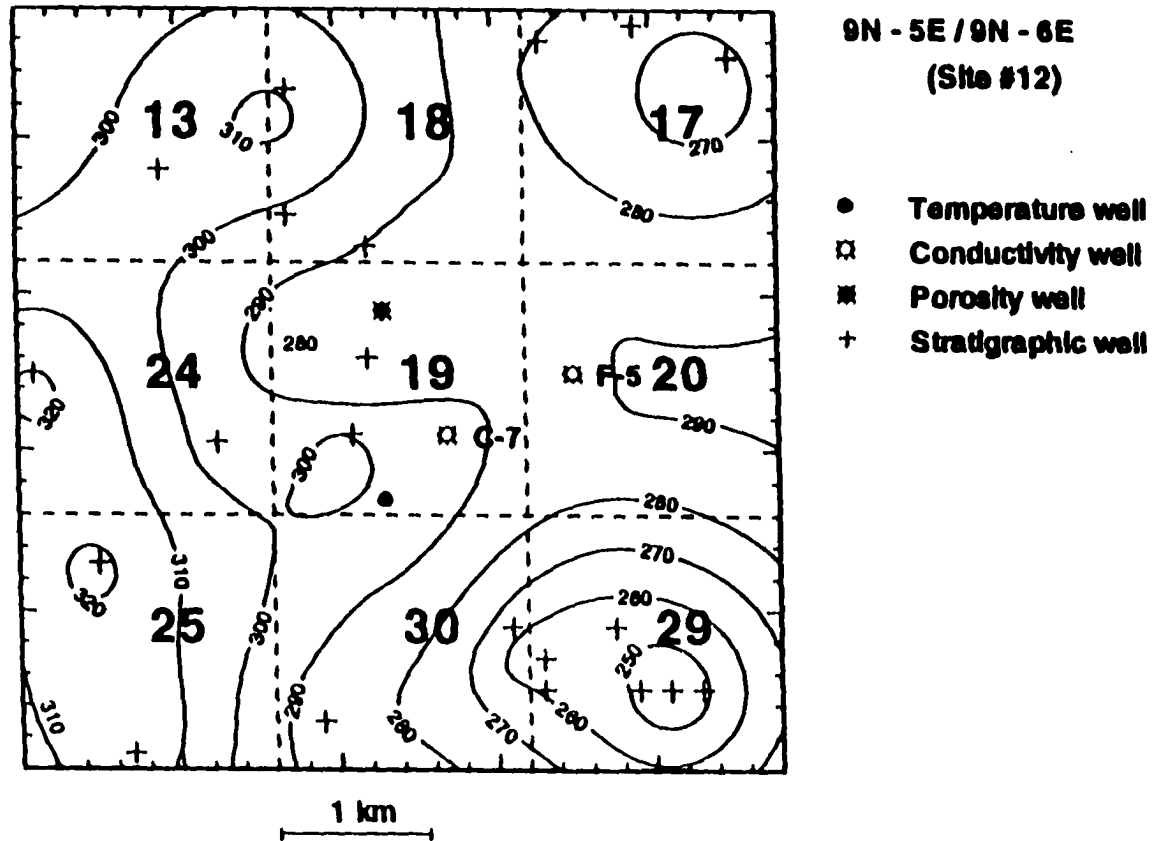


Fig. A24. Stratigraphic map of Checkerboard marl at site #12. The bold numbers in the center of dashed squares represent section numbers of the township and range indicated on the top right side of the figure.

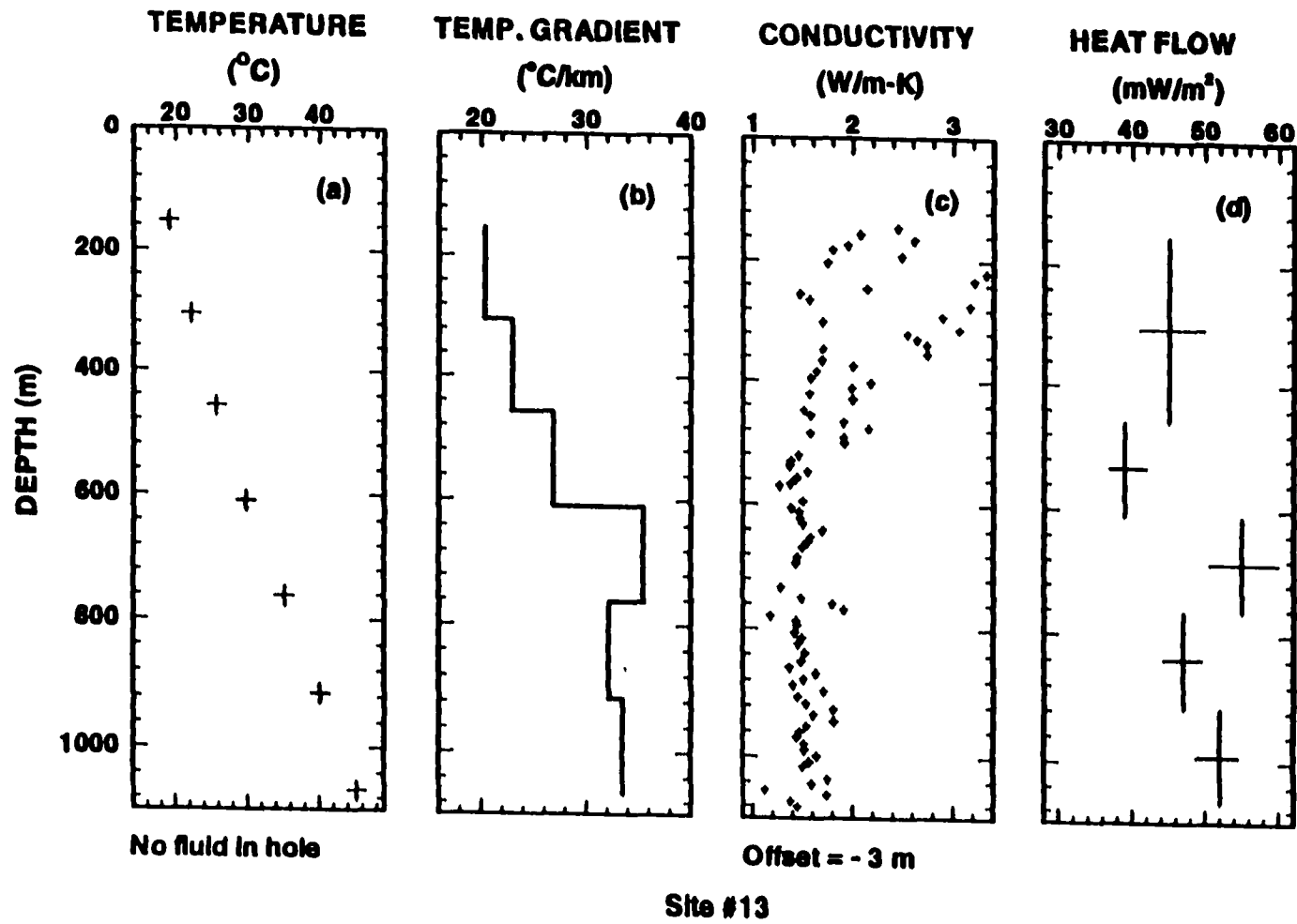


Fig. A25. Temperature (a), thermal gradient (b), thermal conductivity (c), and heat flow (d) distribution with depth at site #13 (for location, see Table 1 and Fig. A26)

EARLSBORO SAND MAP
 (Contours are in meters below sea level)

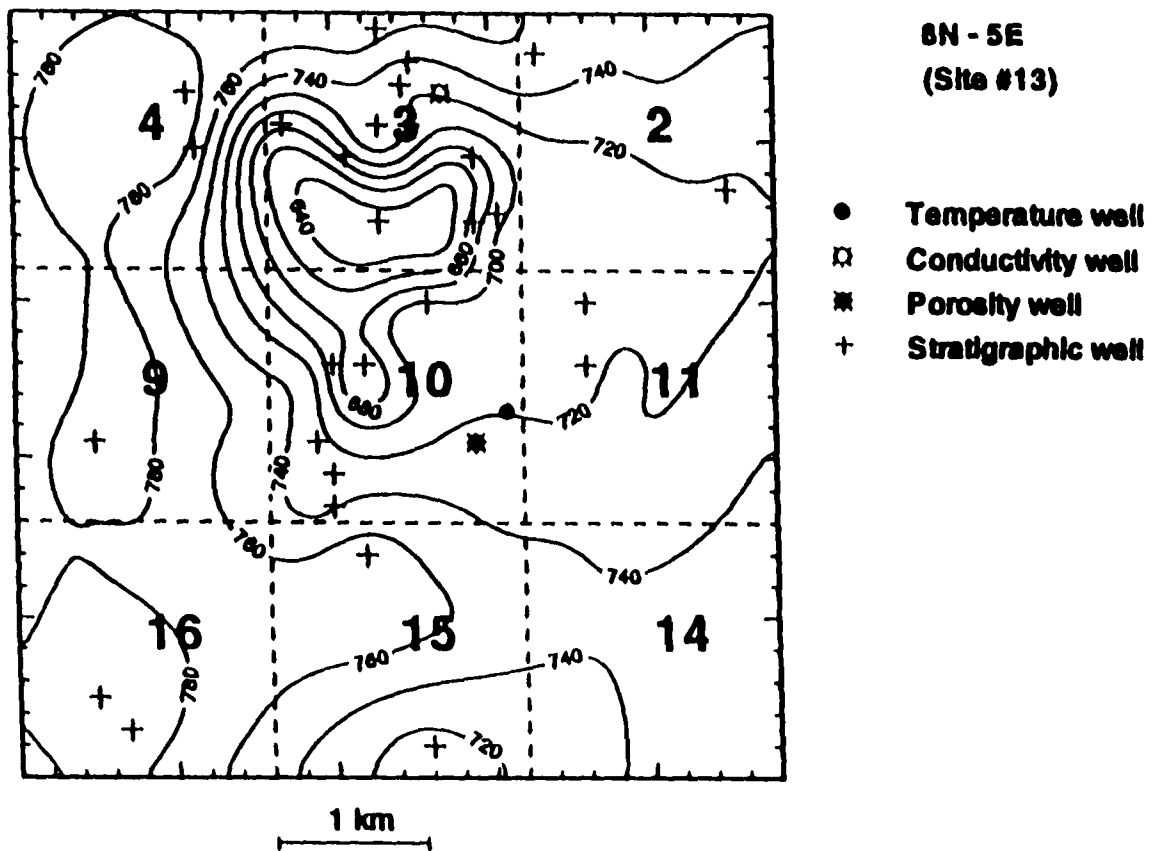


Fig. A26. Stratigraphic map of Earlsboro sand at site #13. The bold numbers in the center of dashed squares represent section numbers of the township and range indicated on the top right side of the figure.

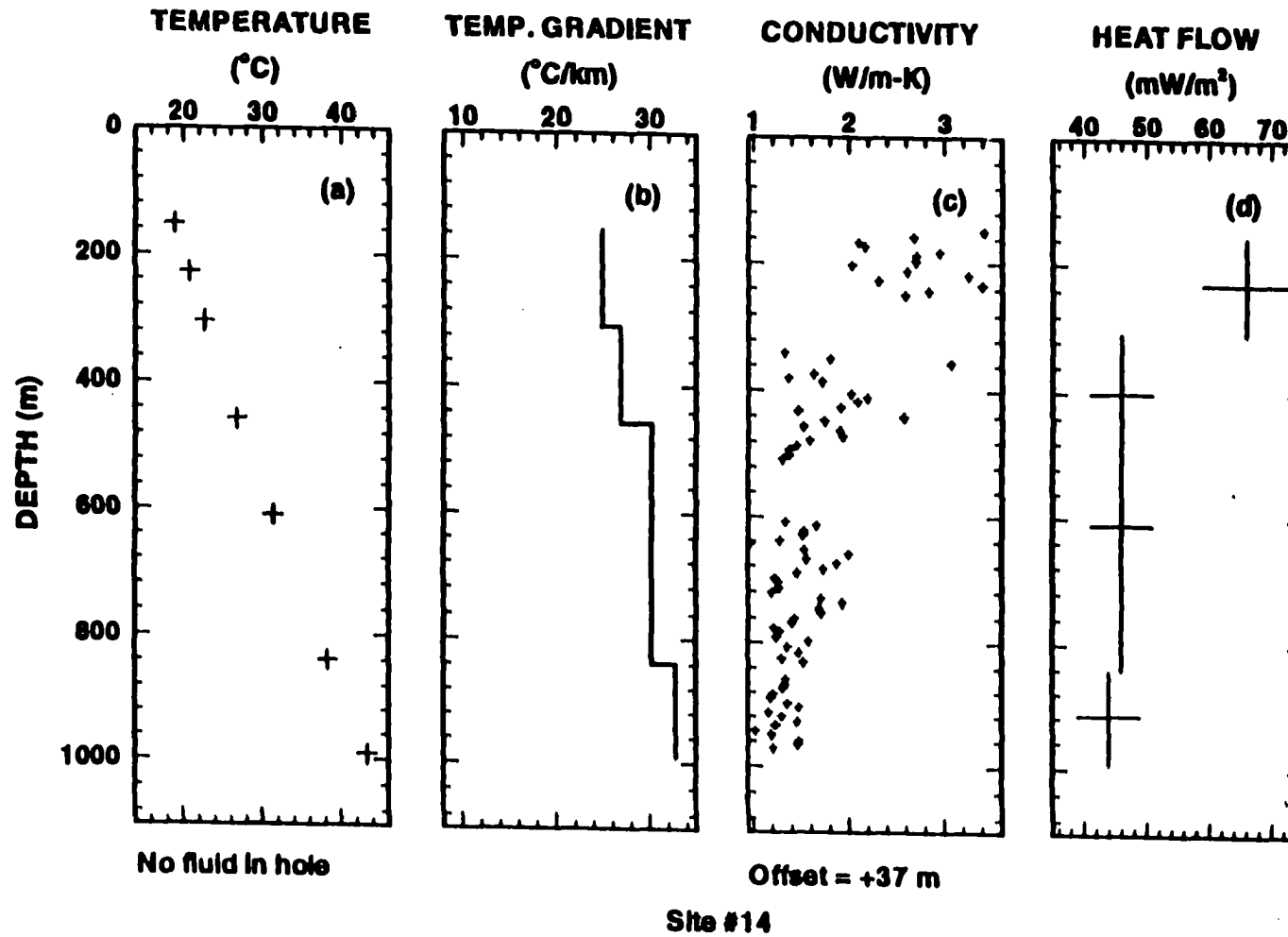


Fig. A27. Temperature (a), thermal gradient (b), thermal conductivity (c), and heat flow (d) distribution with depth at site #14 (for location, see Table 1 and Fig. A28)

EARLSBORO SAND MAP
 (Contours are in meters below sea level)

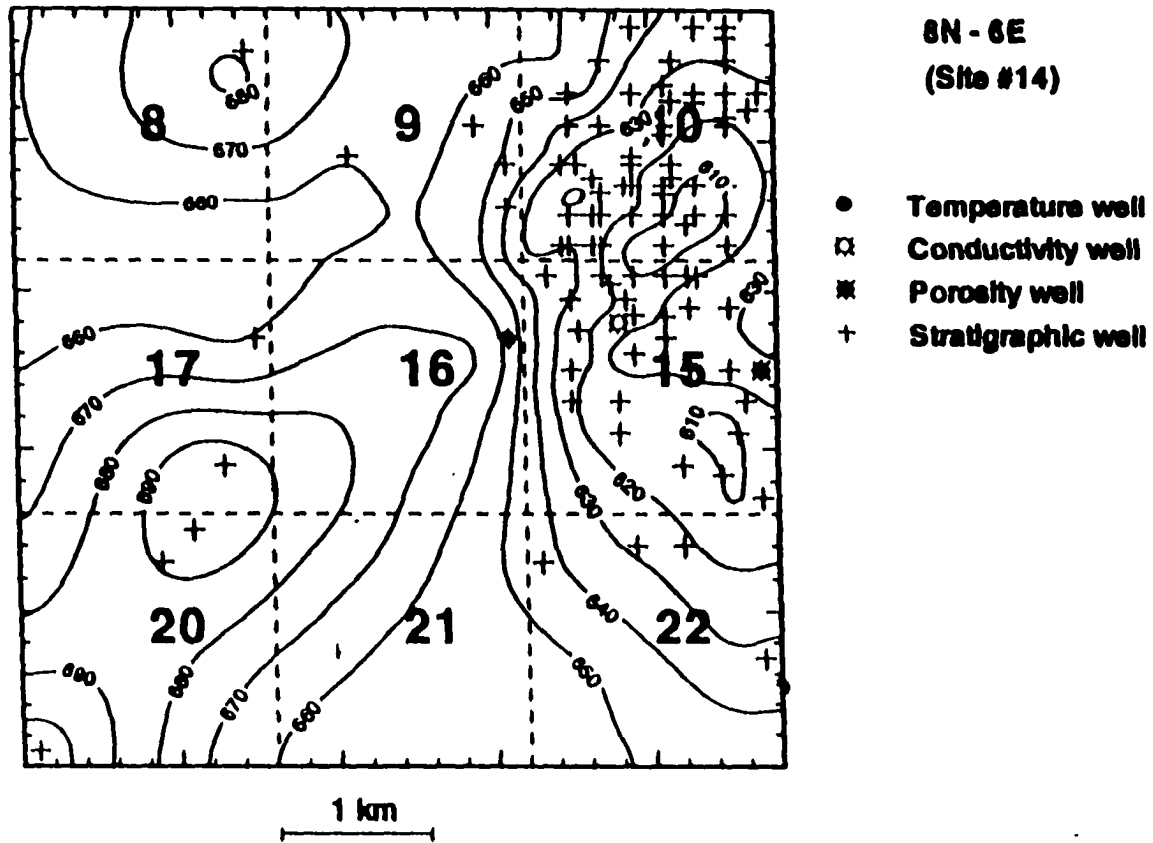


Fig. A28. Stratigraphic map of Earlsboro sand at site #14. The bold numbers in the center of dashed squares represent section numbers of the township and range indicated on the top right side of the figure.

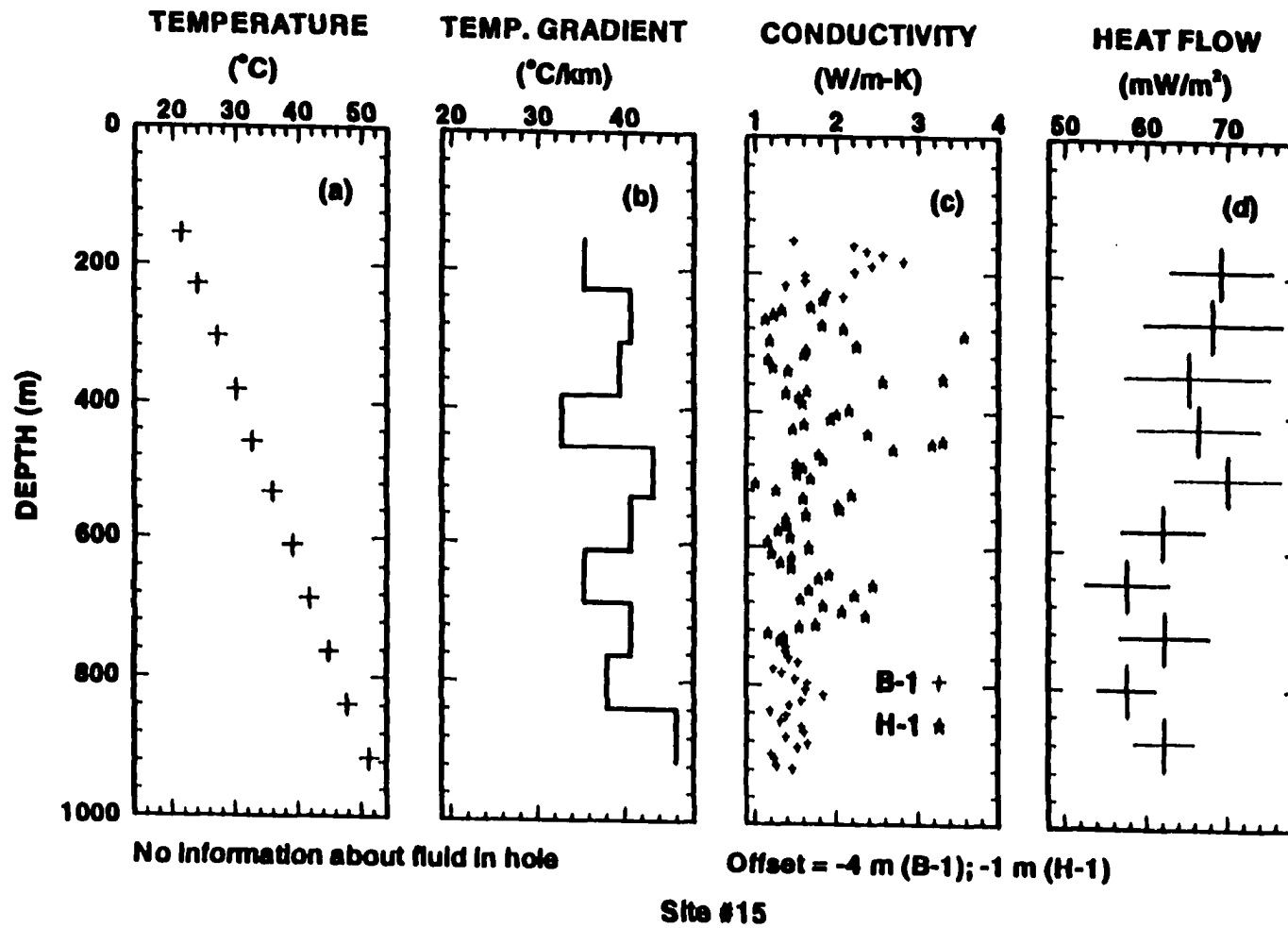


Fig. A29. Temperature (a), thermal gradient (b), thermal conductivity (c), and heat flow (d) distribution with depth at site #15 (for location, see Table 1 and Fig. A30)

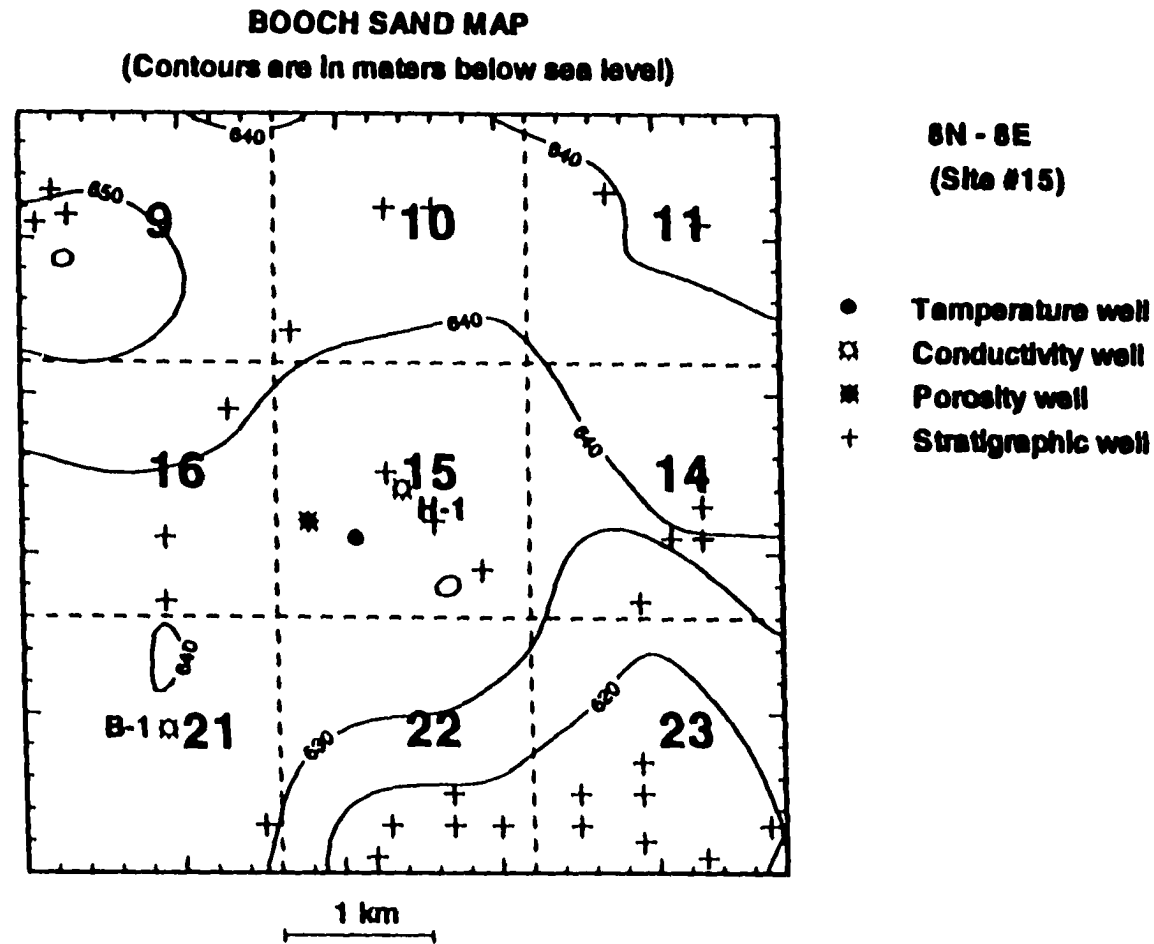


Fig. A30. Stratigraphic map of Booch sand at site #15. The bold numbers in the center of dashed squares represent section numbers of the township and range indicated on the top right side of the figure.

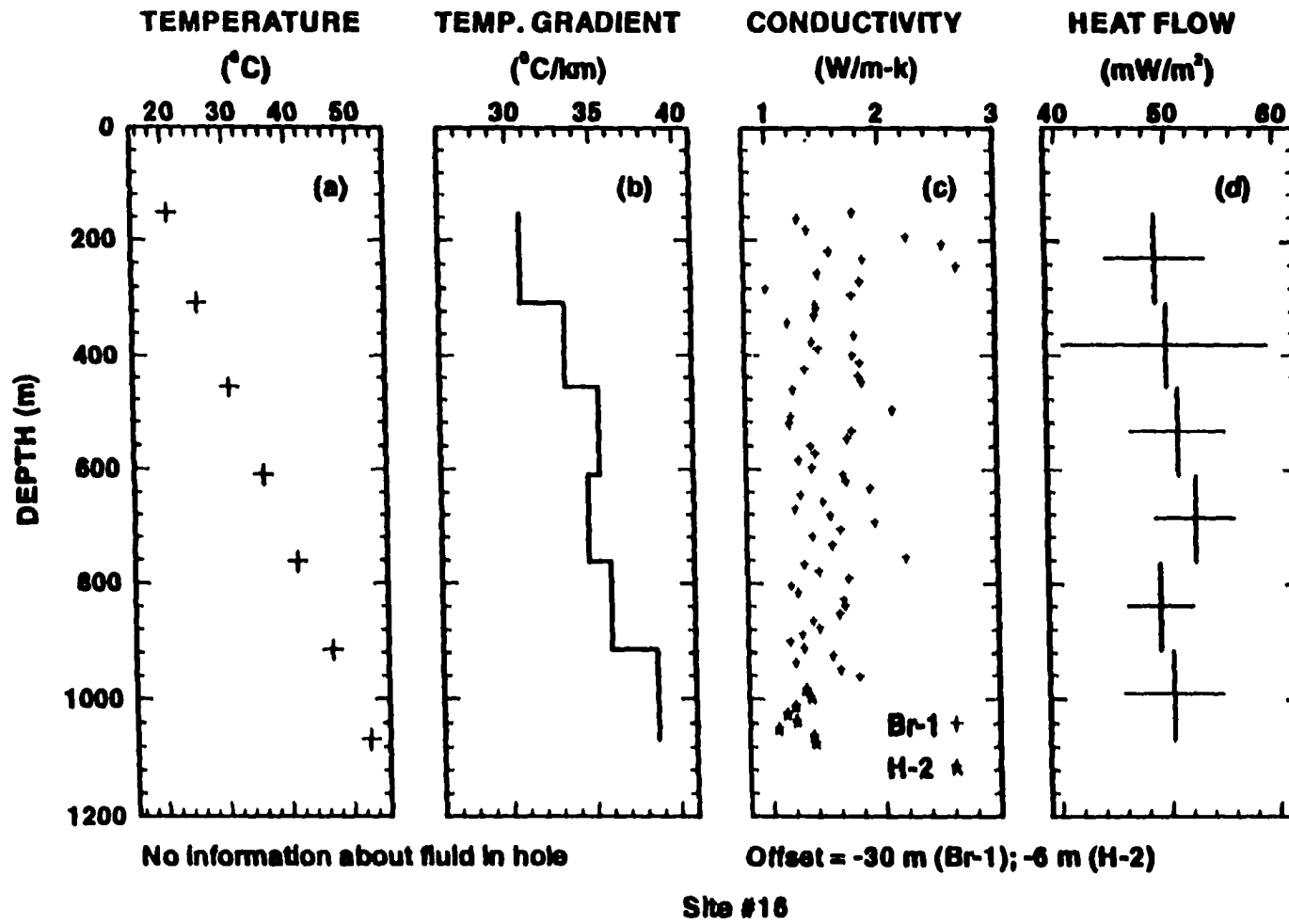


Fig. A31. Temperature (a), thermal gradient (b), thermal conductivity (c), and heat flow (d) distribution with depth at site #16 (for location, see Table 1 and Fig. A32)

BOOCH SAND MAP
 (Contours are in meters below sea level)

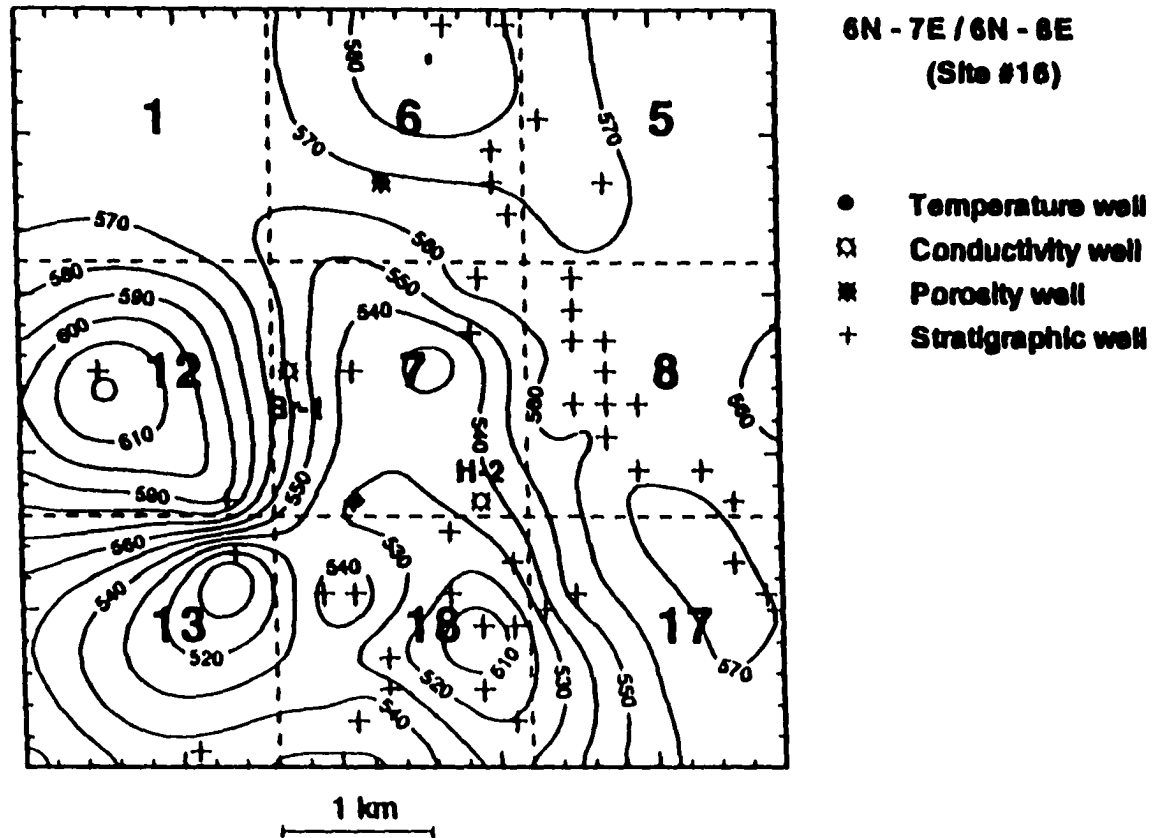


Fig. A32. Stratigraphic map of Booch sand at site #16. The bold numbers in the center of dashed squares represent section numbers of the township and range indicated on the top right side of the figure.

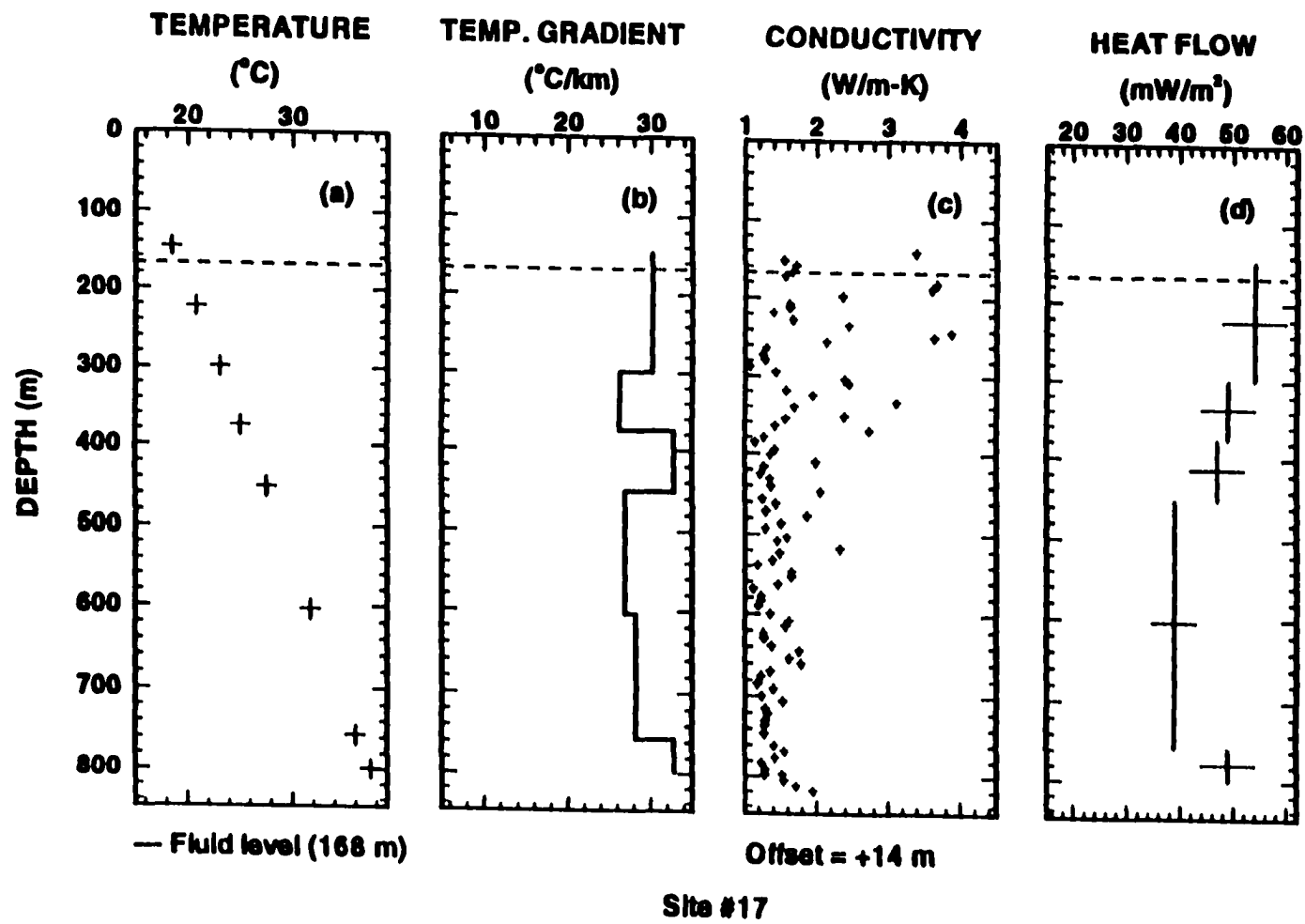


Fig. A33. Temperature (a), thermal gradient (b), thermal conductivity (c), and heat flow (d) distribution with depth at site #17 (for location, see Table 1 and Fig. A34)

SENORA LIMESTONE MAP
 (Contours are in meters below sea level)

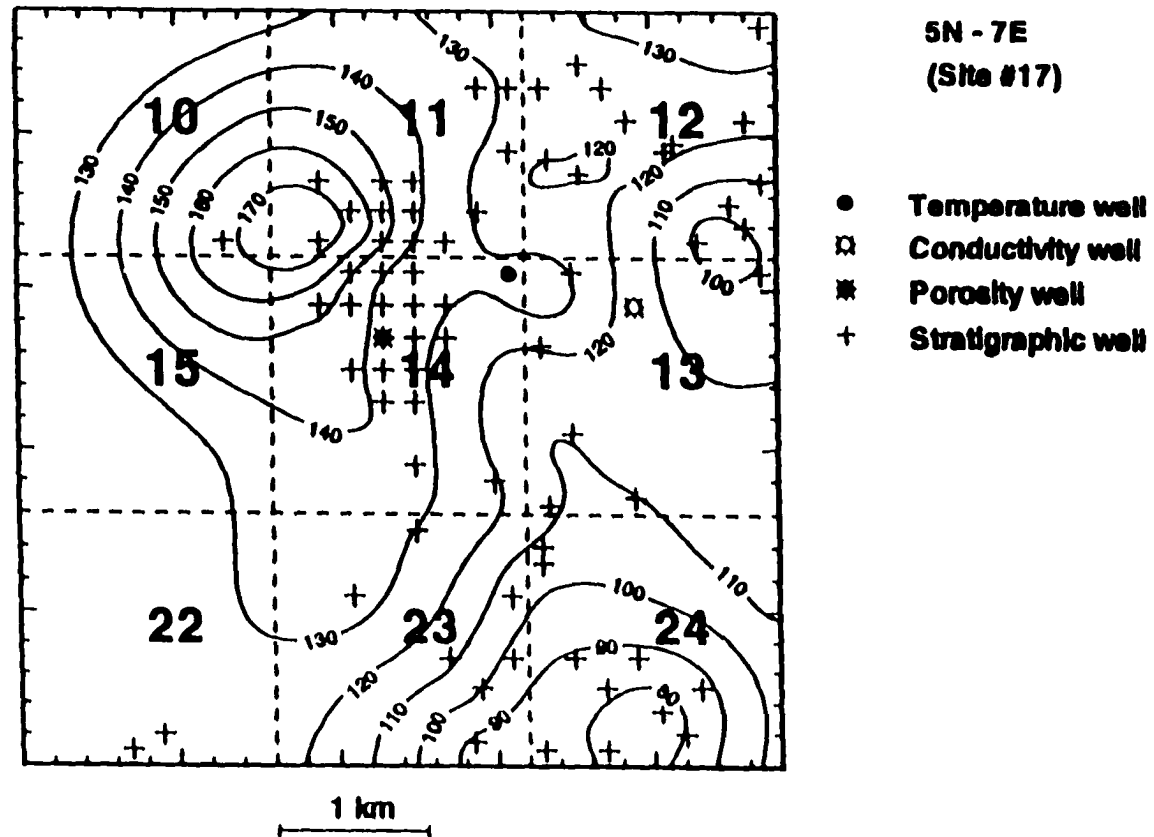


Fig. A34. Stratigraphic map of Senora limestone at site #17. The bold numbers in the center of dashed squares represent section numbers of the township and range indicated on the top right side of the figure.

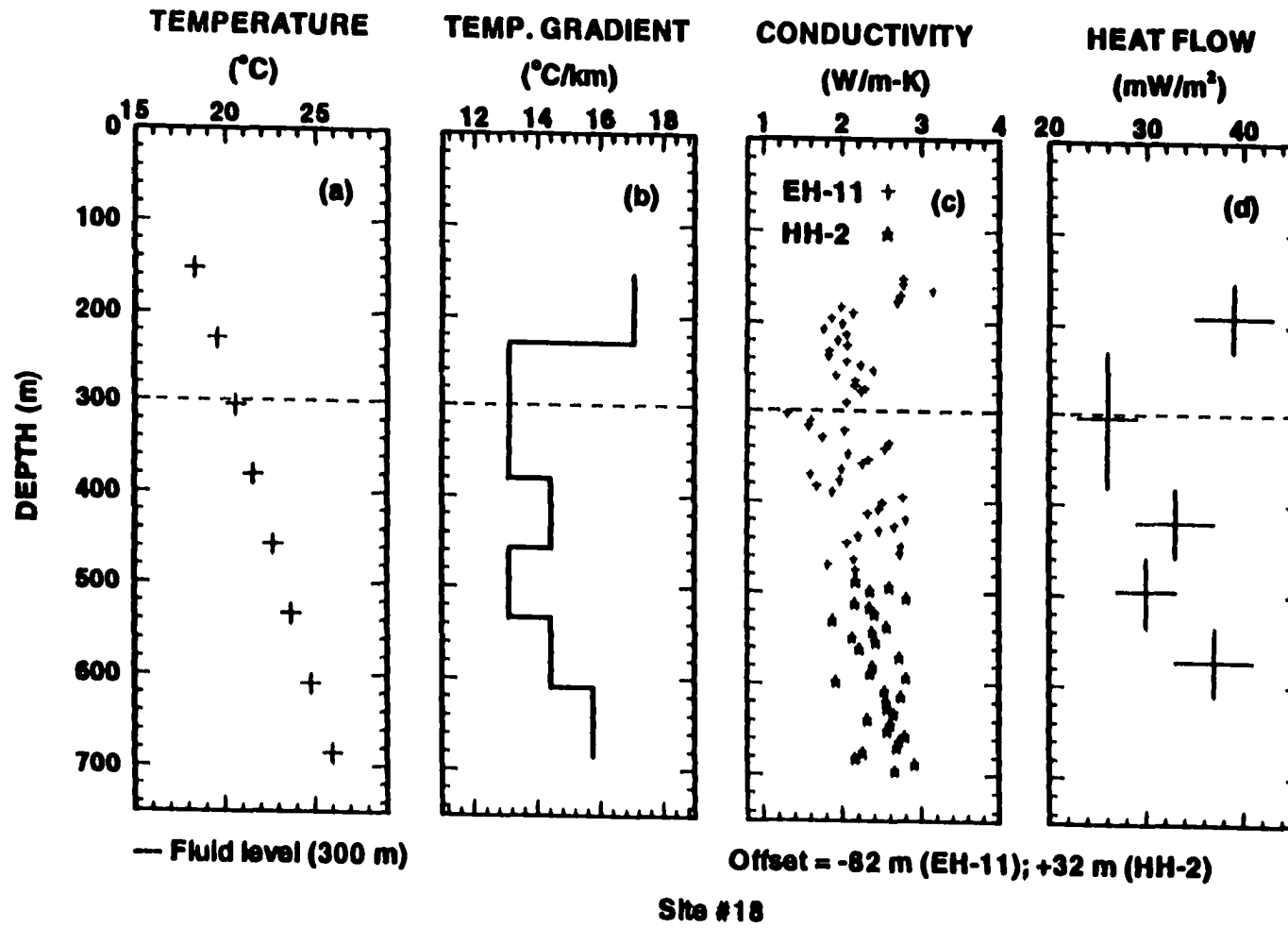


Fig. A35. Temperature (a), thermal gradient (b), thermal conductivity (c), and heat flow (d) distribution with depth at site #18 (for location, see Table 1 and Fig. A36)

TUSSY LIMESTONE MAP
(Contours are in meters below sea level)

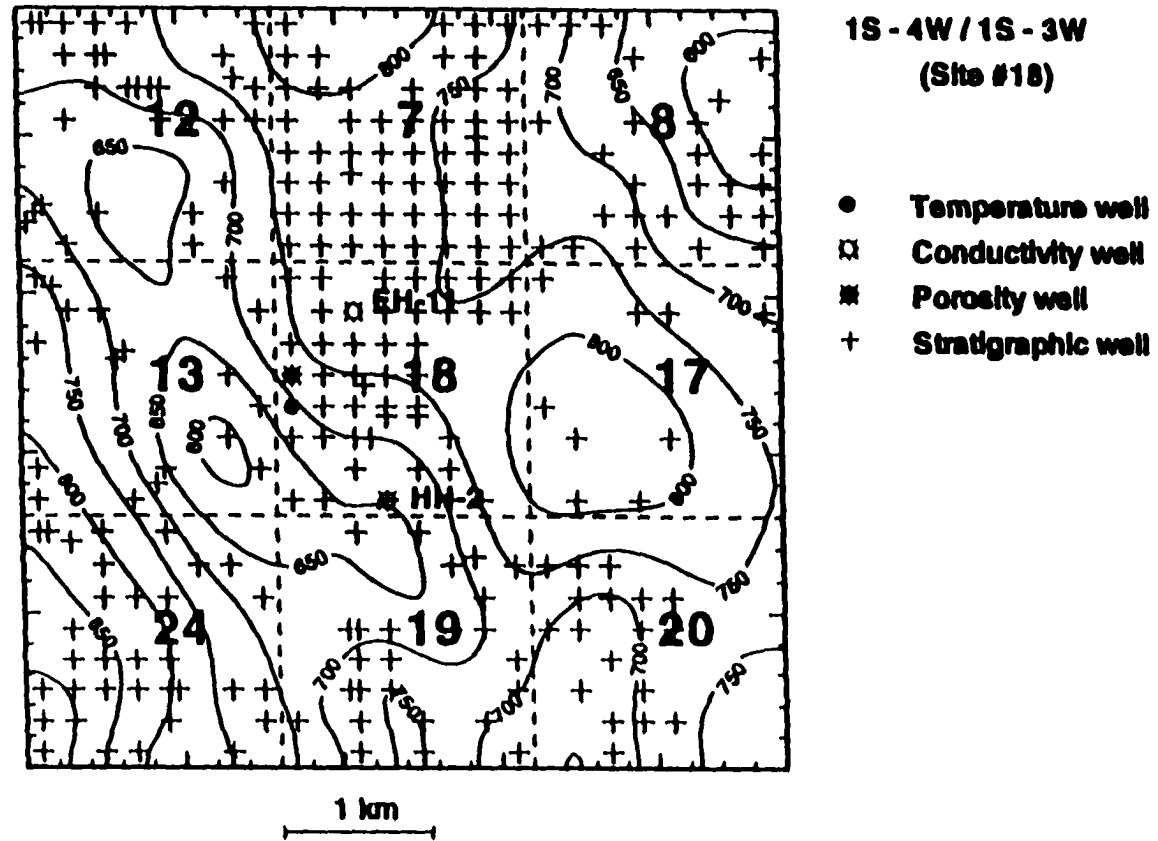


Fig. A36. Stratigraphic map of Tussy limestone at site #18. The bold numbers in the center of dashed squares represent section numbers of the township and range indicated on the top right side of the figure.

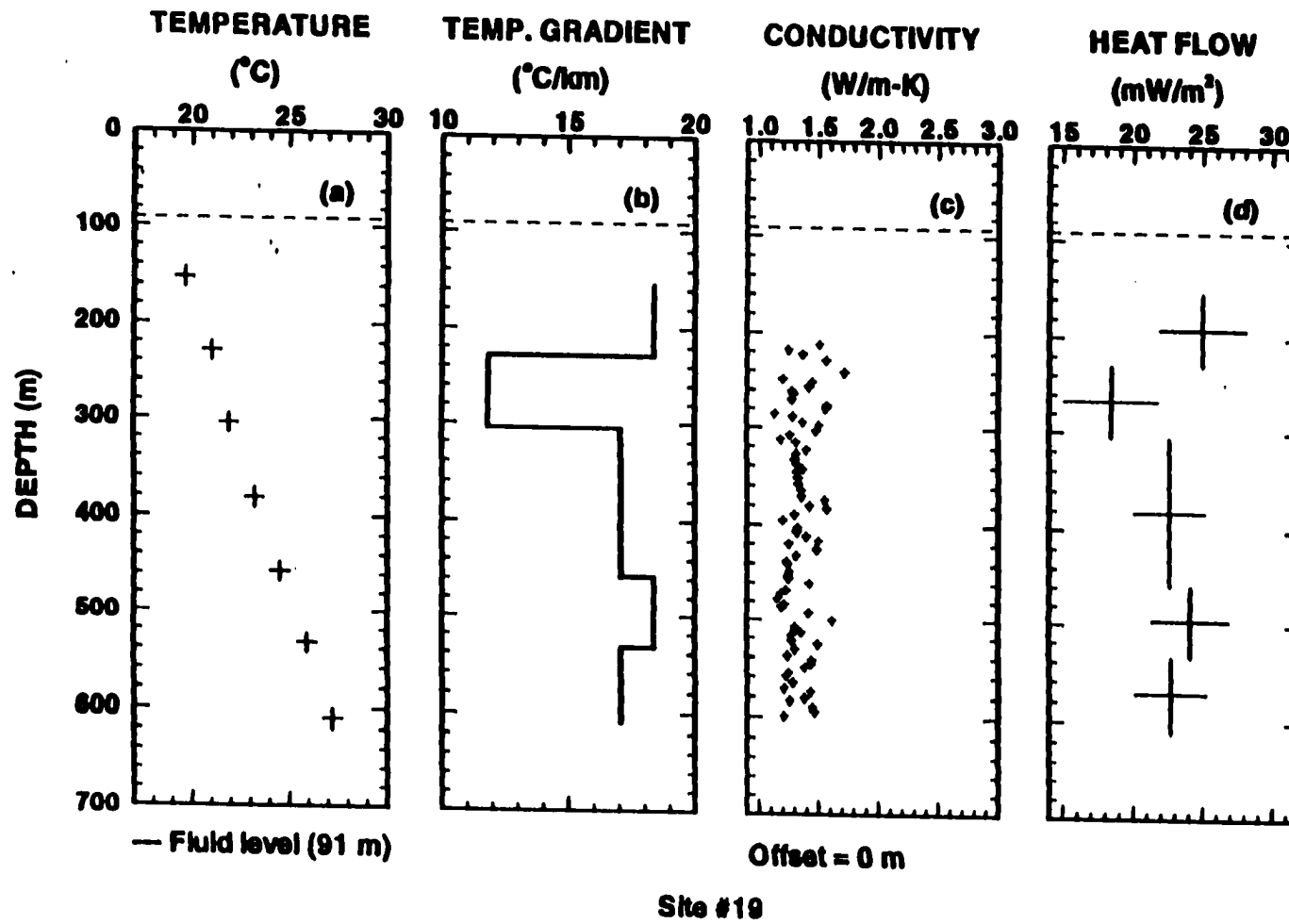


Fig. A37. Temperature (a), thermal gradient (b), thermal conductivity (c), and heat flow (d) distribution with depth at site #19 (for location, see Table 1 and Fig. A38)

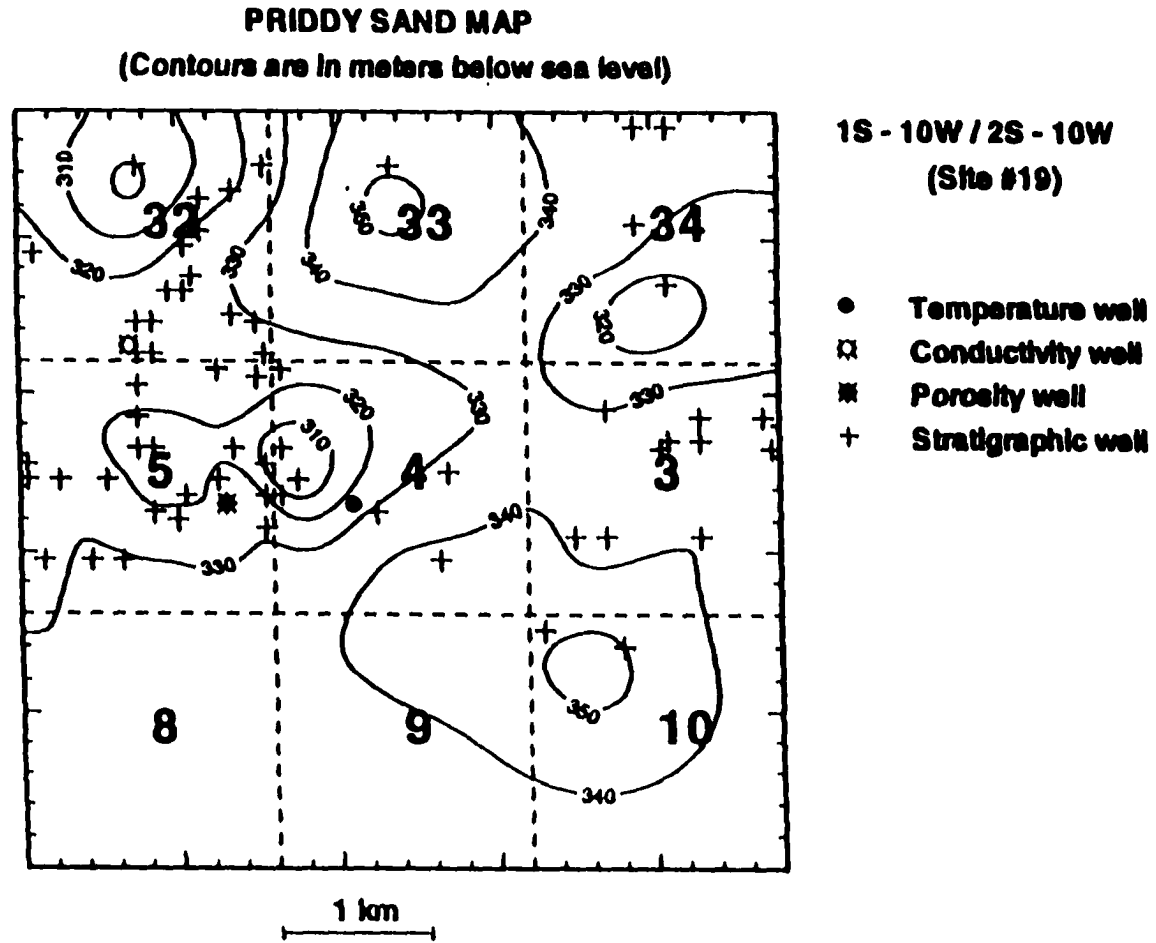


Fig. A38. Stratigraphic map of Priddy sand at site #19. The bold numbers in the center of dashed squares represent section numbers of the township and range indicated on the top right side of the figure.

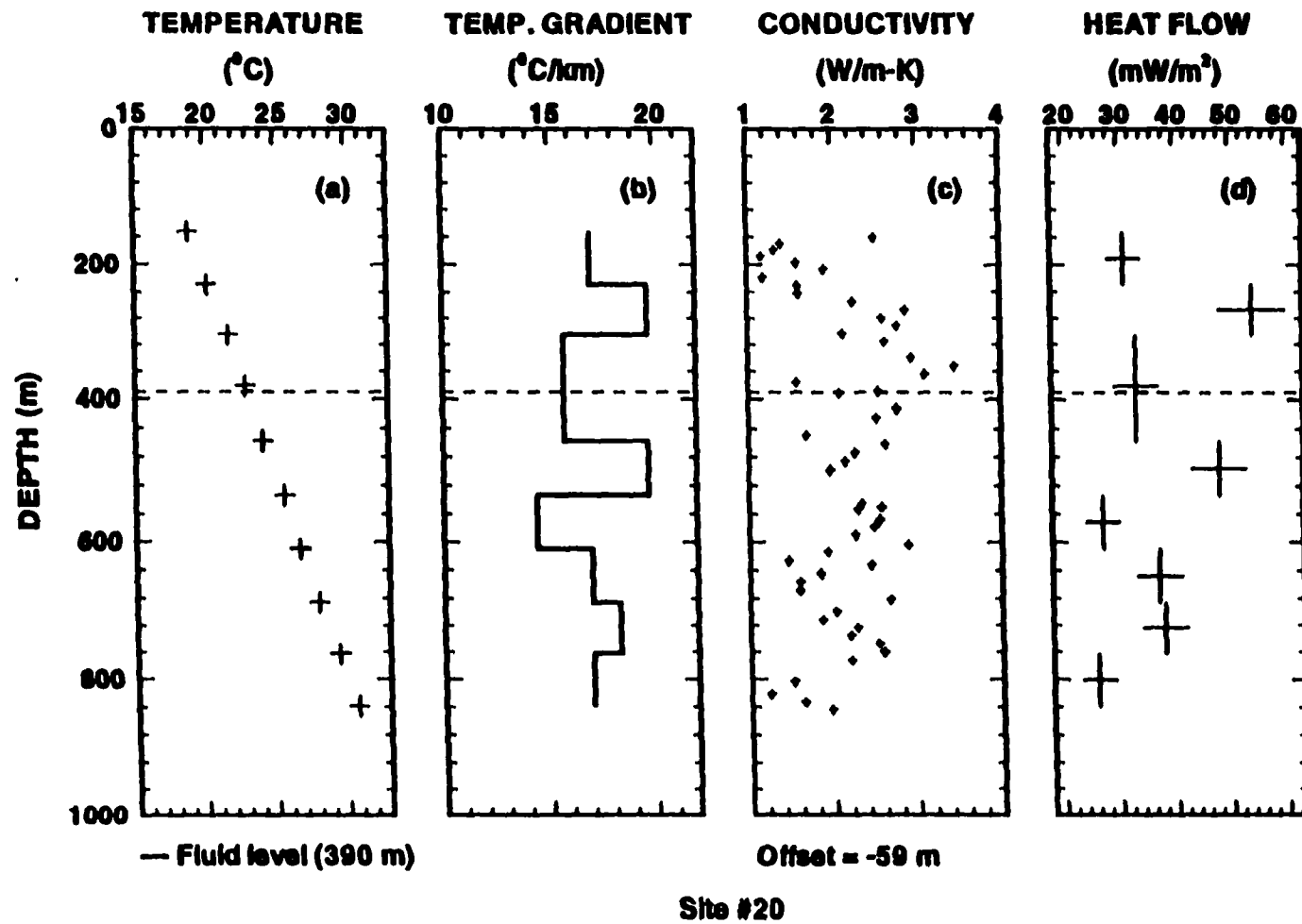


Fig. A39. Temperature (a), thermal gradient (b), thermal conductivity (c), and heat flow (d) distribution with depth at site #20 (for location, see Table 1 and Fig. A40)

CHUBBEE SAND MAP
 (Contours are in meters below sea level)

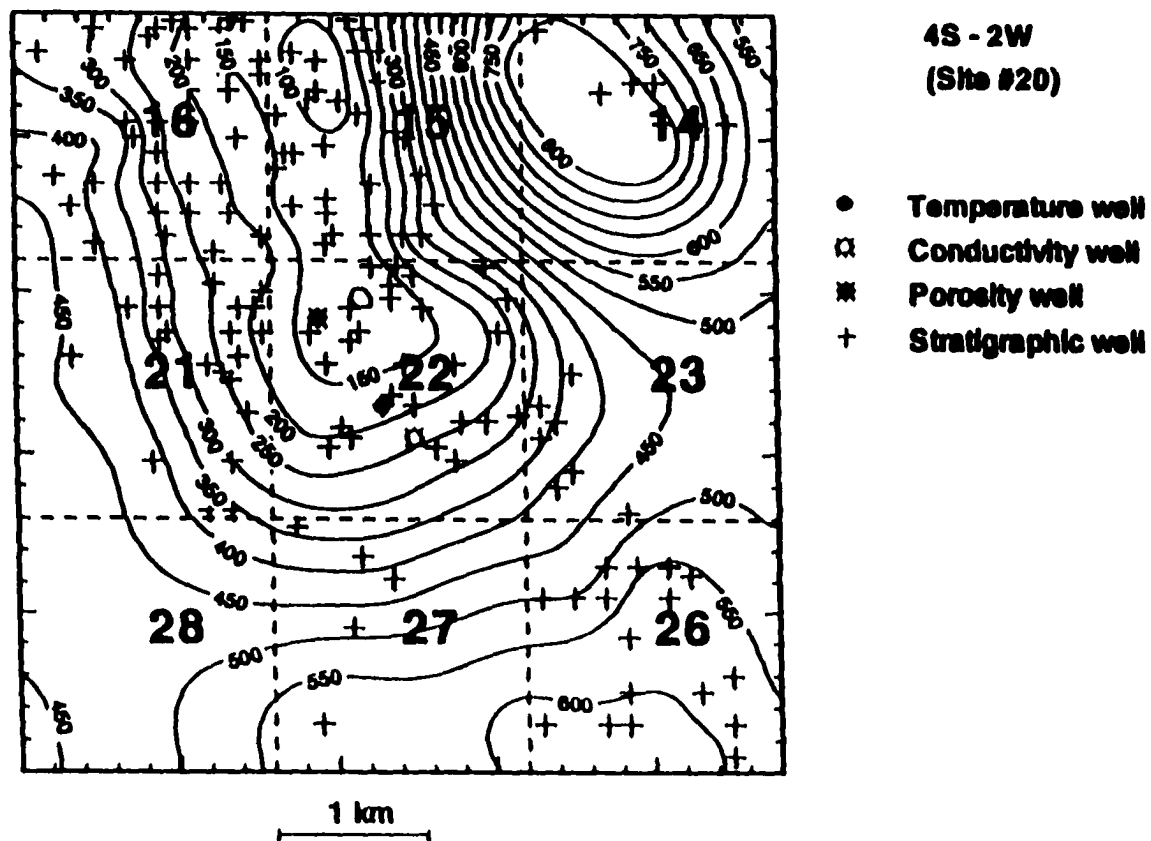


Fig. A40. Stratigraphic map of Chubbee sand at site #20. The bold numbers in the center of dashed squares represent section numbers of the township and range indicated on the top right side of the figure.

APPENDIX B

Minimum interval thermal gradient, maximum interval thermal gradient, and average thermal gradient for each site:

Site #1 (Fig. A1b, Table 1): 34.1°C/km - 40.0°C/km; 36.63°C/km;

Site #2 (Fig. A3b, Table 1): 31.5°C/km - 45.3°C/km; 38.36°C/km

Site #3 (Fig. A5b, Table 1): 31.4°C/km - 51.6°C/km; 34.75°C/km;

Site #4 (Fig. A7b, Table 1): 30.8°C/km - 38.1°C/km; 34.80°C/km;

Site #5 (Fig. A9b, Table 1): 26.2°C/km - 33.5°C/km; 31.12°C/km;

Site #6 (Fig. A11b, Table 1): 27.6°C/km - 39.4°C/km; 31.77°C/km;

Site #7 (Fig. A13b, Table 1): 12.4°C/km - 19.7°C/km; 17.37°C/km;

Site #8 (Fig. A15b, Table 1): 30.2°C/km - 52.5°C/km (the absolute maximum interval thermal gradient); 42.11°C/km;

Site #9 (Fig. A17b, Table 1): 13.7°C/km - 30.1°C/km; 21.15°C/km;

Site #10 (Fig. A19b, Table 1): 32.8°C/km - 48.5°C/km; 41.09°C/km;

Site #11 (Fig. A21b, Table 1): 35.4°C/km - 47.2°C/km; 42.24°C/km (the absolute maximum average thermal gradient);

Site #12 (Fig. A23b, Table 1): 23.6°C/km - 43.9°C/km; 30.07°C/km;

Site #13 (Fig. A25b, Table 1): 20.3°C/km - 35.4°C/km; 28.97°C/km;

Site #14 (Fig. A27b, Table 1): 24.9°C/km - 32.8°C/km; 29.13°C/km;

Site #15 (Fig. A29b, Table 1): 32.8°C/km - 45.9°C/km; 39.01°C/km;

Site #16 (Fig. A31b, Table 1): 30.8°C/km - 38.7°C/km; 34.92°C/km;

Site #17 (Fig. A33b, Table 1): 26.2°C/km - 32.8°C/km; 28.72°C/km;

Site #18 (Fig. A35b, Table 1): 13.1°C/km - 17.1°C/km; 14.11°C/km (the absolute minimum average thermal gradient);

Site #19 (Fig. A37b, Table 1): 11.8°C/km (the absolute minimum interval geothermal gradient); 18.4°C/km; 16.50°C/km;

Site #20 (Fig. A39b, Table 1) 14.4°C/km - 19.7°C/km; 17.10°C/km.

APPENDIX C

Short presentation of thermal conductivity data for each site:

site #1:

Well used for thermal conductivity measurements: Herman #3 (for location, see Table 2 and Fig. A2);

Distance from temperature well: 1000 m;

Depth interval with thermal conductivity measurements: 157 - 1020 m below ground surface;

Stratigraphic offset of conductivity well: + 9 m;

Number of thermal conductivity measurements: 78 (Fig. A1c);

Value interval: 0.95 - 2.5 W/m-K;

In situ harmonic mean of all thermal conductivity measurements (after corrections for anisotropy, temperature, and porosity): 1.11 ± 0.03 W/m-K;

well used for porosity determination: Sims #1 (for location, see Table 3 and Fig. A2);

Depth interval of density log: 37 - 327 m (290 m interval length);

Distance from conductivity well: 1435 m;

Stratigraphic offset of porosity well: + 5 m;

Average porosity: 0.17;

Geologic formations sampled (Fig. 7): Permian, Pennsylvanian, and Mississippian;

Other comments: This site has the lowest harmonic mean of measured thermal conductivities (1.11 ± 0.03 W/m-K). Most thermal conductivity values range between 0.95 - 1.8 W/m-K. Lithologies found during sampling: gray shale, limestone, sandstone. Thermal conductivities do not change with geologic age (Fig. 7). Note the inverse relationship between temperature gradients (Fig. A1b) and thermal conductivities (Fig. A1c).

site #2

Well used for thermal conductivity measurements: McCulloch #1 (for location, see Table 2 and Fig. A4);

Distance from temperature well: 652 m;

Depth interval with thermal conductivity measurements: 460 - 1131 m below ground surface;

Stratigraphic offset of conductivity well: + 47 m;

Number of thermal conductivity measurements: 52 (Fig. A3c);

value interval: 1.14 - 1.70 W/m-K;

In situ harmonic mean of all thermal conductivity measurements (after corrections for anisotropy, temperature, and porosity): 1.38 ± 0.02 W/m-K;

Well used for porosity determination: North #15 (for location, see Table 3 and Fig. A4);

Depth interval of density log: 518 - 945 m (427 m interval length);

Distance from conductivity well: 1087 m;

Stratigraphic offset of porosity well: - 70 m;

Average porosity: 0.09;

Geologic formations sampled (Fig. 7): Permian and Pennsylvanian;

Other comments: Most thermal conductivity values range in a narrow interval (1.2 - 1.6 W/m-K). Lithologies found during sampling: gray shale is predominant; limestone and sandstone are present in small amounts.

Thermal conductivities do not change with geologic age (Fig. 7).

site #3:

Wells used for thermal conductivity measurements: McAninch #1 (M-1) and L. Shower #93 (L-93) (for location, see Table 2 and Fig. A6);

Distance from temperature well: 1,848 m (M-1); 1,040 m (L-93);

Depth interval with thermal conductivity measurements: 168 - 1,033 m; 1,310

- 1,478 m (M-1); 1,310 - 1,478 m (L-93) below ground surface;

Stratigraphic offset of conductivity well: - 28 m (M-1); + 28 m (L-93);

Number of thermal conductivity measurements: 48 (M-1) and 26 (L-93) (Fig. A5c);

Value interval: 1.1 - 3.8 W/m-K;

In situ harmonic mean of all thermal conductivity measurements (after corrections for anisotropy, temperature, and porosity): 1.18 ± 0.03 W/m-K (M-1) and 1.80 ± 0.07 W/m-K (L-93); average value for the entire depth interval: 1.49 ± 0.05 W/m-K;

Well used for porosity determination: Christa #1 (for location, see Table 3 and Fig. A6);

Depth interval of density log: 214 - 820 m (606 m interval length);

Distance from conductivity well: 3239 m (L-93); 3826 m (M-1);

Stratigraphic offset of porosity well: - 35 m (M-1); + 21 m (L-93);

Average porosity: 0.13;

Geologic formations sampled (Fig. 7): Permian, Pennsylvanian, Mississippian, Devonian, and Ordovician;

Other comments: Most thermal conductivity values range between 1 - 2 W/m-K, excepting some basal Mississippian limestone with values between 2 - 3.8 W/m-K. Lithologies found during sampling: gray shale, limestone (predominant); sandstone (secondary). Thermal conductivities do not apparently change with geologic age (Fig. 7).

site #4:

Well used for thermal conductivity measurements: Gravel #1 (for location, see Table 2 and Fig. A8);

Distance from temperature well: 565 m;

Depth interval with thermal conductivity measurements: 105 - 831 m below

ground surface;

Stratigraphic offset of conductivity well: - 6 m;

Number of thermal conductivity measurements: 76 (Fig. A7c);

Value interval: 0.90 - 1.97 W/m-K;

In situ harmonic mean of all thermal conductivity measurements (after corrections for anisotropy, temperature, and porosity): 1.30 ± 0.03 W/m-K;

Well used for porosity determination: Carter #1-B (for location, see Table 3 and Fig. A8);

Depth interval of density log: 118 - 471 m (352 m interval length);

Distance from conductivity well: 478 m;

Stratigraphic offset of porosity well: + 2 m;

Average porosity: 0.21;

Geologic formations sampled (Fig. 7): Permian and Pennsylvanian;

Other comments: Most thermal conductivity values range in a narrow interval, between 1.0 - 1.7 W/m-K. Lithologies found during sampling: gray shale (predominant), limestone, sandstone (secondary). Thermal conductivities do not change with geologic age (Fig. 7). The thermal conductivity values are slightly higher in the upper and lower portions of the well due to a relatively higher amount of sandstone and carbonates.

site #5:

Well used for thermal conductivity measurements: Providence #1 (for location, see Table 2 and Fig. A10);

Distance from temperature well: 2,348 m;

Depth interval with thermal conductivity measurements: 148 - 913 m below ground surface;

Stratigraphic offset of conductivity well: - 4 m;

Number of thermal conductivity measurements: 83 (Fig. A9c);

Value interval: 1.2 - 3.7 W/m-K;

***In situ* harmonic mean of all thermal conductivity measurements (after corrections for anisotropy, temperature, and porosity): 1.53 ± 0.05 W/m-K;**

Well used for porosity determination: Cox #2 (for location, see Table 3 and Fig. A10);

Depth interval of density log: 973 - 1,585 m (612 m interval length);

Distance from conductivity well: 1,870 m;

Stratigraphic offset of porosity well: - 2 m;

Average porosity: 0.04;

Geologic formations sampled (Fig. 8): Permian and Pennsylvanian;

Other comments: Lithologies found during sampling: red sandstone in the upper part of the well (first 300 m), where thermal conductivities range 1.4 - 3.7 W/m-K; red sandstone and gray shale, in the rest of the well, where thermal conductivities vary in a narrow interval (1.2 - 1.9 W/m-K). Thermal conductivities do not change with geologic age (Fig. 8). Note the direct relationship between first temperature gradient, between 180 - 300 m (Fig. A9b) and thermal conductivities (Fig. A9c). The next gradients do not present any relationship with thermal conductivities.

site #6:

Wells used for thermal conductivity measurements: Stewart #1 (S-1) and Dacon #37 (D-37) (for location, see Table 2 and Fig. A12);

Distance from temperature well: 187 m (S-1); 345 m (D-37);

Depth interval with thermal conductivity measurements: 151 - 398 m (S-1) and 414 - 853 m (D-37) below ground surface;

Stratigraphic offset of conductivity well: + 1 m (S-1); + 2 m (D-37);

Number of thermal conductivity measurements: 23 (S-1); 36 (D-37) (Fig. A11c);

Value interval: 1.0 - 4.8 W/m-K;

In situ harmonic mean of all thermal conductivity measurements (after corrections for anisotropy, temperature, and porosity): 2.10 ± 0.10 W/m-K (S-1); 1.82 ± 0.12 W/m-K (D-37); the harmonic mean for the entire site is 1.96 ± 0.11 W/m-K;

Well used for porosity determination: Shamrock Royalty-Tract 3 #W-22 (for location, see Table 3 and Fig. A12);

Depth interval of density log: 427 - 850 m (423 m interval length);

Distance from conductivity well: 739 m (S-1); 1130 m (D-37);

Stratigraphic offset of porosity well: - 28 m (S-1); - 29 m (D-37);

Average porosity: 0.05;

Geologic formations sampled (Fig. 8): Pennsylvanian;

Other comments: Lithologies found during sampling: gray shale and sandstone in S-1 (first 400 m), limestone and shale in D-37 (the depth interval between ~400 - 853 m. Higher than in previous wells, conductivity values reflect the greater amount of carbonates and sandstones sampled in this well.

site #7:

Well used for thermal conductivity measurements: Thompson #1 (for location, see Table 2 and Fig. A14);

Distance from temperature well: 10 m;

Depth interval with thermal conductivity measurements: 111 - 1,224 m below ground surface;

Stratigraphic offset of conductivity well: 0 m;

Number of thermal conductivity measurements: 60 (Fig. A13c);

Value interval: 1.0 - 6.1 W/m-K;

In situ harmonic mean of all thermal conductivity measurements (after corrections for anisotropy, temperature, and porosity): 1.80 ± 0.23 W/m-K;

Well used for porosity determination: Henderson #1-14 (for location, see Table 3 and Fig. A14);

Depth interval of density log: 1538 - 2224 m (686 m interval length);

Distance from conductivity well: 434 m;

Stratigraphic offset of porosity well: - 1 m;

Average porosity: 0.02;

Geologic formations sampled (Fig. 8): Pennsylvanian;

Other comments: Lithologies found during sampling: red sandstone with high thermal conductivity (~4 - ~6 W/m-K) in the first ~300 m, followed by a mixture of shale and red sandstone, ranging narrower (~1 - ~2.W/m-K) in the rest of the well. Note the inverse relationship between the first temperature gradient (Fig. A13b) and thermal conductivities (Fig. A13c) measured in approximately the same depth interval (~100 - ~300 m). For the rest of the well, there is no relationship between thermal gradients and thermal conductivities.

site #8:

Well used for thermal conductivity measurements: Skeleton #2 (for location, see Table 2 and Fig. A16);

Distance from temperature well: 1,826 m;

Depth interval with thermal conductivity measurements: 131 - 850 m below ground surface;

Stratigraphic offset of conductivity well: + 5 m;

Number of thermal conductivity measurements: 53 (Fig. A15c);

Value interval: 1.0 - 5.3 W/m-K;

In situ harmonic mean of all thermal conductivity measurements (after corrections for anisotropy, temperature, and porosity): 2.04 ± 0.14 W/m-K;

Well used for porosity determination: Burnett #1-36 (for location, see Table 3

and Fig. A16);

Depth interval of density log: 618 - 1,157 m (539 m interval length);

Distance from conductivity well: 2,261 m;

Stratigraphic offset of porosity well: - 1 m;

Average porosity: 0.05;

Geologic formations sampled (Fig. 8): Pennsylvanian;

Other comments: Lithologies found during sampling: gray sandstone (predominant) and black shale in the upper ~500 m, followed by black and gray shale and gray sandstone in the bottom part of the well. The thermal conductivity measurements are less numerous and show a quite large scattering in the upper part of the well (0 - ~500 m); then, the number of measurements increases and the variation of thermal conductivities (between ~1.2 - ~3 W/m-K) is mainly due to lithologic variation (large values for sandstones, small values for shales).

site #9:

Wells used for thermal conductivity measurements: Wheeler #4 (W-4) and Wheeler #2 (W-2) (for location, see Table 2 and Fig. A18);

Distance from temperature well: 870 m (W-4); 783 m (W-2);

Depth interval with thermal conductivity measurements: 306 - 1,175 m (W-4) and 1,190 - 1,832 m (W-2) below ground surface;

Stratigraphic offset of conductivity well: + 32 m (W-4); + 25 m (W-2);

Number of thermal conductivity measurements: 54 (W-4); 35 (W-2) (Fig. A17c);

Value interval: 0.94 - 2.4 W/m-K;

In situ harmonic mean of all thermal conductivity measurements (after corrections for anisotropy, temperature, and porosity): 1.37 ± 0.04 W/m-K (W-4); 1.26 ± 0.05 W/m-K (W-2); the harmonic mean for the entire site: 1.33 ± 0.03

W/m-K;

Well used for porosity determination: Jennings "A" #4 (for location, see Table 3 and Fig. A18);

Depth interval of density log: 332 - 1643 m (1311 m interval length);

Distance from conductivity well: 740 m (W-4); 739 m (W-2);

Stratigraphic offset of porosity well: - 38 m (W-4); - 31 m (W-2);

Average porosity: 0.20;

Geologic formations sampled (Fig. 9): Pennsylvanian;

Other comments: Most thermal conductivity values range between 1 - 1.8 W/m-K. Lithologies found during sampling: red sandstone in the upper ~700 m of the well; predominant gray and black shale, with secondary sandstone in the bottom part of the well. There is an apparent direct relationship between thermal gradients (Fig. A17b) and thermal conductivities (Fig. A17c).

site #10:

Well used for thermal conductivity measurements: Johnston #1 (for location, see Table 2 and Fig. A20);

Distance from temperature well: 652 m;

Depth interval with thermal conductivity measurements: 105 - 922 m below ground surface;

Stratigraphic offset of conductivity well: + 26 m;

Number of thermal conductivity measurements: 77 (Fig. A19c);

Value interval: 1.1 - 5.5 W/m-K;

***In situ* harmonic mean of all thermal conductivity measurements (after corrections for anisotropy, temperature, and porosity): 1.85 ± 0.10 W/m-K;**

Well used for porosity determination: Standon Little #6 (for location, see Table 3 and Fig. A20);

Depth interval of density log: 454 - 1,286 m (832 m interval length);

Distance from conductivity well: 1,000 m;

Stratigraphic offset of porosity well: - 47 m;

Average porosity: 0.07;

Geologic formations sampled (Fig. 9): Pennsylvanian;

Other comments: Lithologies found during sampling: gray shale, in the upper half of the well; black shale in the lower half of the well; sandstone is secondary in the middle of the well.

site #11:

Well used for thermal conductivity measurements: Williams #3 (for location, see Table 2 and Fig. A22);

Distance from temperature well: 1,783 m;

Depth interval with thermal conductivity measurements: 212 - 825 m below ground surface;

Stratigraphic offset of conductivity well: - 16 m;

Number of thermal conductivity measurements: 60 (Fig. A21c);

Value interval: 0.96 - 5.5 W/m-K;

In situ harmonic mean of all thermal conductivity measurements (after corrections for anisotropy, temperature, and porosity): 1.77 ± 0.10 W/m-K;

Well used for porosity determination: Thomas Ryan #1-35 (for location, see Table 3 and Fig. A22);

Depth interval of density log: 115 - 1,111 m (996 m interval length);

Distance from conductivity well: 1,435 m;

Stratigraphic offset of porosity well: + 1 m;

Average porosity: 0.08;

Geologic formations sampled (Fig. 9): Pennsylvanian;

other comments: Lithologies found during sampling: black and gray shale (predominant), white sandstone (secondary). Note the inverse relationship

between temperature gradients (Fig. A21b) and thermal conductivities (Fig. A21c).

site #12:

Wells used for thermal conductivity measurements: Fixico #5 (F-5) and Chowing #7 (C-7) (for location, see Table 2 and Fig. A24);

Distance from temperature well: 1,478 m (F-5); 565 m (C-7);

Depth interval with thermal conductivity measurements: 147 - 240 m (F-5); 252 - 921 m (C-7) below ground surface;

Stratigraphic offset of conductivity well: + 8 m (F-5); + 5 m (C-7);

Number of thermal conductivity measurements: 11 (F-5); 74 (C-7) (Fig. A23c);

Value interval: 1.5 - 4.7 W/m-K;

In situ harmonic mean of all thermal conductivity measurements (after corrections for anisotropy, temperature, and porosity): 2.50 ± 0.03 W/m-K (F-5); 1.87 ± 0.05 W/m-K (C-7); harmonic mean for the entire site is 1.93 ± 0.06 W/m-K;

Well used for porosity determination: Nichols #6 (for location, see Table 3 and Fig. A24);

Depth interval of density log: 792 - 1,331 m (539 m interval length);

Distance from conductivity well: 1304 m (F-5); 957 m (C-7);

Stratigraphic offset of porosity well: + 5 m (F-5); + 8 m (C-7)

Average porosity: 0.08;

Geologic formations sampled (Fig. 9): Pennsylvanian;

Other comments: Lithologies found during sampling: red sandstone in the upper part of the well (samples from F-5); red, gray and black shale, red and white sandstone in the rest of the well (samples from C-7). This site shows the disadvantage of using drilling cuttings from two different wells: the different lithologies produce different harmonic means of thermal conductivity

measurements (2.50 W/m-K for F-5 vs. 1.87 W/m-K for C-7).

site #13:

Well used for thermal conductivity measurements: Tiger #3 (for location, see Table 2 and Fig. A26);

Distance from temperature well: 2,087 m;

Depth interval with thermal conductivity measurements: 145 - 1,081 m below ground surface;

Stratigraphic offset of conductivity well: - 3 m;

Number of thermal conductivity measurements: 91 (Fig. A25c);

value interval: 1.1 - 3.3 W/m-K;

In situ harmonic mean of all thermal conductivity measurements (after corrections for anisotropy, temperature, and porosity): 1.63 ± 0.05 W/m-K;

Well used for porosity determination: Hurst #1 (for location, see Table 3 and Fig. A26);

Depth interval of density log: 79 - 1310 m (1231 m interval length);

Distance from conductivity well: 2304 m;

Stratigraphic offset of porosity well: - 2 m;

Average porosity: 0.14;

Geologic formations sampled (Fig. 10): Pennsylvanian and Mississippian;

Other comments: Lithologies found during sampling: gray, red, and black shale (predominant), few limestone, white sandstone (secondary). Thermal conductivities do not change with geologic age (Fig. 10). Note the inverse relationship between temperature gradients (Fig. A25b) and thermal conductivities (Fig. A25c). The upper part of the well (approximately the first 500 m) show a greater scatter of values due to an alternance of shale and sandstone, sometimes limestone.

site #14:

Well used for thermal conductivity measurements: Livingstone #13 (for location, see Table 2 and Fig. A28);

Distance from temperature well: 739 m;

Depth interval with thermal conductivity measurements: 148 - 971 m below ground surface;

Stratigraphic offset of conductivity well: + 37 m;

Number of thermal conductivity measurements: 81 (Fig. A27c);

Value interval: 0.97 - 3.4 W/m-K;

In situ harmonic mean of all thermal conductivity measurements (after corrections for anisotropy, temperature, and porosity): 1.59 ± 0.06 W/m-K;

well used for porosity determination: Goforth #24 (for location, see Table 3 and Fig. A28);

Depth interval of density log: 334 - 959 m (625 m interval length);

Distance from conductivity well: 1000 m;

Stratigraphic offset of porosity well: - 9 m;

Average porosity: 0.15;

Geologic formations sampled (Fig. 10): Pennsylvanian;

Other comments: Lithologies found during sampling: gray shale and sandstone in the upper half of the well, black shale in the bottom half of the well. Note the inverse relationship between temperature gradients (Fig. A27b) and thermal conductivities (Fig. A27c).

site #15:

Wells used for thermal conductivity measurements: Beard #1 (B-1) and Harper #1 (H-1) (for location, see Table 2 and Fig. A30);

Distance from temperature well: 1783 m (B-1); 434 m (H-1);

Depth interval with thermal conductivity measurements: 151 - 233 m; 745 -

918 m (B-1) and 238 - 734 m (H-1) below ground surface;
Stratigraphic offset of conductivity well: - 4 m (B-1); - 1 m (H-1);
Number of thermal conductivity measurements: 37 (B-1); 66 (H-1) (Fig. A29c);
Value interval: 1.0 - 3.6 W/m-K;
In situ harmonic mean of all thermal conductivity measurements (after corrections for anisotropy, temperature, and porosity): 1.56 ± 0.07 W/m-K (B-1); 1.68 ± 0.07 W/m-K (H-1); harmonic mean for the entire site is 1.64 ± 0.05 W/m-K;
Well used for porosity determination: Chamblee #1 (for location, see Table 3 and Fig. A30);
Depth interval of density log: 593 - 1226 m (633 m interval length);
Distance from conductivity well: 1630 m B-1); 652 m (H-1);
Stratigraphic offset of porosity well: + 4 m (B-1); - 2 m (H-1);
Average porosity: 0.07;
Geologic formations sampled (Fig. 10): Pennsylvanian;
Other comments: Lithologies found during sampling: gray shale and sandstone in the upper half of the well; black shale and white sandstone in the bottom half of the well.

site #16:

Wells used for thermal conductivity measurements: Bryant #1 (Br-1) and Holotka #2 (H-2) (for location, see Table 2 and Fig. A32);
Distance from temperature well: 935 m (Br-1); 826 m (H-2);
Depth interval with thermal conductivity measurements: 151 - 961 m (Br-1) and 985 - 1072 m (H-2) below ground surface;
Stratigraphic offset of conductivity well: - 30 m (Br-1); - 6 m (H-2);
Number of thermal conductivity measurements: 63 (Br-1); 8 (H-2) (Fig. A31c);
Value interval: 0.98 - 2.7 W/m-K;

In situ harmonic mean of all thermal conductivity measurements (after corrections for anisotropy, temperature, and porosity): 1.68 ± 0.07 W/m-K (Br-1); 1.25 ± 0.03 W/m-K (H-2); harmonic mean for the entire site is 1.47 ± 0.04 W/m-K;

Well used for porosity determination: Beller Hyde #6-A (for location, see Table 3 and Fig. A32);

Depth interval of density log: 298 - 945 m (647 m interval length);

Distance from conductivity well: 1,391 m (Br-1); 2,174 m (H-2);

Stratigraphic offset of porosity well: - 8 m (Br-1); - 31 m (H-2);

Average porosity: 0.08;

Geologic formations sampled (Fig. 10): Pennsylvanian and Mississippian;

Other comments: Most thermal conductivity values range between 1 - 2 W/m-K. Lithologies found during sampling: gray shale (predominant), few limestone, red sandstone (secondary). Samples from H-2 are only black shales. Thermal conductivities seem to change little with geologic age (Fig. 10). Note the inverse relationship between temperature gradients (Fig. A31b) and thermal conductivities (Fig. A31c).

site #17:

Well used for thermal conductivity measurements: Cully #2 (for location, see Table 2 and Fig. A34);

Distance from temperature well: 870 m;

Depth interval with thermal conductivity measurements: 142 - 819 m below ground surface;

Stratigraphic offset of conductivity well: + 14 m;

Number of thermal conductivity measurements: 90 (Fig. A33c);

Value interval: 1.1 - 3.9 W/m-K;

In situ harmonic mean of all thermal conductivity measurements (after

corrections for anisotropy, temperature, and porosity): 1.53 ± 0.07 W/m-K;
well used for porosity determination: Katy #1 (for location, see Table 3 and Fig. A34);

Depth interval of density log: 287 - 613 m (326 m interval length);

Distance from conductivity well: 1,674 m;

Stratigraphic offset of porosity well: - 22 m;

Average porosity: 0.11;

Geologic formations sampled (Fig. 11): Pennsylvanian;

Other comments: Lithologies found during sampling: gray, red, and black shale, few limestone, white sandstone. The thermal conductivity values are little scattered in the upper part of the well where presence of limestone and sandstone makes the lithology inhomogeneous.

site #18:

Wells used for thermal conductivity measurements: Edge Hardin #11 (EH-11) and Hardin Heirs #2 (HH-2) (for location, see Table 2 and Fig. A36);

Distance from temperature well: 870 m (EH-11); 1783 m (HH-2);

Depth interval with thermal conductivity measurements: 152 - 476 m (EH-11) and 488 - 695 m (HH-2) below ground surface;

Stratigraphic offset of conductivity well: - 82 m (EH-11); +32 m (HH-2);

Number of thermal conductivity measurements: 33 (EH-11); 77 (HH-2) (Fig. A35c);

Value interval: 1.3 - 3.1 W/m-K;

In situ harmonic mean of all thermal conductivity measurements (after corrections for anisotropy, temperature, and porosity): 2.40 ± 0.05 W/m-K (EH-11); 1.35 ± 0.01 W/m-K (HH-2); harmonic mean for the entire site is 2.22 ± 0.04 W/m-K;

Well used for porosity determination: County Line Unit #11-2B (for location,

see Table 3 and Fig. A36);

Depth interval of density log: 395 - 1,127 m (732 m interval length);

Distance from conductivity well: 587 m (EH-11); 1,000 m (HH-2);

Stratigraphic offset of porosity well: + 45 m (EH-11); - 71 m (HH-2)

Average porosity: 0.20;

Geologic formations sampled (Fig. 11): Pennsylvanian

Other comments: This site has the largest harmonic mean of measured thermal conductivities. Lithologies found during sampling: predominant pink and white sandstone; gray and black shale is secondary. Note the trend of increasing of thermal conductivity with depth.

site #19:

Well used for thermal conductivity measurements: Beard #1 (for location, see Table 2 and Fig. A38);

Distance from temperature well: 1783 m;

Depth interval with thermal conductivity measurements: 212 - 599 m below ground surface;

Stratigraphic offset of conductivity well: 0 m;

Number of thermal conductivity measurements: 77 (Fig. A37c);

Value interval: 1.1 - 1.7 W/m-K;

In situ harmonic mean of all thermal conductivity measurements (after corrections for anisotropy, temperature, and porosity): 1.35 ± 0.01 W/m-K;

well used for porosity determination: Freeman #5 (for location, see Table 3 and Fig. A38);

Depth interval of density log: 457 - 767 m (310 m interval length);

Distance from conductivity well: 1,217 m;

Stratigraphic offset of porosity well: + 2 m;

Average porosity: 0.15;

Geologic formations sampled (Fig. 11): Pennsylvanian;

Other comments: Most thermal conductivity values range in a very narrow interval(1.2 - 1.5 W/m-K. Lithologies found during sampling: predominant gray shale with very few limestone and sandstone.

site #20:

Well used for thermal conductivity measurements: Dillard #115 (for location, see Table 2 and Fig. A40);

Distance from temperature well: 304 m;

Depth interval with thermal conductivity measurements: 160 - 844 m below ground surface;

Stratigraphic offset of conductivity well: - 59 m;

Number of thermal conductivity measurements: 53 (Fig. A39c);

value interval: 1.2 - 3.5 W/m-K;

In situ harmonic mean of all thermal conductivity measurements (after corrections for anisotropy, temperature, and porosity): 2.02 ± 0.07 W/m-K;

Well used for porosity determination: Hewitt unit #22-4203 (for location, see Table 3 and Fig. A40);

Depth interval of density log: 16 - 912 m (906 m interval length);

Distance from conductivity well: 1,000 m;

Stratigraphic offset of porosity well: + 114 m;

Average porosity: 0.21;

Geologic formations sampled (Fig. 11): Permian, Pennsylvanian, and Mississippian;

Other comments: Lithologies found during sampling: red and white sandstone, gray and red shale. Thermal conductivities seem to change with geologic age (Fig. 49), from lower values in Permian (~1 - ~2 W/m-K), through higher values in Pennsylvanian (~2 - ~3 W/m-K), to again lower

values in Mississippian (~1 - ~2 W/m-K).

APPENDIX D

Distribution of heat flow intervals for each site:

- site #1 (Fig. A1d): 4 intervals; 37 - 51 mW/m²;
- site #2 (Fig. A3d): 3 intervals; 42 - 60 mW/m²;
- site #3 (Fig. A5d): 9 intervals; 42 - 76 mW/m²;
- site #4 (Fig. A7d): 5 intervals; 40 - 48 mW/m²;
- site #5 (Fig. A9d): 4 intervals; 39 - 56 mW/m²;
- site #6 (Fig. A11d): 9 intervals; 44 - 79 mW/m²;
- site #7 (Fig. A13d): 7 intervals; 19 - 60 mW/m²;
- site #8 (Fig. A15d): 9 intervals; 45 - 123 mW/m²;
- site #9 (Fig. A17d): 9 intervals; 20 - 42 mW/m²;
- site #10 (Fig. A19d): 10 intervals; 54 - 99 mW/m²;
- site #11 (Fig. A21d): 8 intervals; 41 - 101 mW/m²;
- site #12 (Fig. A23d): 5 intervals; 51 - 69 mW/m²;
- site #13 (Fig. A25d): 5 intervals; 39 - 55 mW/m²;
- site #14 (Fig. A27d): 4 intervals; 44 - 66 mW/m²;
- site #15 (Fig. A29d): 10 intervals; 58 - 70 mW/m²;
- site #16 (Fig. A31d): 6 intervals; 49 - 50 mW/m²;
- site #17 (Fig. A33d): 5 intervals; 39 - 54 mW/m²;
- site #18 (Fig. A35d): 5 intervals; 26 - 39 mW/m²;
- site #19 (Fig. A37d): 5 intervals; 18 - 25 mW/m²;
- site #20 (Fig. A39d): 8 intervals; 26 - 54 mW/m²;

REFERENCES

- American Association of Petroleum Geologists and U.S. Geological Survey, 1976, Geothermal gradient map of North America: U.S. Geological Survey, scale 1:5,000,000.
- Amsden, T. W., 1975, Hunton Group (Late Ordovician, Silurian, and Early Devonian (in the Anadarko basin of Oklahoma): Oklahoma Geological Survey Bull. 121, 214 pp.
- Anand, J., Somerton, W. H., and Goma, E., 1973, Predicting thermal conductivities of formations from other known properties: Soc. Pet. Eng. J., v. 13, p. 267 - 273.
- Anderson, G. M., and Macqueen, R. W., 1982, Ore deposit models. 6. - Mississippi Valley-type lead-zinc deposits: Geoscience Canada, v. 9, p. 108 - 117.
- Arbenz, J. K., 1989, The Ouachita system, *in* A. W. Bally and A. R. Palmer (eds.): The Geology of North America - An overview, Boulder, Colorado, Geol. Soc. of America, The Geology of North America, v. A, p. 371 - 396.
- Bachu, S., 1997, Flow of formation waters, aquifer characteristics, and their relation to hydrocarbon accumulation, Northern Alberta Basin: AAPG Bull., v. 81, p. 712 - 733.
- Bachu, S., and Hitchon, B., 1996, Regional-scale flow of formation waters in the Williston basin: AAPG Bull., v. 80, p. 248 - 264.
- Bachu, S., 1993, Basement heat flow in the Western Canada sedimentary basin: Tectonophysics, v. 222, p. 119 - 133.
- Bagley, D. S., London, D., Fruit, D., Cates, K. D., and Elmore, R. D., 1992, Paleomagnetic dating of basinal fluid migration, base-metal mineralization, and hydrocarbon maturation in the Arbuckle Mountains, Oklahoma: Oklahoma Geological Survey Circular 93, p. 289 - 298.
- Banner, J. L., Wasserburg, G. J., Dobson, P. F., Carpenter, A. B., and Moore, C. H., 1989, Isotopic and trace element constraints on the origin and evolution of saline groundwaters from central Missouri: Geochimica et Cosmochimica Acta, v. 53, p. 383 - 398.
- Barker, C., 1996, Thermal modeling of petroleum generation: theory and application, Elsevier, Amsterdam - Lausanne - New York - Oxford -

Shannon - Tokyo, 516 pp.

Barry, B. A., 1978, *Errors in practical measurements in science, engineering, and technology*: John Wiley, New York, 183 pp.

Barthel, C. J., 1985, *Hydrogeologic investigation of artesian spring flow, Sulphur, Oklahoma area*: MS thesis, Univ. Of Oklahoma, 234 pp.

Beck, A. E., 1957, A steady state method for the rapid measurement of the thermal conductivity of rocks: *J. Sci. Instrum.*, v. 34, p. 186 - 189.

Beck, A. E., 1977, Climatically perturbed temperature gradients and their effect on regional and continental heat-flow measurements: *Tectonophysics*, v. 41, p. 17 - 39.

Benfield, A. E., 1947, A heat flow value for a well in California: *Am. J. Science*, v. 245, p. 1 - 18.

Bethke, C. M., and Marshak, S., 1990, Brine migration across North America - The plate tectonics of groundwater: *Ann. Rev. Earth Sci.*, v. 18, p. 287 - 315.

Birch, F., 1950, Flow of heat in the Front Range, Colorado: *Geol. Soc. Am. Bull.*, v. 61, p. 567 - 620.

Birch, F., 1954, Thermal conductivity, climatic variation, and heat flow near Calumet, Michigan: *Am J. Science*, v. 252, p. 1 - 25.

Birch, F., and Clark, H., 1940, The thermal conductivity of rocks and its dependence upon temperature and composition: *Am. J. Sci.*, v. 238, p. 529 - 558, 613 - 635.

Birch, F., Roy, R. F., and Decker, E. R., 1968, Heat flow and thermal history in New York and New England: *in* E. Zen, W. S. White, J. B. Hadley and J. B. Thompson, Jr. (eds.), *Studies of Appalachian Geology: Northern and Maritime*, Intersciences, New York, p. 437 - 451.

Blackwell, D. D., 1967, *Terrestrial heat flow determinations in the northwestern United States*: PhD thesis, 190 pp., Harvard University, Cambridge, Massachusetts.

Blackwell, D. D., and Steele, J. L., 1991 (eds.), *Geothermal map of North America, Colorado*, Geol. Soc. of America, map CSM - 007, 4 sheets, scale 1:5,000,000.

Blackwell, D. D., Steele, J. L., and Carter, L. S., 1994, *United states and Central*

America geothermal data base: Geophysics of North America CD-ROM, U. S. Department of Commerce.

- Borel, R. A., 1995, Geothermics of the Gypsy Site, northcentral Oklahoma: MS thesis, Univ. of Oklahoma, 82 pp.
- Brace, W. F., 1980, Permeability of crystalline and argillaceous rocks: *Int. J. Rock Mech. Min. Sci. & Geomech. Abstr.*, v. 17, p. 241 -251.
- Bredehoeft, J. D., and Papadopulos, I. S., 1965, Rates of vertical groundwater movement estimated from the Earth's thermal profile: *Water Resources Research*, v. 1., p. 325 - 328.
- Bredehoeft, J. D., Wesley, J. B., and Fouch, T. D., 1994, Simulations of the origin of fluid pressure, fracture generation, and the movement of fluids in the Uinta Basin, Utah: *AAPG Bull.*, v. 78, p. 1729 - 1747.
- Brewer, J. A., Good, R., Oliver, J. E., Brown, L. D., and Kaufman, S., 1983, COCORP profiling across the southern Oklahoma aulacogen: overthrusting of the Wichita Mountains and compression within the Anadarko Basin: *Geology*, v. 11, p. 169 - 114.
- Bücker, C., and Rybach, L., 1996, A simple method to determine heat production from gamma-ray log: *Mar. Pet. Geol.*, v. 13, p. 373 - 375.
- Cardott, B. J., 1989, Thermal maturation of the Woodford shale in the Anadarko basin: *in* K. S. Johnson (ed.), *Anadarko basin symposium*, 1988: Oklahoma Geological Survey Circular 90, p. 32 - 46.
- Carr, J. E., McGovern, H. E., and Gogel, T., 1986, Geohydrology of and potential for fluid disposal in the Arbuckle Aquifer in Kansas: U. S. Geological Survey Open-File Report 86-491, 101 pp.
- Carter, L. S., Kelly, S. A., Blackwell, D. D., and Naeser, N. D., 1996, Heat flow and thermal history of the Anadarko Basin, Oklahoma: submitted to *AAPG Bull.*
- Cermák, V., and Rybach, L., 1982, Thermal conductivity and specific heat of minerals and rocks, *in* G. Angenheister (ed.): *Physical properties of rocks*, vol. 1 - a, Springer - Verlag, New York, p. 305 - 403.
- Chapman, D. S., Keho, T. H., Bauer, M.S., and Picard, M. D., 1984, Heat flow in the Uinta Basin determined from bottom hole temperature (BHT) data: *Geophysics*, v. 49, p. 453 - 466.
- Cheung, P. K., 1978, The geothermal gradient in sedimentary rocks in

Oklahoma: MS thesis, Oklahoma State University, 55 pp.

- Cheung, P. K., 1979, Geothermal gradient mapping - Oklahoma: Presented in 7th Formation Evaluation Symposium of Canadian Well Logging Society in Calgary, Canada, October, 1979, 15 pp.
- Clark, S. P., 1966, Handbook of physical constants: Geological Society of America Memoir no. 97, 587 pp.
- Committee for the Magnetic Anomaly Map of North America, 1987: Boulder, Geological Society of America, scale 1:5,000,000, 4 sheets.
- Coveney, R. M. Jr., 1992, Evidence for expulsion of hydrothermal fluids and hydrocarbons in the midcontinent during Pennsylvanian: Oklahoma Geological Survey Circular 93, p. 933 - 943.
- Coveney, R. M. Jr., Goebel, E. D., and Rogan, V. M., 1987, Pressures and temperatures from aqueous fluid inclusions in sphalerite from Midcontinent country rocks: Economic Geology, v. 82, p. 740 - 751.
- Coveney, R. M., and Martin, S. P., 1983, Molybdenum and other heavy metals of the Mecca Quarry and Logan Quarry shales: Economic Geology, v. 78, p. 132 - 149.
- Cranganu, C., and Deming, D., 1996, Heat flow and hydrocarbon generation in the Transylvanian Basin, Romania: AAPG Bull., v. 80, p. 1,641 - 1,653.
- Cranganu, C., and Deming, D., 1997, A heat flow map of Oklahoma: Oklahoma Geology Notes, v. 57, p. 28 -29.
- Davis, H. G., and Northcutt, R. A., 1989, The greater Anadarko basin: an overview of petroleum exploration and development: Oklahoma Geological Survey Circular 90, p. 13 - 24.
- Davis, J. C., 1986, Statistics and data analysis in geology, second edition, John Wiley & Sons, Inc., New York, 646 pp.
- De Bremaecker, J.-C., 1983, Temperature, subsidence, and hydrocarbon maturation in extensional basins: a finite element model: AAPG Bull., v. 67, p. 1,410 - 1,414.
- Deming, D., 1994a, Estimation of the thermal conductivity anisotropy of rock with application to the determination of terrestrial heat flow: J. Geophys. Res., v. 99, p. 22,087 - 22,091.

- Deming, D., 1994b, Factors necessary to define a pressure seal: AAPG Bull., v. 79, p. 1105 - 1009.
- Deming, D., and Borel, R., 1995, Evidence for climatic warming in northeastern Oklahoma from analysis of borehole temperatures: J. Geophys. Res., v. 100, p. 22,017 - 22,032.
- Deming, D., Sass, J. H., and Lachenbruch, A. H., 1996, Heat flow and subsurface temperature, north slope of Alaska: *in* M. J. Johnson and D. G. Howell (eds.), Thermal evolution of sedimentary basins in Alaska: U. S. Geological Survey Bull. 2142, p. 21 - 44.
- Deming, D., Sass, J. H., Lachenbruch, A. H., and De Rito, R. F., 1992, Heat flow and subsurface temperature as evidence for basin-scale groundwater flow, North slope of Alaska: Geological Society of America Bulletin, v. 104, p. 528 - 542.
- Denison, R. E., Lidiak, E. G., Bickford, M. E., and Kisvarsanyi, E. B., 1984, Geology and geochronology of the Precambrian rocks in the central region of the United States: Geol. Surv. Prof. Paper 1241 - C, 20 pp.
- Domenico, P. A., and Palciauskas, V. V., 1973, Theoretical analysis of forced convective heat transfer in regional ground-water flow: Geol. Soc. of America Bull., v. 84, p. 3803 - 3814.
- Elmore, R. D., Sutherland, P. K., and Whito, P. B., 1990, Middle Pennsylvanian recurrent uplift of the Ouachita fold belt and the basin subsidence in the Arkoma basin, Oklahoma: Geology, v. 18, p. 906 - 909.
- Fairchild, R. W., and Davis, R. E., 1983, Hydrologic data for the Arbuckle Mountain area, south-central Oklahoma: U. S. Geological Survey Open-File Report 83-28, 74 pp.
- Fairchild, R. W., Hanson, R. L., and Davis, R. E., 1982, Hydrogeology of the Arbuckle Mountain area, south-central Oklahoma: U. S. Geological Survey Open-File Report 82-775, 156 pp.
- Fairchild, R. W., Hanson, R. L., and Davis, R. E., 1990, Hydrology of the Arbuckle Mountain area, south-central Oklahoma: Oklahoma Geological Survey Circular 91, 112 pp.
- Fay, R. O., 1989, Geology of the Arbuckle Mountains along interstate 35, Carter and Murray Counties, Oklahoma: Oklahoma Geological Survey Guidebook 26, 50 pp.

- Feinstein, S., 1981, Subsidence and thermal history of Southern Oklahoma aulacogen: implications for petroleum exploration: AAPG Bull., v. 65, p. 2,521 - 2,533.
- Fertl, W. H., Chapman, R. E., and Hertz, R. F. (eds.), 1994, Studies in abnormal pressures, Elsevier, Amsterdam - London - New York - Tokyo, 454 pp.
- Förster, A., and Merriam, D., 1996, Heat flow in the Cretaceous of northwestern Kansas: Kansas Geological Survey Journal of Research (in press).
- Fountain, D. M., Salisbury, M. H., and Furlong, K. P., 1987, Heat production and thermal conductivity of rocks from the Pikwitoney-Sachigo continental cross section, central Manitoba: implications for the thermal structure of Archean crust: Can. J. Earth Sci., v. 24, p. 1,583 - 1,594.
- Funnell, R., Chapman, D., Allis, R., and Armstrong, P., 1996, Thermal state of the Taranaki Basin, New Zealand: J. Geoph. Res., v. 101, p. 25,197 - 25,215.
- Furlong, K., and Chapman, D. S., 1987, Crustal heterogeneities and the thermal structure of the continental crust: Geophys. Res. Lett., v.14, p. 314 - 317.
- Garven, G., Ge, S., Person, M. A., and Sverjensky, D. A., 1993, Genesis of stratabound ore deposits in the Midcontinent Basins of North America. 1. The role of regional groundwater flow: Am. J. Sci., v. 293, p. 497 - 568.
- Gilarranz, S., 1964, Determination of regional geothermal gradients in Oklahoma from logs, MS thesis, Univ. of Tulsa, 65 pp.
- Gilbert, M. C., 1983, Timing and chemistry of igneous events associated with the southern Oklahoma aulacogen: Tectonophysics, v. 94, p. 439 - 453.
- Gilbert, M. C., 1992, Speculations on the origin of the Anadarko Basin: in R. Mason (ed.), Basement Tectonics 7, International Basement Tectonics Association Publication no. 7, Kluwer Academic Publishers, Netherlands, p. 195 - 208.
- Goldstein, A. Jr., 1975, Geologic interpretation of Viersen and Cohran's 25-1 Weyerhaeuser well, McCurtain County, Oklahoma: Oklahoma Geology Notes, 35, p. 167 -181.

- Guffanti, M., and Nathenson, M., 1981, Temperature-depth data for selected deep drill holes in the United States obtained using maximum thermometers: U.S. Geological Survey Open File Report 81 - 555.
- Ham, W. E., 1969, Regional geology of the Arbuckle Mountains, Oklahoma: Oklahoma Geol. Survey Guide Book 17, 52 pp.
- Ham, W. E., and Wilson, J. L., 1967, Paleozoic epeirogeny and orogeny in the central United States: American J. of Science, 265, p. 332 - 407.
- Ham, W. E., Denison, R. E., and Meritt, C. A., 1964, Basement rocks and structural evolution of Southern Oklahoma: Oklahoma Geol. Survey Bull., 95, 302 pp.
- Hanson, R. L., and Cates, S. W., 1994, Hydrogeology of the Chickasaw National Recreation Area, Murray County, Oklahoma: U. S. Geological Survey Water-Resources Investigations Report 94-4102, 86 pp.
- Harrison, W. E., and Luza, K. V., 1986, Temperature-gradient information for several boreholes drilled in Oklahoma: Oklahoma Geological Survey Special Publication 86 - 2, 42 pp.
- Harrison, W. R., Prater, M. L., and Cheung, P. K., 1983, Geothermal resources assessment in Oklahoma: Oklahoma Geological Survey Special Publication 83 - 1, 42 pp.
- Heald, K. C., 1930, The study of Earth temperatures in oil fields on anticlinal structures: *in* Earth Temperatures in Oil Fields, American Petroleum Institute Production Bulletin 205, p. 1 - 8.
- Herrin, J. M., and Deming, D., 1996, Thermal conductivities of U.S. coals: J. Geoph. Res., v. 101, p. 25,381 - 25,386.
- Hester, T. C., Schmoker, J. W., and Sahl, H. L., 1992, Structural controls on sediment distribution and thermal maturation of the Woodford shale, Anadarko Basin, Oklahoma: Oklahoma Geological Survey Circular 93, p. 321 - 326.
- Horai, K., 1971, Thermal conductivity of rock-forming minerals: J. Geoph. Res., v. 76, p. 1,278 - 1,308.
- Houseknecht, D. W., 1986, Evolution from passive margin to foreland basin: the Atokan formation of the Arkoma Basin, south-central U.S.A., *in* D. Allen and P. Homewood (eds.): Foreland Basins, Spec. Publ.,

Int. Assoc. Sedimentol., v. 8, p. 327 - 345.

Houseknecht, D. W., Hathon, L. A., and Mcgilvery, T. A., 1992, Thermal maturity of Paleozoic strata in the Arkoma Basin: Oklahoma Geological Survey Circular 93, p. 122 - 132.

Hutchison, I., 1985, The effects of sedimentation and compaction on oceanic heat flow: *Geophysical Journal of the Royal Astronomical Society*, v. 82, p. 439 - 459.

Jessop, A. M., 1990, *Thermal geophysics*, Elsevier, Amsterdam - Oxford - New York - Tokyo, 306 pp.

Johnson, K. S., 1991, Map of aquifers and recharge areas in Oklahoma: Oklahoma State Department of Health and Oklahoma Geological Survey, scale 1:5,000,000, 1 sheet.

Johnson, K. S., Branson, C. C., Curtis, N. M., Jr., Ham, W. E., Marcher, M. V., and Roberts, J. F., 1972, *Geology and earth resources of Oklahoma*: Oklahoma Geological Survey Educational Publication 1, 8 pp.

Johnson, K. S., Amsden, T. W., Denison, R. E., Dutton, S. P., Goldstein, A. G., Rascoe, B., Jr., Sutherland, P. K., and Thompson, D. M., 1988, Southern Midcontinent region, in L. L. Sloss (ed.): *Sedimentary cover - North American Craton*; U. S. Boulder, Colorado, Geol. Soc. of America, *The Geology of North America*, v. D - 2, p. 307 - 359.

Johnson, K. S., and Cardott, B. J., 1992, *Geologic framework and hydrocarbon source rocks of Oklahoma*: Oklahoma Geological Survey circular 92, p. 21 - 37.

Jones, V. L., and Lyons, P. L., 1964, *Vertical-intensity map of Oklahoma*: Norman, Oklahoma Geological Survey Map GM-6, scale 1:750,000.

Jorgensen, D. G., 1989, *Paleohydrology of the Anadarko Basin, central United States*: Oklahoma Geological Survey Circular 90, p. 176 - 193.

Jorgensen, D. G., 1993, *Paleohydrology of the central United States*: U. S. Geol. Survey Bull. 1989-D, 32 pp.

Jorgensen, D. G., Helgesen, J. O., and Imes, J. L., 1993, *Regional aquifers in Kansas, Nebraska, and parts of Arkansas, Colorado, Missouri, New Mexico, Oklahoma, South Dakota, Texas, and Wyoming - geohydrologic framework*: U. S. Geol. Survey Professional Paper 1414-B, 72 pp.

- Joyner, W. B., 1960, Heat flow in Pennsylvania and West Virginia: *Geophysics*, v. 25, p. 1,229 - 1,241.
- Kappelmeyer, O., and Haenel, R., 1974, *Geothermics with special reference to application: Gebruder Borntraeger, Berlin*, 238 pp.
- Kawada, K., 1964, Studies of the thermal state of the Earth: The 17th paper: Variation of thermal conductivity of rocks, 1: *Bull. Earthquake Res. Inst. Univ. Tokyo*, v. 42, p. 631 - 647.
- Kawada, K., 1966, Studies of the thermal state of the Earth: The 17th paper: Variation of thermal conductivity of rocks, 2: *Bull. Earthquake Res. Inst. Univ. Tokyo*, v. 44, p. 1,071 - 1,091.
- Keen, C. E., and Lewis, T., 1982, Measured radiogenic heat production in sediments from continental margin of eastern North America: implications for petroleum generation: *AAPG Bull.*, v. 66, p. 1,402 - 1,407.
- Kisvarsanyi, G., Grant, S. K., Pratt, W. P., and Koenig, J. W. (eds.), 1983, *Proceedings of the international conference on Mississippi Valley-type lead-zinc deposits: University of Missouri - Rolla Press*, 603 pp.
- Kruger, J. M., and Keller, G. R., 1986, Interpretation of crustal structure from regional gravity anomalies, Ouachita Mountains and adjacent Gulf coastal plain: *AAPG Bull.*, v. 70, p. 667 - 689.
- Lachenbruch, A. H., 1969, The effect of two-dimensional topography on superficial thermal gradients: *Geol. Survey Bull.* 1203-E, 86 pp.
- Lachenbruch, A. H., 1970, Crustal temperature and heat production: implication for the linear heat-flow relation: *J. Geophys. Res.*, v. 75, p. 3,291 - 3,300.
- Lachenbruch, A. H., and Marshall, B. V., 1966, Heat flow through the Arctic Ocean floor: the Canada Basin - Alpha Rise Boundary: *J. Geoph. Res.*, vol. 71, p. 1,223 - 1,248.
- Lachenbruch, A. H., and Sass, J. H., 1977, Heat flow in the United States and the thermal regime of the crust: *in* J. G. Heacock (ed.), G. V. Keller, J. E. Oliver and G. Simmons (assoc. eds.): *The Earth's Crust - Its Nature and Physical Properties*, AGU Geophysical monograph 20, p. 626 - 671.
- Langseth, M. G., Grimm, P. J., and Ewing, M., 1965, Heat flow measurements in the East Pacific Ocean: *J. Geoph. Res.*, v. 70, p. 367 - 380.

- Leach, D. L., 1979, Temperature and salinity of the fluids responsible for minor occurrences of the sphalerite in the Ozark region of Missouri: *Economic Geology*, v. 74, p. 931 - 937.
- Lee, Y., and Deming, D., 1997, Heat flow in the Anadarko Basin, and the Oklahoma platform : submitted to *Geology*.
- Lee, Y., Deming, D., and Chen, K. F., 1996, Heat flow and heat production in the Arkoma Basin and Oklahoma Platform, southeastern Oklahoma: *J. Geophys. Res.*, v. 101, p. 25,387 - 25,401.
- Luza, K. V., and Lawson, J. E. Jr., 1983, Seismicity and tectonic relationships of the Nemaha Uplift in Oklahoma, part V (final report): Oklahoma Geological Survey, 115 pp.
- Majorowicz, J. A., and Jessop, A. M., 1981, Regional heat flow patterns in the western Canadian sedimentary basin: *Tectonophysics*, v. 74, p. 209 - 238.
- Mattes, B. W., and Mountjoy, E. W., 1980, Burial dolomitization of the Upper Devonian Miette buildup, Jasper National Park, Alberta, in D. H. Zenger, J. B. Dunham, and R. L. Ethington (eds.), *Concepts and Models of Dolomitization: Soc. Econ. Paleontolog. Mineral. Spec. Publ.*, v. 28, p. 259 - 297.
- McCabe, C., Van der Voo, R., Peacor, D. R., Scotese, C. R., and Freeman, R., 1983, Diagenetic magnetite carries ancient yet secondary remanence in some Paleozoic sedimentary carbonates: *Geology*, v. 11, p. 221 - 223.
- McCutchin, J. A., 1930, Determination of geothermal gradients in oil fields located on anticlinal structures in Oklahoma: in *Earth Temperatures in Oil Fields*, American Petroleum Institute Production Bulletin 205, p. 19 - 61.
- McKee, E. D., and others, 1975, Paleotectonic investigations of the Pennsylvanian System in the United States: U. S. Geological Survey Professional Paper 853, part I, 349 pp.; part II, 192 pp.; part III, 17 plates.
- Mitchell, B. J., and Landisman, M., 1970, Interpretation of a crustal section across Oklahoma: *Geol. Soc. of America Bull.*, v. 81, p. 2,647 - 2,656.
- Mongelli, F., Loddo, M., and Tramacere, A., 1982, Thermal conductivity, diffusivity and specific heat variation of some Travale Field

- (Tuscany) rocks versus temperature: *Tectonophysics*, v. 83, p. 33 - 43.
- Musgrove, M., and Banner, J. L., 1993, Regional ground-water mixing and the origin of saline fluids: Mid-Continent, United States: *Science*, v. 259, p. 1,877 - 1,882.
- Nathenson, M., and Guffanti, M., 1987, Compilation of geothermal-gradient data in the conterminous United States: U.S. Geological Survey Open File Report 87 - 592.
- Nathenson, M., and Guffanti, M., 1988, Geothermal gradients in the conterminous United States: *J. Geophys. Res.*, v. 93, p. 6,437 - 6,450.
- Neuzil, C. E., 1994, How permeable are clays and shales?: *Water Resources Research*, v. 30, p. 145 - 150.
- Northcutt, R. A., and Campbell, J. A., 1996, Geologic provinces of Oklahoma: Trans. of the 1995 American Association of Petroleum Geologists, Mid-Continent Section Meeting, p. 128 - 134.
- Oliver, J., 1986, Fluids expelled tectonically from orogenic belts: Their role in hydrocarbon migration and other geologic phenomena: *Geology*, v. 14, p. 99 - 102.
- Oliver, J., 1992, The spots and stains of plate tectonics: *Earth Science Reviews*, v. 32, p. 77 - 106.
- Osborne, M. J., and Swarbrick, R. E., 1997, Mechanisms for generating overpressure in sedimentary basins: a reevaluation: *AAPG Bull.*, v. 81, p. 1,023 - 1,041.
- Pawlewicz, M. J., 1992, Thermal maturation of the Eastern Anadarko Basin, Oklahoma: *Oklahoma Geological Survey Circular 93*, p. 327 - 329.
- Person, M., Toupin, D., and Eadington, P., 1995, One-dimensional model of groundwater flow, sediment thermal history and petroleum generation within continental rift basins: *Basin Research*, v. 7, p. 81 - 96.
- Pollack, H. N., and Cercone, K. R., 1994, Anomalous thermal maturities caused by carbonaceous sediments: *Basin Research*, v. 6, p. 47 - 51.
- Pollack, H. N., and Chapman, D. S., 1977, On the variation of heat flow, geotherms, and lithospheric thickness: *Tectonophysics*, v. 38, p. 279 - 296.

- Pollack, H. N., Hurter, S. J., and Johnson, J. R., 1993, Heat flow from the Earth's interior: analysis of the global data set: *Reviews of Geophysics*, v. 31, p. 267 - 280.
- Pruatt, M. A., 1975, The southern Oklahoma aulacogen: a geophysical and geological investigation, MS thesis, Univ. of Oklahoma, 60 pp.
- Quigley, T. M., Mackenzie, A. S., and Gray, J. R., 1987, Kinetic theory of petroleum migration, in B. Doligez (ed.), *Migration of hydrocarbons in sedimentary basins*, Ed. Technip, Paris, p. 649 - 665.
- Ratcliffe, E. H., 1959, Thermal conductivities of fused and crystalline quartz: *Br. J. Appl. Phys.*, v. 10, p. 22 - 25.
- Robbins, S. L., and Keller, G. R. Jr., 1992, Complete Bouguer and isostatic residual gravity maps of the Anadarko Basin, Wichita Mountains, and surrounding areas, Oklahoma, Kansas, Texas, and Colorado: *U.S. Geol. Surv. Bull* 1866-G, 11 pp.
- Robertson, E. C., 1988, Thermal properties of rocks: U. S. Geol. Survey Open File Report 88 - 441.
- Roedder, E., 1979, Fluid inclusions as samples of ore fluids, in H. L. Barnes (ed.): *Geochemistry of hydrothermal ore deposits*, John Wiley, New York, p. 685 - 737.
- Roy, R. F., Beck, A. E., and Touloukian, Y. S., 1981, Thermophysical properties of rocks, in *Physical properties of rocks and minerals*, McGraw-Hill CINDAS data ser. Mater. prop., vol. II - 2, edited by Y. S. Touloukian, W. R. Judd, and R. F. Roy, McGraw-Hill, New York, p. 409 - 502.
- Roy, R. F., Blackwell, D. D., and Birch, F., 1968, Heat generation of plutonic rocks and continental heat flow provinces: *Earth Planet. Sci. Lett.*, v. 5, p. 1 - 12.
- Rybach, L., 1976, Radioactive heat production: a physical property determined by the chemistry of rocks, in R. G. J. Streus (ed.): *The physics and chemistry of minerals and rocks*, Wiley & Sons, London, p. 309 - 318.
- Rybach, L., 1986, Amount and significance of radioactive heat sources in sediments, in J. Burrus (ed.): *Thermal Modeling in Sedimentary Basins*, Collections Colloques et Séminaires, 44, Ed. Technip, Paris, p. 311 - 322.

- Rybach, L., 1988, Determination of heat production rate, *in* R. Haenel, L. Rybach and L. Stegena (eds.): *Handbook of terrestrial heat-flow density determination*, Kluwer Acad., Norwell, Mass., p. 125 - 142.
- Sahay, B., and Fertl, W. H., 1989, *Origin and evaluation of formation pressures*, Kluwer Academic Publishers, Dordrecht, 292 pp.
- Sass, J. H., Lachenbruch, A. H., and Munroe, R. J., 1971, Thermal conductivity of rocks from measurements on fragments and its application to heat flow determinations: *J. Geophys. Res.*, v. 76, p. 3,391 - 3,401.
- Sass, J. H., Lachenbruch, A. H., Moses, T. H., and Morgan, P., 1992, Heat flow from a scientific research well at Cajon Pass, California: *J. Geophys. Res.*, v. 97, p. 5,017 - 5,030.
- Sass, J. H., Stone, C., and Munroe, R. J., 1984, Thermal conductivity determinations on solid rock - a comparison between a steady-state divided bar apparatus and a commercial transient line-source device: *J. Volcanol. Geotherm. Res.*, v. 20, p. 145 - 153.
- Schmoker, J. W., 1989, Thermal maturity of the Anadarko Basin: *Oklahoma Geological Survey Circular 90*, p. 25 - 31.
- Schoppel, R. J., and Gilarranz, S., 1966, Use of well log temperatures to evaluate regional geothermal gradients: *Journal of Petroleum Technology*, v. 18, p. 667 - 673.
- Seipold, U., 1990, Pressure and temperature dependence of thermal transport properties of granites: *High Temp. High Pressures*, v. 22, p. 541 - 548.
- Sekiguchi, K., 1984, A method for determining terrestrial heat flow in oil basinal areas: *Tectonophysics*, v. 103, p. 67 - 79.
- Shelton, K. L., Bauer, R. M., and Gregg, J. M., 1992, Fluid inclusion studies if regionally extensive epigenetic dolomites, Bonneterre Dolomite (Cambrian), southeast Missouri: Evidence of multiple fluids during dolomitization and lead - zinc mineralization: *Geol. Soc. of America Bull.*, v. 104, p. 675 - 683.
- Sibbit, W. L., Dodson, J. G., and Tester, J. W., 1979, Thermal conductivity of crystalline rocks associated with energy extraction from hot dry rock geothermal systems: *J. Geophys. Res.*, v. 84, p. 1,117 - 1,124.
- Spicer, H. C., 1964, A compilation of deep Earth temperature data: USA, 1910 - 1945: *U.S. Geological Survey Open File Report 64* - 147.

- Statler, A. T., 1965, Stratigraphy of the Simpson Group in Oklahoma, in T. Herndon (ed.): Symposium on the Simpson group: Tulsa Geological Society Digest, v. 33, p. 162 - 211.
- Stratigraphic Committee, 1971, Cross section of Oklahoma from SW to NE corners of the state: Oklahoma City Geological Society, Inc., 1 sheet.
- Sugawara, A., and Yoshizawa, Y., 1961, An investigation on the thermal conductivity of porous materials and its application to porous rock: Aust. J. Phys., v. 14, p. 469 - 480.
- Sverjenski, D. A., 1986, Genesis of Mississippi Valley-type lead-zinc deposits, Annual Reviews of Earth and Planetary Sciences, v. 14, p. 177 - 199.
- Thompson, T. L., 1976, Plate tectonics in oil and exploration of continental margins: AAPG Bull., v. 60, p. 1,463 - 1,501.
- Thompson, T. L., 1978, Southern Oklahoma oil country in context of plate tectonics (abs): AAPG Bull., v. 62, p. 567.
- Tissot, B. P., Pelet, R., and Ungerer, P., 1987, Thermal history of sedimentary basins, maturation indices, and kinetics of oil and gas generation: AAPG Bull., v. 71, p. 1,445 - 1,466.
- Touloukian, Y. S., Liley, D. E., and Saxena, S. L., 1970, Thermophysical properties of matter, vol. 3, Thermal Conductivity: Nonmetallic liquids and gases, Plenum, New York.
- Ungerer, P., Burrus, J., Doligez, B., Chénet, P. Y., and Bessis, F., 1990, Basin evaluation by integrated two dimensional modeling of heat transfer, fluid flow, hydrocarbon generation, and migration: AAPG Bull., v. 74, p. 309 - 335.
- Van der Voo, R., and French, R. B., 1977, Paleomagnetism of the Late Ordovician Juniata formation and the remagnetization process: J. Geoph. Res., v. 82, p. 5,796 - 5,802.
- Van Orstrand, C. E., 1930, Description of apparatus for the measurement of temperature in deep wells; also, some suggestions in regard to the operation of the apparatus, and the methods of reduction and verification of the observation: in Earth Temperatures in Oil Fields, American Petroleum Institute Production Bulletin 205, p. 9 - 18.
- Vine, J. D., and Tourtelot, E. B., 1970, Geochemistry of black shale deposits a summary report: Economic Geology, v. 65, p. 253 - 273.

- Vitorello, I., and Pollack, H. N., 1980, On the variation of continental heat flow with age and the thermal evolution of continents: *J. Geoph. Res.*, v. 85, p. 983 - 995.
- Wangen, M., 1995, The blanketing effect in sedimentary basins: *Basin Research*, v. 7, p. 283 - 298.
- Waples, D. W., 1980, Time and temperature in petroleum formation: application of Lopatin's method to petroleum exploration: *AAPG Bull.*, v. 64, p. 916 - 920.
- Waples, D. W., 1995a, Maturity modeling : thermal indicators, hydrocarbon generation and oil cracking, *in* L. B. Magoon and W. G. Dow (eds.), *The petroleum system - from source to trap: AAPG Memoir 60*, p. 285 - 306.
- Waples, D. W., 1995b, Modeling of sedimentary basins and petroleum systems, *in* L. B. Magoon and W. G. Dow (eds.): *The petroleum system - from source to trap: AAPG Memoir 60*, p. 307 - 322.
- Weinzierl, J. F., 1922, Subsurface geology of the north part of the Blackwell Field, Oklahoma: MS thesis, University of Oklahoma, Norman, 44 pp.
- Zangerl, R., and Richardson, E. S., 1963, The paleoecologic history of two Pennsylvanian black shales: *Chicago Natural History Museum Fieldiana Geology Memoirs*, v. 4, 352 pp.
- Zenger, D. H., and Dunham, J. B., 1980, Concepts and models of dolomitization - An introduction, *in* D. H. Zenger, J. B. Dunham, and R. L. Ethington (eds.), *Concepts and Models of Dolomitization: Soc. Econ. Paleontolog. Mineral. Spec. Publ.*, v. 28, p. 1 - 9.
- Zoth, G., and Haenel, R., 1988, Thermal conductivity, *in* R. Haenel, L. Rybach and L. Stegena (eds.): *Handbook of terrestrial heat-flow density determination*, eds. Kluwer Acad., Norwell, Mass., p. 449 - 453.